Equilibration of an Atmosphere by Geostrophic Turbulence

by

Malte F Jansen

Submitted to the Department of Earth, Atmospheric, and Planetary Sciences
in partial fulfillment of the requirements for the degree of

Doctor of Philosophy

at the

MASSACHUSETTS INSTITUTE OF TECHNOLOGY

February 2013

Author .....
Department of Earth, Atmospheric, and Planetary Sciences
October 25, 2012

Certified by .....
Raffaele Ferrari
Breene M. Kerr Professor of Oceanography
Thesis Supervisor

Accepted by .....
Robert D. van der Hilst
Schlumberger Professor of Geosciences
Head, Department of Earth, Atmospheric and Planetary Sciences

Equilibration of an Atmosphere by Geostrophic Turbulence

by

Malte F Jansen

Submitted to the Department of Earth, Atmospheric, and Planetary Sciences
on October 25, 2012, in partial fulfillment of the
requirements for the degree of
Doctor of Philosophy

Abstract

A major question for climate studies is to quantify the role of turbulent eddy fluxes in maintaining the observed atmospheric mean state. It has been argued that eddy fluxes keep the mid-latitude atmosphere in a state that is marginally critical to the deepest mode of baroclinic instability, which provides a powerful constraint on the response of the atmosphere to changes in external forcing. A similar criterion does, however not hold in the Southern Ocean, a region whose dynamics are otherwise very similar to the mid-latitude atmosphere. This thesis resolves this apparent contradiction, using a combination of theoretical considerations and eddy-resolving numerical simulations.

It is shown that the adjustment of the extra-tropical troposphere to states of marginal criticality does not follow from a fundamental constraint, but is rather the result of the particular parameters characterizing Earth's troposphere. Both marginally critical and strongly supercritical zonal mean flows can be obtained in planetary atmospheres if external parameters are varied. We argue that changes in the equilibrated mean state over a wide range of simulations can better be understood in terms of a balance between the diabatic forcing and the eddy driven overturning circulation. Using a diffusive closure for the eddy flux of potential vorticity, we can relate the eddy-driven overturning transport to properties of the mean flow, and derive scaling relations for both the baroclinicity and vertical stratification of the equilibrated state.

Thesis Supervisor: Raffaele Ferrari
Title: Breene M. Kerr Professor of Oceanography

Acknowledgments

First and foremost, I want to thank my advisor Raffaele Ferrari, whose support throughout my five years at MIT has been invaluable. I have immensely profited from our various discussions of scientific issues, comments on my papers, as well as help and advise on all kinds of aspects of academic life. I am also grateful to my thesis committee members: Alan Plumb, Paul O'Gorman and Isaac Held, who have helped through comments and discussions to greatly improve this thesis, and who were always available when I was looking for advise. Finally, I would like to thank John Marshall for serving as Chair for my thesis defense, and for providing many valued comments and inspiration along the way.

A big part of my PAOC experience was based on interactions with other students and postdocs. I have greatly enjoyed our reading groups, spontaneous discussion meetings on current (or currently interesting) topics, discussions about each others research, and of course our numerous (scientific and less scientific) lunch conversations. These interactions are a major part of what makes PAOC such a great place to be at. Another part is the availability of the various faculty members and research scientists who have always been welcoming and willing to share their wisdom. In particular, I would like to thank Jean-Michel Campin and the rest of the MITgcm crew for invaluable help on various computing issues.

I also want to thank my wonderful girlfriend Katherine for her support and understanding along the way. Finally, I am deeply grateful to my family and in particular my mother Karin and my father Rainer for being the best parents anyone could hope for. To them this thesis is dedicated.

Contents

List of Figures

List of Tables

Chapter 1

Introduction

1.1 Background

The extra-tropical atmosphere, as well as large parts of the ocean, are filled with turbulent motions on a variety of scales. The largest and most energetic eddies in the atmosphere have scales in excess of 1000km, while the large eddies in the ocean are typically on the order of 100km in size. These large-scale geostrophic eddies play a critical role in the climate system, as they are a major contributor to the transport of heat and other properties. In particular, almost all the atmospheric transport of heat from the subtropical latitudes to the polar regions, is achieved by turbulent eddies and waves.

Understanding the character of these eddy transports is crucial if we want to understand the response of the planets climate, and in particular the equator-to-pole temperature gradient, to changes in the external forcing, such as encountered with past and future climate change. Heuristic arguments have been put forward to predict the turbulent adjustment to changes in the external forcing, both for the atmosphere and the ocean. Surprisingly the arguments put forward for the two fluids are remarkably different, despite the dynamical similarities between the two fluids. The goal of this thesis is to revisit the arguments developed for the atmosphere and explore how generally they hold, and why they seem to break down in the ocean.

The nature of the turbulent fluxes in the atmosphere changes with the latitude

under consideration. In the tropical troposphere, the saturated moist entropy is well mixed in the vertical: this well homogenized state is marginally critical to convective instability and turbulence acts to maintain the system in equilibrium. The implication is that whatever the changes in external forcing, the turbulent fluxes will respond so as to keep saturated moist entropy homogeneous.

The problem is more complex in the midlatitude atmosphere. Here the turbulent eddies originate from baroclinic instabilities of the mid-latitude jets, and feed on the available potential energy associated with the equator-to-pole temperature gradient. Unlike convective instability, which primarily redistributes properties in the vertical, baroclinic eddies redistribute entropy and momentum both in the horizontal and in the vertical. There is no agreed upon theory on how the baroclinic flow equilibrates, and this is the topic of this thesis. A common argument is that, in analogy to the tropical problem, the turbulent eddy fluxes keep the mid-latitude atmosphere in a state that is marginally critical to baroclinic instability. The prediction has some observational support in the atmosphere (Stone, 1978), though the generality of the argument has been challenged by some numerical studies (e.g. Panetta and Held, 1988; Thuburn and Craig, 1997; Barry et al., 2000; Zurita-Gotor, 2008). Most puzzling is the fact that the marginal criticality condition is not satisfied in the Southern Ocean, even though this ocean is characterized by a reentrant baroclinically unstable current and is dynamically very similar to the mid-latitude atmosphere. Yet, the failure of the marginal criticality argument for the ocean has not received much attention.

The original argument for baroclinic adjustment, as advocated by Stone (1978), is based on the condition for marginal criticality in the two layer quasi-geostrophic (QG) model, which can be written as

$$\xi \equiv \frac{fs}{\beta H} = 1, \tag{1.1}$$

where ξ is the criticality parameter, H is the lower layer depth, s is the slope of the interface, f is the Coriolis parameter and $\beta = \partial_y f$. Condition (1.1) states that the QG PV gradient in the lower layer vanishes due to a cancellation between the planetary

vorticity gradient β and the "thickness" gradient $\frac{fs}{H}$. If H is assumed to scale as the tropopause height and s is the isentropic slope in the atmosphere, then condition (1.1) predicts that in a marginally critical state isentropes leaving the surface in the subtropics will reach the tropopause at about the pole, which is in general agreement with the observed state of the atmosphere.

The theory of baroclinic adjustment is very appealing, but some limitations need to be considered. First, any argument for adjustment to marginal criticality requires that the time-scale of the turbulent equilibration is fast compared to the time-scale over which the system is restored to an unstable state by the external forcing. The thermal structure of the atmosphere is restored by radiation, which acts on a time-scale on the order of tens of days. This is much longer than the time required by convection to stabilize the stratification in the tropics, making convective adjustment a very powerful constraint. Eddies in the extra-tropics, however, act on a time-scale comparable to the radiative restoring, and do not satisfy the baroclinic adjustment condition (e.g. Barry et al., 2000).

Second, the marginal criticality condition as formulated in Eq. (1.1) is specific to the two-layer model and it is not clear to what extent it can be applied to continuously stratified models. One obvious approach to generalize the two-layer model result to the continuously stratified problem, is to make use of the fact that the two level QG equations accurately describe the behavior of the barotropic and first baroclinic mode of the continuously stratified system. The condition in Eq. (1.1) therefore implies more generally a threshold for the stability of the deepest interior modes. However, shallower modes, and in particular surface-intensified "Charney" modes, which are thought to play an important role in Earth's atmosphere, may still be unstable, even if $\xi < 1$.

Held (1978, 1982) proposed an alternative argument for the equilibration of the extra-tropical atmosphere, based on the vertical extent of Charney modes in a continuously stratified QG model. The argument does not rely on the assumption that the atmosphere is marginally critical, but arises from the vertically integrated zonal momentum budget of a turbulent atmosphere. He notes that the zonal momentum

budget constrains the eddy PV flux to extend vertically over the Charney depth

$$h_{Ch} = \frac{fs}{\beta}. \tag{1.2}$$

If the height of the tropopause is given by the vertical extent of these eddy fluxes, i.e. $H \sim h_{Ch}$, Eq. (1.2), directly implies a criticality parameter around one. In general, however, the tropopause height is set by a more complex interplay between eddy fluxes and the radiative restoring (Held, 1982). Eq. (1.2) then implies that significant eddy fluxes are expected to extend over the entire depth of the troposphere if $\xi \gtrsim 1$, while eddy fluxes are primarily confined to a shallow layer near the surface if $\xi \ll 1$, which may ultimately render eddy transports ineffective in this limit.

Held's result is akin to the relation between the criticality parameter and the vertical structure of the eddy diffusivity pointed out by Green (1970). Using a diffusive closure for the eddy fluxes of QG PV, the zonal momentum budget puts a constraint on the vertical decay of the eddy diffusivity rather than the eddy flux itself. As shown in Green (1970) the eddy diffusivity has to decay in the vertical over the depth of the troposphere for any finite criticality parameter[1]. For $\xi \approx 1$ the eddy diffusivity needs to decay from its surface value to about zero at the tropopause. For $\xi \ll 1$ the eddy diffusivity needs to decay over a depth scale much smaller than the tropopause height, while only little vertical structure is required if $\xi \gg 1$. This raises the question of what determines the vertical structure of the eddy diffusivity, and whether it can change to allow for changes in the criticality parameter.

Schneider (2004) argues that the result of Green (1970) is specific to the QG approximation, and a different result is obtained from the vertically integrated zonal momentum budget in primitive equations. He integrates the isentropic zonal momentum budget from the surface to the tropopause and uses a diffusive closure for the eddy fluxes of PV and surface potential temperature. Unlike in the QG approximation, he finds that the vertically integrated zonal momentum budget can be closed with a vertically constant eddy diffusivity. Moreover, he argues that this assump-

[1]Green (1970) does not explicitly talk about the "criticality parameter", but introduces a parameter γ which is essentially the inverse of the criticality parameter as used in this thesis.

tion directly implies that the criticality parameter needs to be close to one. The adjustment of the extra-tropical atmosphere to states with $\xi \approx 1$ is thus argued to result directly from the vertically integrated zonal momentum budget, if eddies mix PV at an approximately constant rate throughout the depth of the troposphere. The difference between Schneider's (2004) result, and the one obtained using the QG approximation, is argued to stem from an inadequate representation of isentropic intersections with the surface in the QG equations. Notice, that Schneider's (2004) result resembles the marginally criticality condition of Stone (1978), but it does not require (or imply) marginal criticality to baroclinic instability of the full, continuously stratified, primitive equation system.

Schneider's (2004) result seems to put a strong upper bound on the criticality parameter. Supercritical flows are in general assumed to be associated with a strong barotropization of the turbulent eddies (Rhines, 1979; Held and Larichev, 1996). Should ξ be larger than one, the turbulent eddies would be expected to be strongly barotropic, implying that the eddy diffusivity is approximately constant in the vertical. This results in a contradiction, because Schneider (2004) claims that $\xi \sim 1$ if the eddy diffusivity is depth independent. Schneider concludes that strongly supercritical states cannot be achieved in primitive equation systems (Schneider and Walker, 2006).

An important implication of the limitation of the criticality parameter ξ to order one is that turbulence in planetary atmospheres would be prevented from producing a significant up-scale energy transfer. The latter relies upon a separation between the deformation scale, at which turbulent eddies are generated through baroclinic instability of the zonal flow, and the halting scale, which has to be larger than the scale of the instability. Held and Larichev (1996), using the two-layer QG model, show that such a scale separation is contingent on ξ being larger than one. In agreement with the observation that the criticality parameter is close to one, no significant separation between the scale of the instability and the halting scale appears to exist in Earth's atmosphere (e.g. Merlis and Schneider, 2009, and references therein).

The marginal criticality arguments reviewed above are quite general and may be

expected to apply to baroclinic flows in atmospheres as well as in the ocean. The Southern Ocean is a good test case, because it is characterized by an uninterrupted circumpolar flow, the Antarctic Circumpolar Current (ACC) – ocean flows at other latitudes are blocked laterally by continents resulting in a different equilibration problem. Analogous to the mid-latitude atmosphere, dynamic fluxes of entropy and momentum are here dominated by turbulent eddies arising from baroclinic instability of the mean zonal current (e.g. Karsten and Marshall, 2002, and references therein). One should therefore expect the arguments for baroclinic adjustment to hold in the ACC region. However, observations and numerical models of the Southern Ocean show that the ACC region is supercritical, with QG PV gradients much larger than β, and also displays an up-scale energy transfer due to nonlinear eddy-eddy interactions (Scott and Wang, 2005; Tulloch et al., 2011).

The goals for this thesis are to (1) resolve the apparent contradiction between theories for the equilibration of the extra-tropical atmosphere and the observed equilibration of the Southern Ocean, (2) develop a more general understanding of how turbulent eddies equilibrate an atmosphere, and (3) analyze in how far results obtained from QG theory can be applied to primitive equation systems.

1.2 Outline

The main body of this thesis is composed of 5 chapters, the first 4 of which represent separate papers that have either been published or are in preparation for publication. Chapter 2 appeared in the Journal of Atmospheric Sciences (Jansen and Ferrari, 2012) and is here reproduced identically, save for cuts in the introduction[2]. Chapter 3 is currently in revision for publication in the Journal of Atmospheric Sciences, and chapters 4 and 5 are in preparation for submission. The topics of each chapter as well as their connections are outlined in the following.

Chapter 2 uses the observed difference in the adjustment of the extra-tropical atmosphere and Southern Ocean as a motivation for a series of idealized simulations in

[2]The American Meteorological Society maintains the copyright for this chapter.

which fluid properties are varied to span air-like and water-like characteristics. The parameter that will be controlled is the thermal expansion coefficient, which determines the buoyancy contrast associated with a given temperature contrast. Temperature contrasts between water masses in the ocean are comparable to those in the atmosphere, but the associated buoyancy contrasts are much smaller due to the much smaller thermal expansion coefficient of sea water. It will be shown that by varying this parameter we can obtain mid-latitude atmosphere-like, marginally critical states, as well as significantly supercritical states, which resemble some of the properties observed in the Southern Ocean.

The ability to obtain marginally critical as well as supercritical mean states, by varying only the thermal expansion coefficient of the fluid, calls into question the generality of theories which argue for baroclinic adjustment of the extra-tropical atmosphere to marginal criticality. Apart from being specific to the two layer model, Stone's (1978) argument for baroclinic adjustment to marginal criticality is expected to hold only as long as the time-scale over which eddies mix properties across the baroclinic zone is much shorter than the time-scale of radiative restoring. This assumption is already violated for typical atmospheric conditions, and becomes even more inapplicable in simulations with small, ocean-like, thermal expansion coefficients, which cause much weaker eddy velocities. The breakdown of Stone's (1978) result, for the simulations discussed in chapter 2 is thus not particularly surprising. The theory of Schneider (2004), however, results from a fundamental constraint on the zonal momentum budget and ought to hold for any choice of parameters.

The argument for the turbulent equilibration of atmospheres to states of marginal criticality, brought forward by Schneider (2004), is reviewed in chapter 3. Schneider's (2004) theory is based on the vertically integrated zonal momentum budget in isentropic coordinates, closed with a diffusive closure for the eddy fluxes of PV and surface potential temperature. The result obtained by Schneider (2004), however, depends crucially on his definition of mean and eddy fluxes on isentropes which intersect with the surface. It is argued that this definition is unphysical, and the applied diffusive closure is not supported by numerical simulations. Instead, we argue for

an alternative definition, first proposed by Koh and Plumb (2004). Following this approach, it is shown that the zonal momentum budget cannot be closed with a vertically constant eddy PV diffusivity, in agreement with results found using QG theory (Green, 1970). Order one criticalities are obtained if the eddy diffusivity decays from its surface value to about zero over the depth of the troposphere, which is likely to be the case in Earth's atmosphere. Large criticality parameters, however, are possible if the eddy diffusivity decays only weakly in the vertical, consistent with results from QG models. This helps to explain the numerical studies discussed in chapter 2, as well as other studies which have found supercritical mean states in primitive equation models (Zurita-Gotor, 2008; Zurita-Gotor and Vallis, 2010).

The revised relation between the criticality parameter and the vertical structure of the eddy diffusivity is tested against atmospheric re-analysis data and numerical simulations in chapter 4. Analyis of re-anaysis data confirms the predicted vertical decrease in the eddy diffusivity over the extra-tropical troposphere. The relation is further supported quantitatively in a series of numerical simulations with varying Coriolis parameter, f, and planetary vorticity gradient, β. Changes in these parameters prove to be an efficient way to obtain mean states with a wide range of criticality parameters from $\xi \approx 1$ to $\xi \gg 1$. In agreement with the results of chapter 3, these changes in the criticality parameter are associated with correspondingly large changes in the vertical structure of the eddy diffusivity.

Chapters 2 through 4 show unambiguously that large-scale turbulence does not generally adjust an atmosphere to states of marginal criticality. In chapter 5 we thus return to the challenge of predicting how the atmospheric baroclinicity and stratification adjusts in response to changes in the forcing or other external parameters. We argue that changes in the criticality parameter can best be understood in terms of a balance between the diabatic forcing and adiabatic eddy fluxes. Using the diffusive closure for the eddy fluxes proposed by Held and Larichev (1996), one can derive a predictive scaling argument for the criticality parameter. The derived scaling relation reproduces the numerical results discussed in chapters 2 and 4. Finally, we will argue that the scaling relation can be extended to predict both the equator to pole

temperature gradient, and the bulk static stability.

In chapter 6 we return to a brief comparison between our results for the turbulent equilibration of an atmosphere and the corresponding equilibration problem of the Southern Ocean, which motivated this thesis. It will be shown that the fundamental arguments applied in this thesis are similar to those that have been used in the oceanographic literature. Chapter 7 summarizes the results of this thesis and provides some concluding remarks.

Chapter 2

Transition to Supercriticality in a Primitive Equation System

2.1 Introduction

It has been argued that eddy fluxes keep the mid-latitude atmosphere in a state that is marginally critical to baroclinic instability, which provides a powerful constraint on the response of the atmosphere to changes in external forcing (e.g. Stone, 1978). However, no comparable criterion appears to exist for the ocean. This is particularly surprising for the Southern Ocean, a region whose dynamics are very similar to the mid-latitude atmosphere, but observations and numerical models suggest that the currents are supercritical. This chapter aims to test the generality of the idea of adjustment to marginal criticality, making use of our knowledge of the difference between the equilibration in the atmosphere and ocean.

When comparing ocean and atmospheric jets, two differences are most apparent. First, the ocean is primarily driven mechanically by surface wind stresses, while the atmosphere is a heat engine driven by differential heating throughout the troposphere (e.g. Wunsch and Ferrari, 2004). Second, the two fluids have different properties (density, compressibility, ...). In this chapter we will focus on the second difference. All simulations use an atmosphere-like thermal forcing. Nevertheless, it will show that by varying only fluid properties it is possible to obtain atmosphere-like, marginally

critical states, as well as more ocean-like, supercritical states. This shows that supercritical mean states can be obtained in thermally forced systems, if only external parameters are varied, calling into question the generality of the theory of atmospheric adjustment to marginal criticality.

We will consider an idealized, thermally forced, zonally-re-entrant, channel configuration, using a Boussinesq fluid. Within the idealized framework of a Boussinesq fluid, differences in the fluid properties between air and water are captured by the very different thermal expansion coefficients. Motivated by the observed differences between the atmosphere and ocean, we will therefore consider thermal expansion coefficients spanning from atmospheric (air) to oceanic (water) values. It will be shown that eddies become ineffective at maintaining the system in a marginally critical state in the more ocean-like limit of small thermal expansion coefficients.

The role of the thermal expansion coefficient in setting dynamical properties of the system will be discussed in section 2.2. In section 2.3 we introduce a theoretical framework for the eddy-equilibration of an idealized thermally forced Boussinesq system, using primitive equations in isentropic coordinates. In section 2.4 we present a series of numerical simulations using a diabatically forced, primitive equation model in a channel configuration. It is shown that marginally critical as well as supercritical states can be found simply by varying the thermal expansion coefficient. A summary and discussion of the results is offered in section 2.5.

2.2 Representation and Implications of Fluid Properties in an Idealized Boussinesq Framework

We idealize the problem of turbulent adjustment by considering a Boussinesq fluid in a thermally forced zonally re-entrant channel. This configuration maintains all the physics that are essential to test the ideas discussed in the introduction, while omitting some of the complicating factors found in real geophysical fluids. In particular, it allows us to continuously vary fluid properties from atmospheric to oceanic values,

without changing the dynamical equations.

Fluid differences enter the dynamical equations only via the equation of state, which in the Boussinesq system becomes an equation for buoyancy. Consistent with the Boussinesq approximation, buoyancy is assumed to depend linearly on potential temperature only, i.e.

$$b = g\alpha(\theta - \theta_0), \tag{2.1}$$

where θ_0 is some reference potential temperature and $\alpha = -\frac{1}{\rho}\frac{\partial \rho}{\partial \theta}$ is the thermal expansion coefficient. Within the Boussinesq approximation, the differences between air and water are thus captured by the thermal expansion coefficient α (the dynamics depends only on gradients of buoyancy and are thus independent of the reference potential temperature θ_0). For typical oceanic conditions the thermal expansion coefficient is about $\alpha \approx 1 - 3 \times 10^{-4}$ K^{-1}. For a dry atmosphere, where the equation of state is well approximated by the ideal gas law, on the other hand

$$\alpha = -\frac{1}{\rho}\frac{\partial \rho}{\partial \theta} = \frac{1}{\theta} \approx 3.6 \times 10^{-3}\mathrm{K}^{-1}, \tag{2.2}$$

where the partial derivative is to be taken at constant pressure, and we assumed a typical potential temperature $\theta \approx 280$ K. The thermal expansion coefficient of air is thus about 10-40 times bigger than that of ocean water. Since planetary-scale potential temperature contrasts are of similar order in the atmosphere and ocean (due to the strong coupling between the two fluids), the much larger thermal expansion coefficient causes buoyancy contrasts to be about 10-40 times larger in the atmosphere, resulting into much stronger circulations.

One of the key differences between the mid-latitude atmosphere and the Southern Ocean are the different deformation scales, which are largely set by the different thermal expansion coefficients of the two fluids. Assuming that the stratification is approximately constant in the vertical, and using the linear equation of state (2.1), the deformation radius scales as

$$L_d \sim \frac{\sqrt{\Delta_v b H}}{f} \sim \frac{\sqrt{g\alpha\Delta_v \theta H}}{f}, \tag{2.3}$$

where $\Delta_v b$ and $\Delta_v \theta$ denote the vertical buoyancy and potential temperature differences and H is the depth of the troposphere or the thermocline. The vertical temperature differences are of the same order as the horizontal ones, and they are of the same order in the atmosphere and ocean. Hence the difference in the deformation radii between the atmosphere and the ocean arise from two main parameters: the large differences in the thermal expansion coefficients and the different depth scales. α is about 10-40 times larger in the atmosphere than in the ocean, while H is $\sim$ 10km for the troposphere but only $\sim$ 1km for the ocean's thermocline. Together these differences account for the observation that the deformation scale of the atmosphere is larger than that of the ocean by a factor of $\sqrt{100} - \sqrt{400} \sim 10 - 20$.

2.3 Macroturbulent Adjustment in an Isentropic Framework

We introduce a theoretical framework to address the question of how macroturbulence sets the equilibrated thermal structure of a thermally forced primitive equation (PE) system. The discussion will be presented in the framework of the full primitive equations expressed in isentropic coordinates. A simplified derivation based on the QG approximation is given in appendix A. While the QG-based discussion has some obvious shortcomings, it captures the essence of the results derived below. On a first reading, one might therefore skip to appendix A and then proceed directly to the numerical simulations discussed in section 2.4.

We will first discuss dynamical constraints on the zonal momentum balance inspired by the work of Koh and Plumb (2004) and Schneider (2004, 2005). Departing from Schneider (2004), who integrates the zonal momentum budget over the whole depth of the troposphere, we will integrate only to the top of the Surface Layer (SL), i.e. that part of the atmosphere that includes all isentropes that intersect with the surface at some longitude or time, as sketched in Fig. 2-1. (The reasons for this will be discussed later.) In order to close the SL momentum budget we will derive an

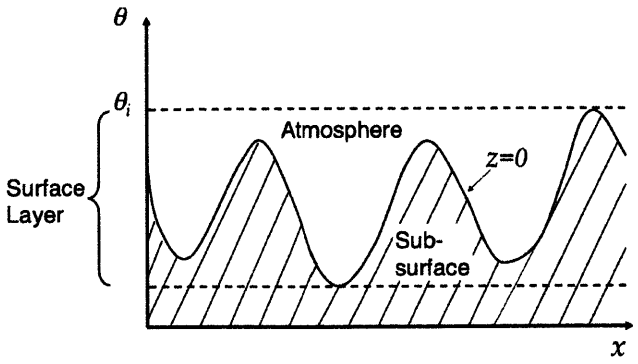

Figure 2-1: Sketch of the Surface Layer (SL). The undulating bottom surface of the atmosphere shown in the longitude–potential temperature (x,θ) plane. The SL comprises all isentropes that intersect with the surface at some longitude and time.

additional constraint for the total meridional mass transport in the SL. Armed with these two constraints, we will be able to relate the turbulently adjusted mean state to the radiative forcing. For simplicity all arguments and simulations presented here assume a Boussinesq fluid in a flat-bottomed re-entrant channel configuration. Notice, however, that the same qualitative results are obtained for an ideal gas atmosphere on a spherical planet.

2.3.1 Dynamical constraint: the zonal momentum balance

We start with the vertically integrated, temporal and zonal mean isentropic zonal momentum balance discussed in Schneider (2005). For a Boussinesq fluid in a statistically steady state in the limit of small Rossby numbers (appropriate for large scale ocean and atmospheric flows), this can be approximated as

$$\int_{b_{min}}^{b_i} \overline{h_b}\,\overline{v}^* db \approx -\int_{b_{min}}^{b_i} \frac{\overline{h_b}\overline{\hat{v}\hat{P}}^* + \overline{h_b}\overline{J_F^y}^*}{\overline{P}^*} db - \frac{f}{\overline{P}^*(\overline{b_s}^s)}\overline{v'_{gs}b'_s}^s \tag{2.4}$$

where v is the full meridional velocity and v_{gs} is the meridional geostrophic velocity at the surface, b is buoyancy, b_s the surface buoyancy, b_{min} the minimum buoyancy in the domain and b_i a buoyancy level above the SL. $h_b = \mathcal{H}(b - b_s)\partial_b z$ is the isentropic thickness and z the height of the isentrope b. The thickness is multiplied by

the Heaviside function so that it vanishes when isentropes intersect the ground. The potential vorticity is $P = \frac{f}{\partial_b z}$, consistent with the small Rossby number assumption[1]. J_F^y represents frictional forces. The overbar $\overline{()}$ denotes an isentropic zonal and temporal average, $\overline{()}^* = \overline{h_b()}/\overline{h_b}$ is the thickness weighted zonal average, and $\overline{()}^s$ denotes a zonal and temporal average along the surface. Primes denote departures from the zonal averages and hats departures from the thickness weighted averages.

Eq. (2.4) looks similar to its QG analogue: Eq. (2.A2) derived in appendix A by averaging the zonal QG momentum budget. It states that the net volume transport (or "residual transport") between the surface and the isentropic surface b_i is driven by the interior meridional PV flux $\overline{\hat{v}\hat{P}}^*$, and the surface geostrophic buoyancy flux, $\overline{v'_{gs}b'_s}^s$. Hence QG theory can be used to qualitatively understand the momentum budget of a baroclinic jet. There are, however, important quantitative differences between the PE and QG budgets. In QG, the SL is infinitesimally thin and contributes only the buoyancy flux, while the PV flux acts only in the interior. In PE, the SL spans up to half of the troposphere in the real atmosphere (e.g. Schneider, 2004). In particular, the surface buoyancy flux represents the eddy form drag generated by outcropping isentropes in the SL.

In order to transform Eq. (2.4) into a constraint for the mean variables, we need a closure for the eddy fluxes of PV and surface buoyancy. Mixing length arguments (Rhines and Young., 1982), and numerical studies (e.g. Pavan and Held, 1996), suggest that the eddy fluxes are down their mean gradients, such that

$$\overline{\hat{v}\hat{P}}^* = -D\partial_y\overline{P}^* \,, \quad \overline{v'_{gs}b'_s}^s = -D\partial_y\overline{b_s}^s \,, \tag{2.5}$$

with an eddy diffusivity D that, for simplicity, is here assumed constant in the vertical. As discussed in Appendix B, all the key relationships derived below are recovered if

[1]In the following we are also neglecting the contribution of the mean-flow vorticity gradient to the mean PV gradient. If the mean flow is primarily baroclinic, this is equivalent to assuming a small Burger number for the mean flow, which is also appropriate for the large-scale flow in the atmosphere and ocean. In the presence of strong barotropic jets, the vorticity gradient associated with the mean jets can become more significant locally, but this contribution approximately vanishes when averaging over the width of the entire baroclinic zone.

we allow for vertical variations in the eddy diffusivity, with D replaced by a bulk eddy diffusivity which tends to be dominated by its near surface value. Ignoring frictional forces, which are small in the free troposphere (Schneider, 2005), the isentropic mass flux equation (2.4) becomes

$$\int_{b_{min}}^{b_i} \overline{h_b}\,\overline{v}^* db \approx D \int_{b_{min}}^{b_i} \frac{\overline{h_b}\partial_y \overline{P}^*}{\overline{P}^*} db + \frac{f}{\overline{P}^*(\overline{b_s}^s)} D \partial_y \overline{b_s}^s . \tag{2.6}$$

Using that $P = f/\partial_b z$ and $h_b = \mathcal{H}(b - b_s)\partial_b z$, the thickness weighted average of PV can be written as $\overline{P}^* = \overline{h_b P}/\overline{h_b} \approx \overline{\mathcal{H}(b-b_s)f}/\overline{h_b} = \Pi f/\overline{h_b}$, where $\Pi = \overline{\mathcal{H}(b-b_s)}$ denotes the fraction of the isentrope that is above the surface[2]. We can now rewrite the first term on the R.H.S. of Eq. (2.6) as

$$\begin{aligned}
\int_{b_{min}}^{b_i} \frac{\overline{h_b}\partial_y \overline{P}^*}{\overline{P}^*} db &\approx \int_{b_{min}}^{b_i} (\overline{h_b}\frac{\beta}{f} - \partial_y \overline{h_b} + \frac{f}{\overline{P}^*}\partial_y \Pi) db \\
&= \frac{\beta}{f}\overline{z}(b_i) - \partial_y \overline{z}(b_i) - \overline{\frac{f}{\overline{P}^*(b_s)}\partial_y b_s}^s \\
&\approx \frac{\beta}{f}\overline{z}(b_i) - \partial_y \overline{z}(b_i) - \frac{f}{\overline{P}^*(\overline{b_s}^s)}\partial_y \overline{b_s}^s .
\end{aligned} \tag{2.7}$$

The approximation in the last step can be formalized by expanding variables around $\overline{b_s}$, following a similar derivation for the surface buoyancy flux term sketched in Schneider (2005, Eq. (11)). Using the relationship in Eq. (2.7), Eq. (2.6) can now be written as

$$\Psi_Q(b_i) \approx D\left(s(b_i) - \frac{\beta}{f}\overline{z}(b_i)\right) , \tag{2.8}$$

where $s(b_i) = \partial_y \overline{z}(b_i)$ denotes the slope of the isentrope b_i and $\Psi_Q(b_i) \equiv -\int_{b_{min}}^{b_i} \overline{h}\,\overline{v}^* db$ is the isentropic overturning streamfunction (the subscript Q reminds that Ψ_Q is related to the diabatic forcing Q, as discussed below).

Eq. (2.8) states that the net isentropic mass transport in the SL is proportional

[2]Notice that we here use the PV definition used by Koh and Plumb (2004) or "convention II" discussed by Schneider (2005). However, if it is assumed that the isentropic slope varies little over the depth of the SL, "convention I" of Schneider (2005) yields a result very similar to Eq. (2.8) except for an additional factor of 3/2 in front of the slope on the R.H.S.. Notice however that, as will be discussed below, the differences do become crucial if the integration is taken over the whole depth of the tropopause instead of over just the surface layer, as done in Schneider (2004).

to the eddy diffusivity times an effective SL PV gradient, which is given by the sum of the vertical integral of the planetary vorticity gradient and the isentropic slope at the top of the SL. This effective SL PV gradient is similar to the PV gradient in the bottom layer of a layered QG model, supporting the interpretation that the lower layer of a two-layer QG model might be regarded as representative of the SL. The effective PV gradient in this layer is generally dominated by the contribution of the surface potential temperature gradient, appearing on all isentropes in the SL. Note, however, that the vertical extent of the SL is not fixed (as in a layered QG model) but can adjust e.g. to changes in the forcing.

Notice, that our approach differs from Schneider (2004), who stretched the integral in (2.6) all the way to the tropopause, where $\Psi_Q(b_t) = 0$ by definition, and obtained the condition that the criticality parameter has to be close to one. However, the result obtained by integrating Eq. (2.6) all the way to the tropopause depends crucially on assumptions for computing PV on isentropes below the surface (which Schneider (2005) refers to as "conventions I and II"), and on the vertical structure of the eddy diffusivity under the respective conventions. By integrating (2.6) only over the SL, our result does not depend on these somewhat arbitrary "conventions" or on the exact vertical structure of the eddy diffusivity.

In the limit of weak diabatic circulation, i.e. $|\Psi_Q/D| \ll |s(b_i)|$, the relation (2.8) simplifies to a statement analogous to the marginal criticality condition of the two layer QG model, with the layer depth given by the depth of the SL, i.e.

$$\frac{fs(b_i)}{\beta\overline{z}(b_i)} \approx 1\,. \tag{2.9}$$

Similar to the marginal criticality condition of the two layer QG model, Eq. (2.9) states that the effective PV gradient integrated over the SL has to vanish. The SL thus becomes the analogue to the lower layer in the two-layer QG model. The relevance of this limit for typical atmospheric conditions will, however, be questioned in the following section, where we will derive a scaling for the diabatic circulation Ψ_Q and show that Ψ_Q/D is typically not small compared to $s(b_i)$.

2.3.2 Thermodynamic constraint: isentropic mass budget

A relation between the isentropic mass transport and the diabatic forcing can be derived from the time and zonal mean continuity equation in isentropic coordinates

$$\partial_y(\overline{h_b v}) + \partial_b(\overline{h_b Q}) = 0\,, \tag{2.10}$$

where $Q = \frac{db}{dt}$ denotes the diabatic forcing. Eq. (2.10) can be integrated meridionally and vertically to yield

$$\Psi_Q(y, b_i) \equiv -\int_{b_{min}}^{b_i} \overline{h_b v}(y, b')db' = \int_{y_s}^{y} \overline{h_b Q}(y', b_i)dy'\,, \tag{2.11}$$

where we used that h_b vanishes on sub-surface isentropes and thus $\overline{h_b Q}(y, b_{min}) = 0$ for all y. Here y_s denotes the southernmost latitude where the isentrope b_i intersects with the surface, or the southern boundary of the channel if it does never intersect the surface.

By integrating (2.11) from y_s to the northern boundary of the domain y_{max}, we can further show that in equilibrium the net heating along an isentrope has to vanish, so that we can replace the diabatic heating in the SL by the diabatic cooling above[3]. We thus have

$$\Psi_Q(y, b_i) = \int_{y_s}^{y} \overline{h_b Q}(y', b_i)dy' = -\int_{y}^{y_{max}} \overline{h_b Q}(y', b_i)dy' \approx -\int_{y}^{y_t} \overline{h_b Q}(y', b_i)dy'\,, \tag{2.12}$$

where $y_t(b_i)$ denotes the latitude at which the isentrope b_i intersects with the tropopause. Eq. (2.12) is derived assuming that the net heating over a certain buoyancy class $\overline{h_b Q}$ is negligible above the tropopause, an assumption equivalent to assuming that the isentropic mass transport is small above the tropopause, which is confirmed in the simulations discussed below and in atmospheric analysis (e.g. Bartels et al., 1998, Fig. 1). If b_i is chosen to be the buoyancy just above the SL, the relationship in (2.12)

[3]Notice, that we here assumes an isentrope which intersects with the surface somewhere in the domain. Since the stratification becomes very weak near the southern end of the domain in the simulations discussed here, this holds true for almost all isentropes in the domain (see figure 2-5).

implies that the overturning $\Psi_Q(b_i)$ at the top of the SL is given by the integrated cooling along the isentrope b_i above the SL. This cooling must be balanced by a similar warming within the SL. Ψ_Q is thus given by the total amount of heat transported out of the SL and into the interior within the buoyancy class b_i.

Eq. (2.12) can now be used to derive a scaling for the diabatic overturning streamfunction Ψ_Q. Let us assume that the diabatic forcing can be represented by a radiative relaxation, that is $Q \sim -(b - b_{eq})/\tau_r$ with a restoring time scale τ_r to an equilibrium buoyancy b_{eq}. This is indeed the form of radiative forcing used in the simulations described below and in many idealized studies of the atmosphere (e.g. Held and Suarez, 1994; Schneider, 2004). Using (2.12) we can then argue that

$$\Psi_Q \sim \frac{\Delta b_{eq}\, l}{\tau_r \partial_z \bar{b}}\,, \tag{2.13}$$

where l is the meridional length of the isentrope b_i, and Δb_{eq} denotes the variation of the equilibrium buoyancy along the isentrope b_i (see Fig. 2-2 for a sketch). The relation (2.13) assumes that the radiative imbalance $b - b_{eq}$ along each isentrope above and below the top of the SL scales with the variation of the radiative equilibrium buoyancy along the respective isentrope Δb_{eq}, and is derived in detail in Appendix C. Note, that Δb_{eq} is not fixed, but depends on the mean state and in particular on the isentropic slope. However, changes in Δb_{eq} are small across all the simulations discussed in this paper.

2.3.3 Implications for the equilibrium state and criticality

The scaling for Ψ_Q can be used to show that the condition (2.9) (which can be viewed as a generalization of the QG marginal criticality condition, with the layer depth replaced by the depth of the SL) cannot be expected to hold generally. The requirement for Eq. (2.9) to hold is that $\frac{\Psi_Q}{Ds(b_i)} \ll 1$, which with (2.13) becomes

$$\frac{\Psi_Q}{Ds(b_i)} \sim \frac{\Delta b_{eq}\, l}{D\tau_r \partial_y \bar{b}} \sim \frac{\Delta b_{eq}}{\Delta_y \bar{b}} \frac{l^2/D}{\tau_r} \ll 1\,. \tag{2.14}$$

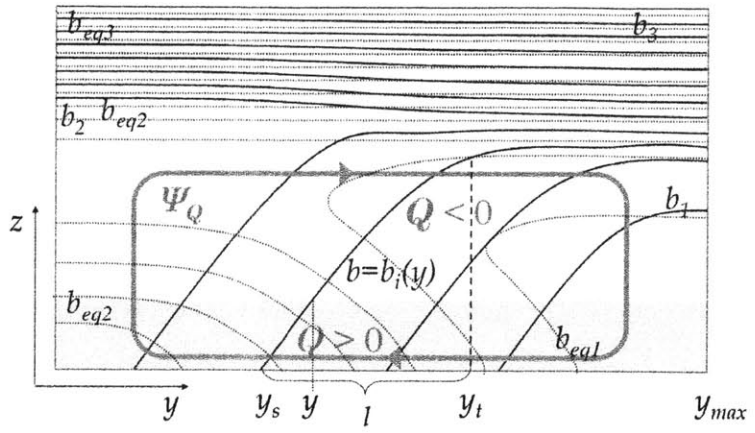

Figure 2-2: Sketch of the diabatically driven overturning circulation Ψ_Q. The solid and dotted black lines denote isentropes of the mean and radiative equilibrium states, respectively, with $b_3 = b_{Eq3} > b_2 = b_{Eq2} > b_1 = b_{Eq1}$. The shading indicates the surface layer, which at latitude $y = y_1$ extends up to the buoyancy $b = b_i(y_1)$. Note that the net heating and cooling integrated along the isentrope b_i over the distance l (that is from its intersection with the surface to its intersection with the tropopause) approximately vanishes (see section 2.3.2.3.2).

Here $\Delta_y \bar{b} \sim l\, \partial_y \bar{b}$ denotes the horizontal buoyancy difference over the meridional extent l of the isentrope b_i (note that the y-derivative is here taken at constant z). Generally $\Delta b_{eq} \gtrsim \Delta_y \bar{b}$, because $\Delta b_{eq} \gtrsim \Delta_y b_{eq}$ since the vertical tilt of the isentropes adds a positive contribution to the buoyancy contrast along an isentrope (if the restoring profile is statically unstable), and $\Delta_y b_{eq} \gtrsim \Delta_y \bar{b}$ since the meridional temperature gradient is generally weaker than the temperature gradient in radiative equilibrium. The relation (2.14) thus implies that the diabatic term Ψ_Q/D can be small only if $\frac{l^2/D}{\tau_r} \ll 1$, that is the time-scale of eddy-diffusion over the length of an isentrope, l^2/D, has to be short compared to the restoring time-scale τ_r. Equivalently, the time scale over which eddy fluxes modify the mean state needs to be fast compared to the time-scale of diabatic restoring. This is not true for typical atmospheric conditions and for the numerical simulations discussed below.

In typical atmospheric conditions and in the simulations described below, the diffusive time-scale is not small compared to the radiative restoring time scale. In this case the effective SL PV gradient does not vanish, because $s(b_i) - \beta f^{-1} \bar{z}(b_i) \approx \psi_Q/D > 0$ for the common situation where net warming in the SL is compensated by

net cooling above. This further implies that the net isentropic slope will generally be steeper than predicted by the condition $s(b_i) - \beta f^{-1}\overline{z}(b_i) = 0$ (see Eq. (2.9)).

Our simulations suggest that typically $\frac{fs(b_i)}{\beta\overline{z}(b_i)} \gg 1$ and the leading order balance in the momentum budget (2.8) is between the diabatic overturning and the eddy diffusivity acting on the thickness gradient integrated over the SL,

$$s(b_i) \approx \frac{\Psi_Q}{D}. \tag{2.15}$$

The relation (2.15) has important implications for the criticality parameter defined as

$$\xi = \frac{fs}{\beta H_t}, \tag{2.16}$$

which is the form used in most studies on extratropical adjustment (e.g. Zurita-Gotor and Vallis, 2011, and references therein). Here H_t denotes the depth of the tropopause and s represents a characteristic isentropic slope (whose exact definition varies in different studies). Interpreting s as the isentropic slope at the top of the SL, (2.15) predicts

$$\xi \sim \frac{f}{\beta H_t}\frac{\Psi_Q}{D}, \tag{2.17}$$

where Ψ_Q here denotes the net mass transport over the SL, which is generally found to be close to the total overturning transport (e.g. Held and Schneider, 1999). For any given planet ($\frac{f}{\beta}$ fixed), the criticality parameter ξ thus depends on the relation between the forcing (and the associated Ψ_Q), the eddy diffusivity, and the depth of the troposphere. Baroclinic adjustment theories, which predict constant ξ, would demand that D scales as Ψ_Q/H_t. This is, however, not what we find in the numerical experiments analyzed below.

A slightly more general form of (2.15) can be used to compare the equilibration in atmosphere-like and ocean-like settings. If the mechanical surface stress in Eq. (2.4) is retained, a the more general scaling for the isentropic slope is obtained

$$s(b_i) \approx \frac{\Psi_Q - \Psi_{Ek}}{D}. \tag{2.18}$$

For the atmospheric case $\Psi_{Ek} << \Psi_Q$, which leaves us with the relation (2.15). In a nearly adiabatic oceanic channel, on the other hand, $\Psi_Q << \Psi_{Ek}$, which leaves us with the scaling $s(b_i) \approx -\frac{\Psi_{Ek}}{D}$. A scaling similar to Eq. (2.18) is discussed in Marshall and Radko (2003) for the isentropic slope at the bottom of the mixed layer in the ACC.

2.4 Transition to Supercritical States in a Channel Model

The arguments presented above are tested by analyzing numerical simulations that explicitly resolve the macroturbulence whose effect on the mean-fields we are trying to understand. As in the theoretical discussion above, we idealize the problem by considering a Boussinesq fluid in a zonally re-entrant channel model.

2.4.1 Model setup

We use a hydrostatic, incompressible, cartesian coordinate configuration of the MIT GCM (Marshall et al., 1997). The geometry is a zonally reentrant channel, 15,000 km long, bounded meridionally by side walls with free slip boundary conditions at y=± 4500km, and vertically by a rigid lid at z=H=10.2km and a flat bottom at z=0, with free slip and no-slip conditions, respectively. We employ a vertical viscosity of $\nu_z = 10^{-1}$ m^{2}s^{-1} and a diffusive convective adjustment scheme with a diffusivity of $\kappa_{conv} = 10^2$ m^{2}s^{-1}. No explicit horizontal diffusion of temperature or momentum is used, but a 4th order Shapiro filter (Shapiro, 1970) is employed to remove small scale grid noise. The vertical resolution is 400m in the interior but refines to 50m at the surface, adding up to a total of 29 levels. The horizontal resolution for all experiments is 50km.

While details of the simulations can be sensitive to the model resolution, the bulk quantities which are of primary interest here are found to be robust. The strongest resolution dependence is expected for the most supercritical simulations with the

smallest deformation radii. A simulation with doubled horizontal resolution suggests that the criticality parameter decreases slightly (on the order of 10%) in this limit[4]. A small decrease in the criticality parameter for increased horizontal resolution is to be expected due to reduced dissipation of EKE by the numerical filter (see also Appendix D), but does not affect our conclusions.

We use a β-plane, where the Coriolis parameter increases linearly as

$$f = f_0 + \beta y\,, \tag{2.19}$$

whith $f_0 = 1\times10^{-4}s^{-1}$ and $\beta = 1.6\times10^{-11}m^{-1}s^{-1}$ for all simulations presented in the chapter. With this choice the Coriolis parameter varies strongly but stays positive throughout the domain. We use the linear equation of state given in Eq. (2.1) with varying thermal expansion coefficients.

The simulations are forced through relaxation to an equilibrium temperature profile which is chosen to mimic some of the key features of radiative forcing in the atmosphere. The potential temperature in radiative equilibrium is specified as a function of y and z as

$$\theta_{eq} = \theta_{min} + \Delta_z\theta\left(\frac{z}{H}\right)^3 + \mathrm{e}^{-\frac{z^2}{h^2}}\Delta\theta_s(y) \tag{2.20}$$

with $\theta_{min} = 233\mathrm{K}$, $\Delta_z\theta = 180K$ and $h = 4km$. The meridional dependence of the surface temperature is given as

$$\Delta\theta_s(y) = \begin{cases} \Delta\theta_{s0} + \Delta_y\theta & \text{for} \quad y < -L_c \\ \Delta\theta_{s0} + \frac{\Delta_y\theta}{2}(1 - \sin(\pi y/(2L_c))) & \text{for} \quad -L_c \le y \le L_c \\ \Delta\theta_{s0} & \text{for} \quad y > L_c \end{cases} \tag{2.21}$$

where $\Delta\theta_{s0} = 10\mathrm{K}$, $\Delta_y\theta = 80\mathrm{K}$ and $L_c = 3500$ km. The resulting equilibrium poten-

[4]The simulation used for this sensitivity experiment is discussed in chapter 4 and uses $f = 8\times10^{-4}\mathrm{s}^{-1}$ and $\beta = 0.8\times10^{-11}\mathrm{m}^{-1}\mathrm{s}^{-1}$. This is the most supercritical simulation considered in this thesis and has a similar deformation radius to the simulation with the smallest thermal expansion coefficient discussed in this chapter. The criticality parameter in this simulation decreased by about 13% in response to a doubling of the horizontal resolution.

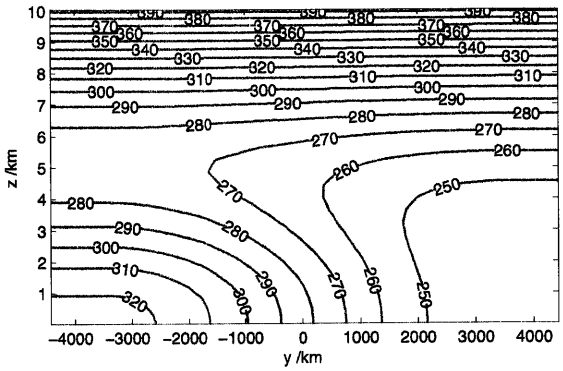

Figure 2-3: Equilibrium potential temperature for thermal restoring in K. (CI: 10K)

tial temperature section is shown in Fig. 2-3. It is characterized by a baroclinic zone with a width of 7000 km and an equilibrium meridional surface temperature difference of 80 K. The equilibrium potential temperature vertical gradient is everywhere convectively unstable near the surface, while a stable radiative-equilibrium stratification is prescribed at higher altitudes to mimic the radiative effects of ozone in the stratosphere. The relaxation time-scale is chosen as $\tau_{int} = 50$ days in the interior, but decreases to $\tau_s = 14$ days at the surface as

$$\tau(z)^{-1} = \tau_{int}^{-1} + (\tau_s^{-1} - \tau_{int}^{-1})\mathrm{e}^{-(z/h_s)^2}\,, \tag{2.22}$$

with an e-folding scale $h_s = 400$m.

All simulations are spun up until a quasi-steady state is reached and statistics are calculated as an average over at least 400 days after the equilibration is reached.

2.4.2 Results

We ran 8 simulations with thermal expansion coefficients varying from $\alpha = 1.6 \times 10^{-4}\mathrm{K}^{-1}$ to $\alpha = 1.44 \times 10^{-2}\mathrm{K}^{-1}$, thus spanning almost two orders of magnitudes in α and one order of magnitude in deformation radii. α is varied by a factor of two between all "neighboring" simulations, except for the last simulation with $\alpha = 1.6 \times 10^{-4}\mathrm{K}^{-1}$, a value 30% smaller than the previous to last run with $\alpha = 2.25 \times 10^{-4}\mathrm{K}^{-1}$. Any

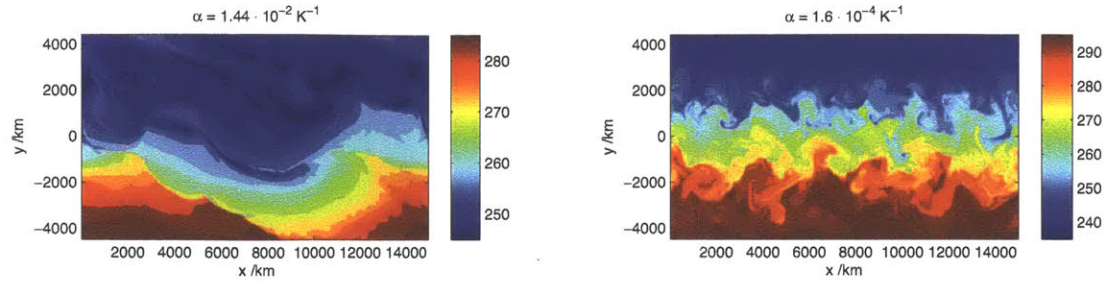

Figure 2-4: Snapshots of surface potential temperature (in K) for the simulations with $\alpha = 1.44 \times 10^{-2}K^{-1}$ (left) and with $\alpha = 1.6 \times 10^{-4}K^{-1}$ (right)

further reduction of α would cause the deformation scale to be under-resolved in the model. Notice also, that for the Boussinesq equations to be an accurate description of a physical fluid we need density variations to be small, such that $|\rho - \rho_0|/\rho_0 = \alpha(\theta - \theta_0) << 1$, a constraint that determined the upper bound for the thermal expansion coefficient α.

Fig. 2-4 shows surface temperature snapshots from the simulations with the smallest and largest thermal expansion coefficients, after the initial equilibration period. Both snapshots show turbulent behavior, though arguably more wave-like in the large α simulation. Also evident is a reduction of the typical eddy scale, which is similar to the domain scale for the largest α but significantly smaller for the smallest α.

The equilibrated time- and zonal-mean states of four representative simulations with $\alpha = 2.25 \times 10^{-4}\mathrm{K}^{-1}$, $\alpha = 9.0 \times 10^{-4}\mathrm{K}^{-1}$, $\alpha = 3.6 \times 10^{-3}\mathrm{K}^{-1}$ and $\alpha = 1.44 \times 10^{-2}\mathrm{K}^{-1}$ are shown in Fig. 2-5. For $\alpha \geq 3.6 \times 10^{-3}\mathrm{K}^{-1}$, we find that isentropes have moderate slopes, such that isentropes leaving the surface close to the southern end of the domain reach the tropopause close to the northern boundary. The baroclinic eddy kinetic energy is large over a major part of the domain and the zonal winds, which have a large barotropic component, change from westerlies in the southern part of the domain to easterlies in the north, thus implying a southward eddy flux of zonal momentum. Simulations with $\alpha \leq 9 \times 10^{-4}\mathrm{K}^{-1}$, on the other hand show at least one pronounced westerly jet in the interior domain, co-located with a maximum in EKE. Analysis of the temporal evolution of the jets (not shown), reveals that they

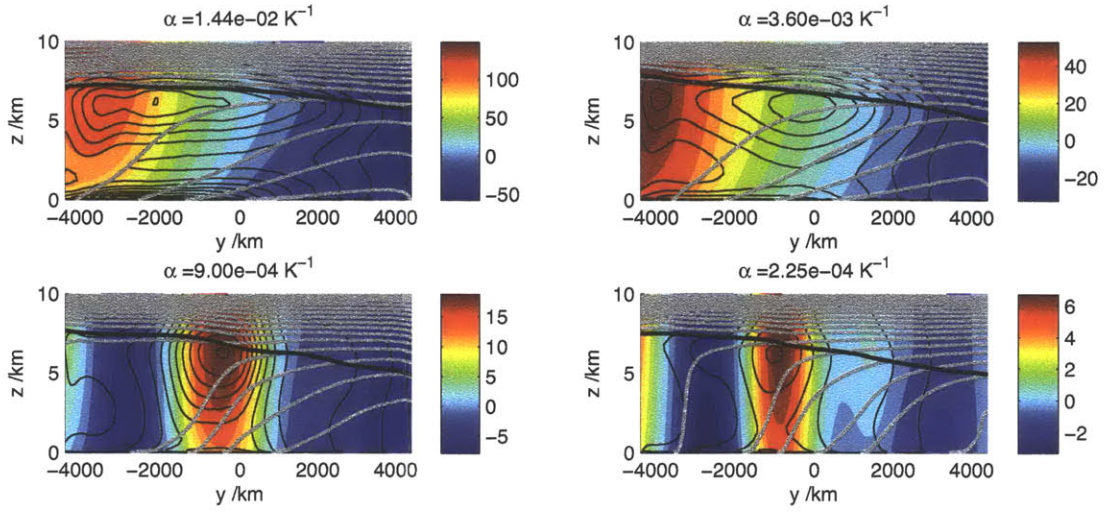

Figure 2-5: Time- and zonal-mean fields of potential temperature (thick grey lines), EKE (thin black lines), zonal wind (shading - in m/s) and the tropopause height, defined as the height at which $\frac{d\theta}{dz} = 10^{-2}Km^{-1}$ (thick black line), for simulations with varying thermal expansion coefficients α (see graph titles). The contour interval for isentropes is 10K. Contour intervals for EKE are, from top left to bottom right: 40 m^2s^{-2}, 20 m^2s^{-2}, 10 m^2s^{-2}, 3 m^2s^{-2}.

are largely stationary with only weak meandering. The time-mean plots in Fig. 2-5 are therefore qualitatively similar to the structure at any instance. The EKE, as well as the strength and the width of the jets, gets smaller as α is reduced. The reduction of kinetic energy is expected because the available potential energy in the equilibrium state decreases with α as $APE \sim \langle b''^2 \rangle H / \langle b_z \rangle \sim g\alpha \langle \theta''^2 \rangle H / \langle \theta_z \rangle$, where $\langle\,\rangle$ denotes a domain-wide horizontal average and $(\,)''$ denotes deviations from that average.

A prominent steepening of the isentropes over the troposphere is observed for small thermal expansion coefficients, $\alpha \leq 9 \times 10^{-4}\mathrm{K}^{-1}$, a clear indication of changes in the criticality. This is confirmed if we compute the criticality parameter as

$$\xi \equiv \frac{f\partial_y \overline{\theta}}{\beta \Delta_V \overline{\theta}}, \tag{2.23}$$

where $\Delta_V \overline{\theta} \equiv \overline{\theta}(H_t) - \theta_s$ denotes a bulk stability based on the potential temperature difference between the tropopause (here defined as the height at which $\frac{d\theta}{dz} =$

$10^{-2}Km^{-1}$) and the surface[5]. The horizontal temperature gradient $\partial_y\overline{\theta}$ in (2.23) is evaluated as an average over the lower half of the troposphere. Definition (2.23) has the advantage that it is not sensitive to the choice of a particular level at which we evaluate the isentropic slope. The results presented here, however, do not qualitatively depend on the exact definition used for the criticality parameter.

Fig. 2-6 shows the criticality parameter calculated as an average over the baroclinic zone between y=-3500km and y=3500km, and locally at the latitude of the maximum EKE. The domain averaged criticality parameter seems to approach a value close to 1 for large thermal expansion coefficients, but increases steadily for values smaller than the atmosphere-like expansion coefficient $\alpha_A = 3.6 \times 10^{-3}\mathrm{K}^{-1}$. The criticality parameter at the latitude of maximum EKE also increases as α is decreased, but shows a much more irregular behavior with a large jump in ξ between the simulations with $\alpha = 1.8 \times 10^{-3}\mathrm{K}^{-1}$ and $\alpha = 9 \times 10^{-4}\mathrm{K}^{-1}$. Comparison with Fig. 2-5 shows that this jump coincides with the emergence of an interior westerly jet which is co-located with the maximum EKE.

Held and Larichev (1996) argue that the criticality parameter ξ can be related to the ratio between the deformation scale, where EKE is produced by baroclinic instability, and the Rhines scale, where a possible up-scale energy transfer is halted. In a marginally critical state the two scales ought therefore to be similar, resulting in no significant up-scale energy transfer. We calculated the deformation scale according to

$$L_d = \frac{2}{f}\int_0^{H_t} (\partial_z \overline{b})^{1/2} dz \tag{2.24}$$

(which is consistent with the WKB approximation for the first vertical eigenmode), and the Rhines scale as

$$L_\beta = 2\pi \frac{EKE_T^{1/4}}{\beta^{1/2}}, \tag{2.25}$$

where EKE_T denotes the barotropic EKE. Fig. 2-7 shows the domain averaged deformation and Rhines scales for all simulations. Consistent with what we found for

[5]Isentropes here tend to flatten out in the Ekman layer in our simulations. Hence we use the model temperature above this Ekman layer, at a height of about 300m, as the "surface" temperature.

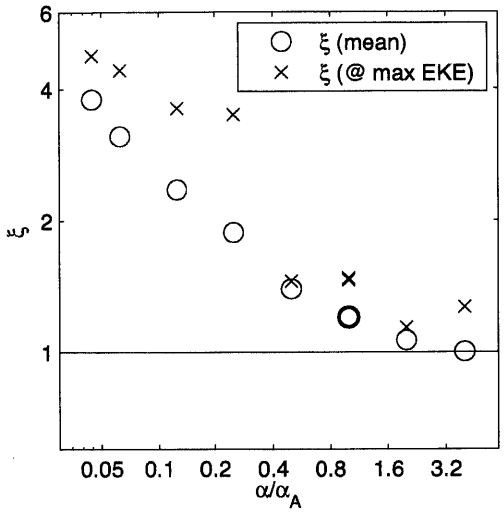

Figure 2-6: Supercriticality ξ averaged over the domain between y=-3500km and y=3500km (circles) and at the latitude of maximum EKE (crosses), as a function of the thermal expansion coefficient α normalized by the atmosphere like value of $\alpha_A = 3.6 \times 10^{-3}$ K^{-1}. The bold markers denote the simulation with an atmosphere-like thermal expansion coefficient.

ξ, the two scales are similar only for the experiments with the largest values of α. For smaller values of α, the deformation scale decreases much more rapidly than the Rhines scale.

The argument above assumed that (1) baroclinic instability produces EKE near the deformation scale and (2) energy is then transferred up to the Rhines scale. To test both assumptions we (1) performed a linear instability analysis and (2) calculated the eddy scale from the barotropic eddy kinetic energy spectrum.

Scales of baroclinic instability are calculated as in Smith (2007), based on the meridional planetary QGPV gradient, averaged over the domain between $y = -3500$km and $y = 3500$km. For all simulations the fastest growth rates are found for a deep tropospheric eigenmode with a wavelength close to the deformation scale calculated according to (2.24), as shown in Fig. 2-7.

The dominant eddy scales are estimated from the barotropic eddy kinetic energy spectra, for the same region, using a Hanning window in the meridional direction to avoid Gibbs phenomena due to non-periodic data. The eddy scale was then calculated

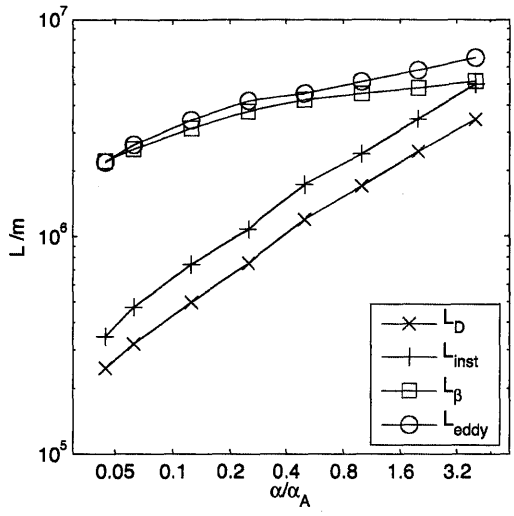

Figure 2-7: Deformation scale (crosses), Rhines scale (squares), the scale of the fastest growing wave (plusses) and the barotropic eddy scale (circles), as a function of the normalized thermal expansion coefficient α/α_A. All scales are based on averages over the domain between y=-3500km and y=3500km. See text for details.

as the inverse centroid of the barotropic EKE spectrum as proposed by Schneider and Liu (2009)

$$L_e = 2\pi \frac{\int (k^2+l^2)^{-1/2} E(k,l) dk dl}{\int E(k,l) dk dl}, \tag{2.26}$$

where $E(k,l)$ is the energy density as a function of the zonal and meridional wavenumbers. We find that the barotropic eddy scale is well approximated by the Rhines scale (Fig. 2-7). The results therefore suggest that, as the thermal expansion coefficient is reduced, eddies become ineffective in keeping the mean state at a criticality close to one, and undergo an up-scale energy transfer from the instability scale to the Rhines scale. This is confirmed by a detailed analysis of the spectral EKE budget presented in Appendix D.

To compare the numerical results to the theory discussed earlier, and in particular to the prediction of Eq.(2.17), we need estimates for the isentropic mass transport Ψ_Q and the eddy diffusivity D. We calculated the total isentropic mass transport by remapping the flow field into isentropic coordinates and integrating up to the

buoyancy b_i at which the mass transport $\overline{h_b v}$ changes sign

$$\Psi_Q \equiv -\int_{b_{min}}^{b_i} \overline{h_b v}(y, b')db' . \tag{2.27}$$

We then calculated the mean isentropic mass transport over the baroclinic zone between $y = -3500$km and $y = 3500$km for all simulations. The eddy diffusivity is calculated from the near-surface[6] flux-gradient relationship for buoyancy as $D = -\frac{\overline{v'b'}^s}{\partial_y \bar{b}^s}$. Again mean values over the baroclinic zone between $y = -3500$km and $y = 3500$km are presented for all simulations.

The resulting mean overturning mass transport and eddy diffusivity estimates are shown in Fig. 2-8. While both the isentropic mass transport and the eddy diffusivity decrease as the thermal expansion coefficient is reduced, the eddy diffusivity decreases much more rapidly: the eddy diffusivity varies by a factor of about 15 over the range of simulations, while the isentropic mass transport changes only by about a factor of 3. In agreement with Eq. (2.15), this results in a steepening of the isentropes. Qualitatively, we can therefore understand the steepening of the isentropes as resulting from a reduction in the eddy diffusivity, which in turn is expected from the reduction of the deformation scale and baroclinicity with the thermal expansion coefficient α.

The steepening of the isentropes here translates directly to an increase in the criticality parameter, since the latter varies much more than the height of the tropopause. Noting that the "planetary scale" β/f is also constant in the simulations shown here, the scaling for the criticality parameter is here dominated by changes in the isentropic slope, i.e. ξ is directly proportional Ψ_Q/D. As shown in Fig. 2-9 this is confirmed well by the numerical simulations.

[6]Due to the use of no-slip boundary conditions in the simulations discussed here, the actual eddy flux vanishes at the surface, we therefore evaluated the flux-gradient relationship to calculate the eddy diffusivity above the surface Ekman layer at 300m height. Note that the theoretical predictions derived in section 2.3 assume a down-gradient flux for the geostrophic eddy flux of surface buoyancy $\overline{v_g' b'}^s$, which is best approximated by the flux just above the Ekman layer.

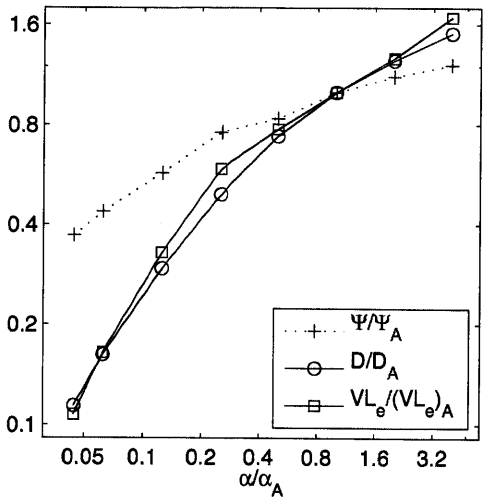

Figure 2-8: Isentropic mass transport Ψ (plusses), and eddy diffusivity D estimated from a near-surface buoyancy flux-gradient relationship (circles) and from the barotropic eddy-velocity and -scale (squares), for varying thermal expansion coefficient. All quantities are normalized by their respective value in the simulations with atmospheric thermal expansion coefficient $\alpha_A = 3.6 \times 10^{-3}\mathrm{K}^{-1}$ and averaged over the domain between y=-3500km and y=3500km (see text).

2.4.3 Deriving a Scaling Relation for the Criticality Parameter

The scaling law for ξ can be turned into a predictive theory for the mean state, if Ψ_Q and D are expressed in terms of external parameters and the mean state itself. Mixing length arguments (e.g. Pavan and Held, 1996) suggest that the eddy diffusivity can be approximated by the product of the eddy scale and the barotropic eddy velocity, that is

$$D \sim L_e EKE_t^{1/2} \tag{2.28}$$

This scaling is shown to work in Fig. 2-8, and the eddy scale is well approximated by the Rhines scale in our simulations $L_e \approx L_\beta$ (Fig. 2-7). If we use the scaling $L_\beta \sim \xi L_d$ proposed by Held and Larichev (1996), for fully developed QG turbulence, we have

$$D \sim L_\beta EKE_t^{1/2} \sim L_\beta^3 \beta \sim \xi^3 \beta L_d^3 . \tag{2.29}$$

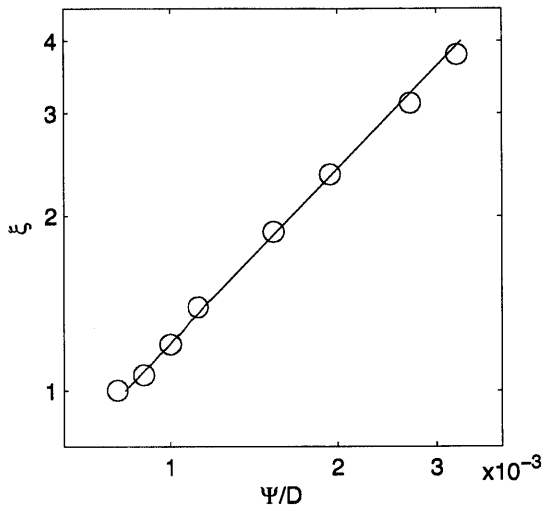

Figure 2-9: Supercriticality ξ against the ratio of the isentropic mass transport and the eddy diffusivity (Ψ/D). The black line denotes a slope of 1. All quantities are averaged over the baroclinic zone between y=-3500km and y=3500km (see text).

While the first relation in Eq. (2.29) holds over the whole range of simulations, some caution must be used in applying Held and Larichev (1996)'s scaling relation, because it is formally valid only for $L_\beta \gg L_d$, i.e. for strongly supercritical simulations. Fig. 2-10 shows that, despite the limited scale-separation, the simulations broadly support the scaling in Eq. (2.29) as long as $\alpha < \alpha_A$ and $\xi > 1$. The scaling relation, however, breaks down for the marginally critical simulations with $\alpha \gtrsim \alpha_A$, which show much weaker eddy diffusivities than predicted by Eq. (2.29). A scaling for the isentropic mass transport Ψ_Q was derived in section 2.3.2.3.3, Eq. (2.13), as $\Psi_Q \sim \frac{\Delta \bar{b}_{Eq} l}{\partial_z \bar{b} \tau_r}$, where $\Delta \bar{b}_{Eq}$ denotes the variation of the equilibrium buoyancy along the isentrope b_i, and l denotes the distance between the latitudes where the isentrope b_i intersects with the surface and the tropopause. Using that $l \sim \frac{\bar{b}_z}{\bar{b}_y} H_t$ and $b = g\alpha(\theta - \theta_0)$ we find that

$$\Psi_Q \sim \frac{\Delta \bar{b}_{Eq} H_t}{\partial_y \bar{b} \tau_r} \sim \frac{\Delta \bar{\theta}_{Eq} H_t}{\partial_y \bar{\theta} \tau_r}. \tag{2.30}$$

The scaling for the mass transport (2.30) has no explicit dependence on the thermal expansion coefficient, which is here varied much more strongly than any other mean-

state variable. This explains why changes in the total isentropic mass transport are in general much smaller than changes in the eddy diffusivity, which does instead depend explicitly on the thermal expansion coefficient via its dependence on the deformation scale as per. Eq. (2.29). The weak variations in Ψ_Q are dominated by variations in $\partial_y\overline{\theta}$ and $\Delta\overline{\theta}_{Eq}$. Fig. 2-10 shows the scaling (2.30), but considering only variations in Ψ_Q due to changes in $\partial_y\overline{\theta}$. This captures the variations in Ψ_Q well for simulations with $\alpha \geq 9 \times 10^{-4}\mathrm{K}^{-1}$, for which the isentropic slope changes little. The simulations with smaller α, however, show significantly weaker overturning circulations, which is due to the reduction in $\Delta\overline{\theta}_{Eq}$ as the isentropes steepen (see Fig. 2-3). As we will show later, variations in $\Delta\overline{\theta}_{Eq}$ are, however, negligible in the final scaling for the criticality parameter, and can be ignored for present purposes. Notice also that the scaling (2.30) further assumed that the diabatic forcing is given by the radiative relaxation. An additional diabatic term arises from the convective adjustment scheme. This term is generally small compared to the heating associated with the relaxation scheme in our simulations.

We can now derive a scaling for the criticality parameter ξ in the supercritical regime in terms of mean state variables. Substituting (2.30) and (2.29) back into (2.17) and rearranging terms yields

$$\xi \sim \left(\frac{1}{\tau_r f}\frac{\Delta\overline{\theta}_{Eq}}{a\partial_y\overline{\theta}}\right)^{1/4}\left(\frac{L_d}{a}\right)^{-3/4} \tag{2.31}$$

where $a = \frac{f}{\beta}$ denotes the dynamical planetary scale which, for our simulations (as well as for earth's atmosphere) is comparable to the width of the baroclinic zone. Eq. (2.31) predicts that variations in the criticality are dominated by variations in the deformation scale L_d, which decreases strongly as α is decreased. As confirmed by Fig. 2-11, we therefore find that the criticality parameter in the supercritical limit is to a good approximation proportional to the -3/4th power of the deformation scale. Since the reduction in the deformation scale is dominated by the reduction in α, this qualitatively explains the observed increase in the criticality parameter as α is reduced. Since $\frac{\Delta\overline{\theta}_{Eq}}{a\partial_y\overline{\theta}} \sim O(1)$ and $\tau_r f \sim O(10^2)$, we may further note, that the

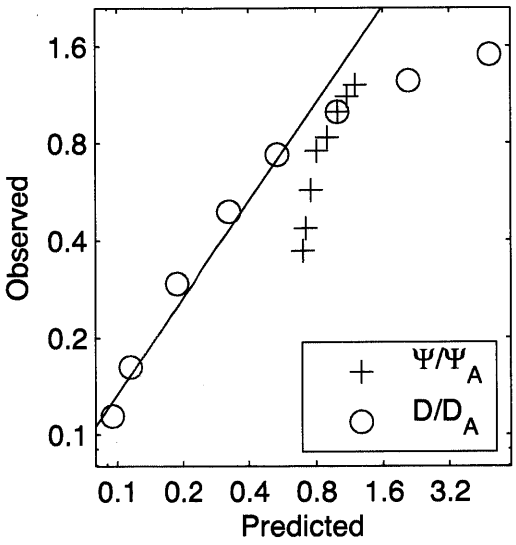

Figure 2-10: Eddy diffusivity D against the scaling in Eq. (2.29) (circles), and Isentropic mass transport Ψ, against the inverse horizontal temperature gradient $(\partial_y \theta)^{-1}$ (see Eq. 2.30). All quantities are averaged over the baroclinic zone between y=-3500km and y=3500km and normalized by their respective values in the atmosphere-like simulation with $\alpha = 3.6 \times 10^{-3}\mathrm{K}^{-1}$. The black line denotes a slope of 1.

pre-factor in Eq. (2.31) is on the order of $\left(\frac{1}{\tau_r f}\frac{\Delta\bar{\theta}_{Eq}}{a\partial_y\theta}\right)^{1/4} \sim 0.2 - 0.4$. Eq. (2.31) thus suggests that supercritical states may only be expected if $L_d/a \ll 1$, which is in general agreement with the results shown in Fig. 2-11.

The scaling (2.31) breaks down for simulations in which L_d/a becomes larger than about 0.2 and the criticality approaches one. The dependence of the criticality parameter ξ on the deformation scale then flattens out and seems to asymptote towards a constant value close to one. This is in qualitative agreement with results from previous studies (e.g. Schneider, 2004; Schneider and Walker, 2006), who find that the criticality parameter of diabatically forced systems stays close to one over a wide range of parameters and forcings. The flattening out of the scaling relation between ξ and L_d/a is here associated dominantly with the breakdown of the diffusive scaling law (2.29), which is not expected to hold in the marginal critical limit and predicts much larger eddy diffusivities than observed in these simulations.

The saturation of the criticality parameter to one, for simulations where the Held

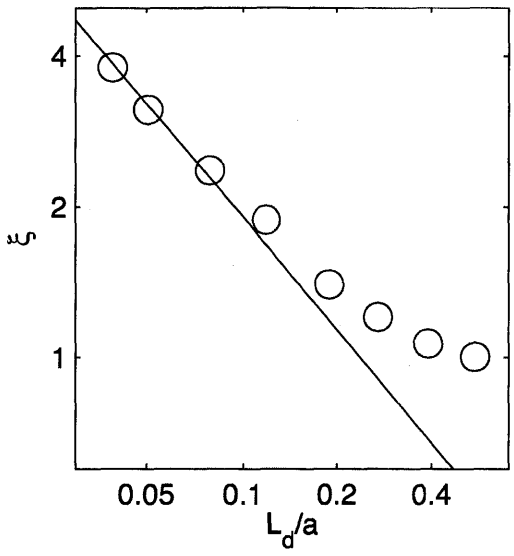

Figure 2-11: Supercriticality ξ against the normalized deformation scale L_d/a (see Eq. 2.31). The black line denotes a slope of -3/4 (Note that the axes are logarithmic). All quantities are averaged over the baroclinic zone between y=-3500km and y=3500km.

and Larichev (1996) scaling relation breaks down, might seem to support traditional ideas of baroclinic adjustment. These predict that eddy activity will decrease rapidly once the criticality parameter gets close to one, because the system becomes neutral to baroclinic instability, or unstable modes become shallow (e.g. Zurita-Gotor and Lindzen, 2007), and references therein). Whether this reasoning is appropriate for the simulations presented here is, however, not clear. Preliminary simulations suggest that the breakdown of the Held and Larichev (1996) scaling for the eddy diffusivity is here at least partially associated with an increasing role of bottom friction in this limit, which might be via a direct influence of friction on the eddies themselves or indirectly via the modification of the mean flow and a "barotropic governor" mechanism (James and Gray, 1986). The important role that bottom friction can play in controlling the eddy diffusivity has recently been discussed by Thompson and Young (2007). When and how exactly the transition to marginally critical states occurs, however, is beyond the scope of this study but will be the subject of future work.

It should also be noted that the eddy diffusivity scaling in (2.29) relies on the

assumption that the eddy scale is proportional to the Rhines scale. However, our qualitative argument that the criticality increases for small α holds as long as the eddy diffusivity decreases as the thermal expansion coefficient is decreased. In the real ocean and atmosphere, where other processes (such as bottom friction) can prevent eddies from growing much beyond the deformation scale, Green (1970), Stone (1972) and many other authors since have proposed different scalings for the diffusivity. Yet, all these scaling share the property that the eddy diffusivity decreases as α is reduced.

Finally one might ask whether there is a limit to the validity of the proposed scalings in the supercritical limit. One limitation comes from the assumption, implied in the scalings above, that the heat transport is dominated by large scale eddies as opposed to convection, and that the stratification is dominantly statically stable. While this is true for all simulations discussed here, we do observe an increasing role of convection as the thermal expansion coefficient is reduced and the criticality increases, suggesting that there might be a limit where convective transports will start to dominate. Whether such a limit is universal or specific to a certain set of parameters and forcing, however, is an open question.

2.5 Summary and Discussion

We showed that states with marginally critical as well as supercritical states with much steeper isentropic slopes can be obtained in a diabatically forced system, if the thermal expansion coefficient is varied. Equilibrium states with criticality parameters close to one ($\xi \approx 1$) are found for large thermal expansion coefficients, which are associated with deformation scales on the same order as the planetary scale. Supercritical mean-states ($\xi > 1$) are obtained for small thermal expansion coefficients, which are associated with deformation scales much smaller than the planetary scale. As the thermal expansion coefficient is reduced, deformation-scale eddies become less effective at stabilizing the mean-state, which causes an increase in the isentropic slope and thus in the criticality parameter. The higher criticality parameter allows for a more turbulent state with an up-scale energy transfer from the scale of the instabil-

ity to the Rhines scale due to nonlinear eddy-eddy interactions. In summary, in the marginally critical limit we find weakly nonlinear, deformation-scale eddies that are efficient in modifying the mean state. For supercritical states, instead, eddies are less efficient in modifying the mean state, but nonlinear eddy-eddy interactions become more important.

The results found in the limit of large thermal expansion coefficients resemble those observed in the real atmosphere, which is close to marginal criticality and dominated by weakly nonlinear eddies close to the deformation scale (e.g. O'Gorman and Schneider, 2007, and references therein). The results found in the limit of small thermal expansion coefficients, on the other hand, display some of the characteristics found in the Southern Ocean, which is not in a state close to marginal criticality and where nonlinear eddy-eddy interactions are believed to be important in setting the observed eddy scale (e.g. Scott and Wang, 2005). One difference, however, is that in the Southern Ocean the scale of the eddies is not generally set by the Rhines scale. This is likely because the up-scale energy flux is arrested earlier by bottom drag and or topography.

The variations in the criticality parameter over our simulations are dominated by changes in the isentropic slope, which in turn are shown to be well captured by the scaling

$$s \sim \frac{\Psi_Q}{D}, \tag{2.32}$$

where Ψ_Q is the eddy-driven diabatic overturning circulation and D is the eddy diffusivity. We showed that the diabatic overturning is to first order independent of the thermal expansion coefficient. The scaling (2.32) therefore implies that the increase in criticality parameter for small expansion coefficients can be understood as stemming from a decrease in the eddy diffusivity as the deformation scale is reduced. In the limit of small thermal expansion coefficients, in which deformation scales are much smaller than the planetary scale, we can employ scalings for Ψ_Q and D to show that the criticality parameter is to leading order proportional to the -3/4 power of the deformation scale. In the limit of large thermal expansion coefficients (and deformation

scales on the same order as the planetary scale), the criticality parameter asymptotes to a constant value close to unity. This latter limit is in agreement with previous studies which suggested that the atmosphere maintains a criticality parameter close to unity over a wide range of forcings and parameters, though the exact mechanisms responsible for this result remain unclear and will be subject of a future study.

It is worth noting, that our results imply that supercritical, more strongly turbulent states are found in the limit of weaker buoyancy contrast to which the system is restored (since $\Delta b = g\alpha\Delta\theta$). These states are also characterized by an overall weaker EKE. The non-dimensional ratio of the EKE to the square of the mean baroclinic shear does, however, increase with the criticality, as predicted by QG studies (Held and Larichev, 1996).

Our results are in qualitative agreement with recent work by Zurita-Gotor and Vallis (2011), who also find that the criticality parameter exceeds one in the limit of weak equilibrium horizontal temperature gradients, if the depth of the tropopause is constrained by the radiative restoring profile, as in our simulations. Our results are also consistent with results shown in Schneider and Walker (2006), if one compares appropriate sets of simulations. In most of the simulations discussed in Schneider and Walker (2006), the convective adjustment scheme restores to a finite stratification to mimic the stabilizing effects of moisture. In these simulations the adjustment scheme becomes active in the limit of small buoyancy gradients, and prevents the system from reaching supercritical mean states – the system becomes sub-critical, once the stratification is set by the convection scheme. However, the authors also perform a series of simulations in which convective adjustment restores to a convectively neutral profile, as in our simulations. In agreement with our results, these simulations suggest equilibration to supercritical mean states in the limit of small buoyancy gradients.

An alternative perspective to equilibration of jets in the ocean and atmosphere is provided by the theory of transient stable amplification and adjustment to a generalized marginally stable state (Farrell and Ioannou, 2009, and references therein). The theory has so far been derived using the QG approximation and prescribes the vertical stratification. This is a major limit for applying the theory to our work whose focus

is on the changes in stratification and deformation radius. Moreover, the eddy-eddy fluxes, which are crucial in setting the large-scale adjustment, are not predicted by the theory. A test of the parameterizations used to close the problem, and a generalization of these ideas to primitive equation systems would be a welcome contribution to the discussion.

APPENDIX A

Deriving a Scaling for the Criticality in a Quasi-Geostrophic Framework

The scalings for the overturning circulation, derived in Section 2.3 for the more general primitive equations, can be recovered in a qualitative way using the continuously stratified QG equations. We will first discuss dynamical constraints on the zonal momentum balance. In order to close the momentum budget we will then need a closure for the eddy fluxes, and a constraint for the meridional overturning mass transport. Armed with these two closures, we will be able to relate the turbulently adjusted mean state to the applied forcing. For simplicity all arguments and simulations presented here will assume a QG Boussinesq fluid in a flat-bottomed re-entrant channel configuration.

2.A.1 Dynamical constraint: the zonal momentum balance

We start from the zonal momentum balance, which in the QG transformed eulerian mean (TEM) formulation can be written as

$$-f_0\overline{v}^* = \overline{v'q'}\,, \tag{2.A1}$$

where $\overline{v}^* = -\partial_z\psi^*$ denotes the residual meridional velocity, with the residual streamfunction $\psi^* \equiv -\int_0^z \overline{v}dz' + \frac{\overline{v'b'}}{\partial_z b_0}$ and the reference buoyancy profile b_0. The QG PV is $q = f_0 + \beta y + \zeta_g + f_0\partial_z\frac{b}{\partial_z b_0}$, with ζ_g the geostrophic relative vorticity. Frictional forces have been ignored, because they are weak in the simulations used in this study. Zonal averages are here taken at constant z. We can integrate (2.A1) from the surface (for

simplicity here again assumed to be flat at $z = 0$) to some height z to get

$$f_0\psi^*(z) = \int_0^z \overline{v'q'}dz' + f_0\frac{\overline{v'b'}}{\partial_z b_0}(0)\,, \tag{2.A2}$$

where we used that $\psi^*(0) = \frac{\overline{v'b'}}{\partial_z b_0}(0)$.

Assuming a diffusive closure for the eddy fluxes of PV and surface buoyancy and ignoring the contribution of relative vorticity to the PV, we find

$$\psi^*(z) = -\int_0^z D\left(\frac{\beta}{f_0} + \frac{\partial_{yz}\bar{b}}{\partial_z b_0}\right)dz' - D\frac{\partial_y \bar{b}}{\partial_z b_0}(0)\,. \tag{2.A3}$$

If z is chosen close to the surface so that we can assume that the eddy diffusivity is approximately constant over the regarded layer, we get

$$\psi^*(z) = D\left(s(z) - \frac{\beta}{f_0}z\right) \tag{2.A4}$$

where $s = -\frac{\partial_y \bar{b}}{\partial_z b_0}$. Eq. (2.A4) is the QG analog of Eq. (2.8) and shows that the residual transport below any level z is proportional to the eddy diffusivity times the effective PV gradient vertically integrated below z. The latter is given by the sum of the vertical integral of the planetary vorticity gradient and the isentropic slope at the top of the layer, and thus bears close resemblance to the PV gradient in the bottom layer of a layered QG model.

If we choose z to be a small height just above the surface, the β-term in (2.A4) can be neglected and we obtain a scaling for the isentropic slope near the surface,

$$s = \frac{\psi^*}{D}\,. \tag{2.A5}$$

Substituting the expression (2.A5) for the slope into the definition of the supercriticality, we find,

$$\xi \sim \frac{f}{\beta H_t}\frac{\psi^*}{D}\,, \tag{2.A6}$$

which is the QG analog of Eq. (2.17). For any given planet ($\frac{f}{\beta}$ fixed), the supercriti-

cality ξ thus depends on the relation between the residual overturning ψ^* (which, as shown in the following section, can be related directly to the diabatic forcing), the eddy diffusivity, and the depth of the troposphere.

2.A.2 Thermodynamic constraint: isentropic mass budget

Similar to our discussion in section 2.3b, we want to relate the residual overturning streamfunction ψ^* to the diabatic forcing using the thermodynamic equation

$$\partial_t \overline{b} = -\partial_y \psi^* \partial_z b_0 + \overline{Q}\,, \tag{2.A7}$$

where $Q = \frac{db}{dt}$ is the diabatic forcing. In steady state, we can integrate (2.A7) horizontally, to get

$$\psi^* = \int_{y_{min}}^{y} \frac{\overline{Q}}{\partial_z b_0} dy' = -\int_{y}^{y_{max}} \frac{\overline{Q}}{\partial_z b_0} dy'\,, \tag{2.A8}$$

where y_{min} and y_{max} denote the southern and northern boundaries, respectively, where ψ^* is assumed to vanish. Condition (2.A8) is the QG analog of Eq. (2.12); however due to the assumption of horizontal isentropes, implicit in the QG equations, the along-isentrope integration in (2.12) becomes a horizontal integration over the entire width of the domain

We can now derive a scaling for the residual overturning streamfunction ψ^* based on Eq. (2.A8). We will assume that the diabatic forcing can be represented by a radiative relaxation, that is $Q = -\frac{b-b_{eq}}{\tau_r}$ with a restoring time scale τ_r and an equilibrium buoyancy profile b_{eq}. This is the form of radiative forcing used in our simulations and in many idealized studies of the atmosphere (e.g. Held and Suarez, 1994; Schneider, 2004). Using Eq. (2.A8) we then find

$$\psi^* \sim \frac{QL}{\partial_z b_0} \sim \frac{(b - b_{eq})L}{\partial_z b_0 \tau_r}\,. \tag{2.A9}$$

Here L denotes the width of the domain, which naturally replaces the length of the isentrope (l) appearing in the isentropic coordinate scaling, consistent with the assumption that the isentropic slope is weak compared to the aspect ratio, implied in

the QG approximation. Eq. (2.A9) is the QG analog to the scaling in Eq. (2.13). In the main paper, we further relate the thermal disequilibrium $(b - b_{eq})$ to the variation of the equilibrium buoyancy along an isentrope, Δb_{eq}. This argument cannot readily be transferred to the QG framework. However, we will discuss in chapter 4 how the radiative disequilibrium can instead be related to the vertical stratification, if we use the full (primitive equation) thermodynamic budget in physical coordinates.

APPENDIX B

Implications of Vertical Structure in the Eddy Diffusivity

If we are to allow for the eddy diffusivity to have some vertical structure, the closure relationships for the eddy fluxes become

$$\overline{\hat{v}\hat{P}}^{*} = -D(b)\partial_y \overline{P}^{*} \,, \quad \overline{v'_{gs} b'_s}^{s} = -D_s \partial_y \overline{b_s}^{s} \,, \tag{2.B1}$$

where $D_s = \overline{D(b)}^{s}$. Note, that D can of course also have a y dependence, which is not made explicit here since all relationships hold locally at any given y. Substituting these closures in the vertically integrated momentum budget in Eq. (2.6) yields,

$$\int_{b_{min}}^{b_i} \overline{h_b}\,\overline{v}^{*} db \approx \int_{b_{min}}^{b_i} D(b) \frac{\overline{h_b}\partial_y \overline{P}^{*}}{\overline{P}^{*}} db + \frac{f}{\overline{P}^{*}(\overline{b_s}^{s})} D_s \partial_y \overline{b_s}^{s} \,. \tag{2.B2}$$

Following the same steps used to derive Eq. (2.7), we can write the first term on the R.H.S. of (2.B2) as

$$\begin{aligned}
\int_{b_{min}}^{b_i} D(b) \frac{\overline{h_b}\partial_y \overline{P}^{*}}{\overline{P}^{*}} db &\approx \int_{b_{min}}^{b_i} D(b)(\overline{h_b}\frac{\beta}{f} - \partial_y \overline{h_b} + \frac{f}{\overline{P}^{*}}\partial_y \Pi) db \\
&= D_{SL} \int_{b_{min}}^{b_i} (\overline{h_b}\frac{\beta}{f} - \partial_y \overline{h_b}) db + \int_{b_{min}}^{b_i} D(b) \frac{f}{\overline{P}^{*}} \partial_y \Pi db \\
&\approx D_{SL} \left(\frac{\beta}{f} \overline{z}(b_i) - \partial_y \overline{z}(b_i) \right) - D_s \frac{f}{\overline{P}^{*}(\overline{b_s}^{s})} \partial_y \overline{b_s}^{s} \,,
\end{aligned} \tag{2.B3}$$

where we defined a bulk SL diffusivity,

$$D_{SL} \equiv \frac{\int_{b_{min}}^{b_i} D(b)(\overline{h_b}\frac{\beta}{f} - \partial_y \overline{h_b}) db}{\int_{b_{min}}^{b_i} (\overline{h_b}\frac{\beta}{f} - \partial_y \overline{h_b})} db \,. \tag{2.B4}$$

The weighting factor in the definition of the bulk SL eddy diffusivity can be written as $\overline{h_b}\frac{\beta}{f} - \partial_y\overline{h_b} = \overline{h_b}\frac{\beta}{f} - \overline{\mathcal{H}(b-b_s)\partial_{yb}z} + \overline{\delta(b-b_s)\partial_b z \partial_y b_s}$, and is generally dominated by the contribution of the (negative) surface buoyancy gradient over the SL (e.g Schneider, 2005). In practice D_{SL} can therefore be expected to be well approximated by to the surface diffusivity D_s.

APPENDIX C

A Scaling for the Diabatically Forced Overturning Ψ_Q

We here derive a scaling for the diabatically forced overturning Ψ_Q (Eq.2.11), which is set by the heating integrated along the lower part of an isentrope, which has to be balanced by a similar cooling above,

$$\Psi_Q \equiv \int_{y_s}^{y} \overline{hQ}(y', b_i)dy' \approx -\int_{y}^{y_t} \overline{hQ}(y', b_i)dy' . \tag{2.C1}$$

Here y_s and y_t denote the southern- and northernmost latitude at which the isentrope b_i is above the surface and below the tropopause, at any time and longitude (or alternatively the southern and northern boundaries of the domain). If, for simplicity, we assume that the stratification between the surface and the tropopause changes little along the isentrope b_i, then we can approximate (2.C1) as

$$\Psi_Q \approx \partial_z \overline{b}^{-1} \int_{y_s}^{y} \overline{Q}(y', b_i)dy' \approx -\partial_z \overline{b}^{-1} \int_{y}^{y_t} \overline{Q}(y', b_i)dy' , \tag{2.C2}$$

We now want to choose b_i such that it separates the regions of heating (below) and cooling (above), i.e. such that $Q(y', b_i) > 0$ for $y' < y$ and $Q(y', b_i) < 0$ for $y' > y$ (choosing b_i just above the SL generally fulfills this condition to a good approximation, since diabatic heating is usually confined to the SL while cooling is found above). We then find that

$$\Psi_Q \approx \frac{1}{2}\partial_z \overline{b}^{-1} \int_{y_s}^{y_t} |\overline{Q}(y', b_i)|dy' , \tag{2.C3}$$

Assuming a restoring condition such that $Q = -(b_i - b_{eq})/\tau_r$, where b_{eq} denotes the

radiative equilibrium buoyancy and τ_r the restoring timescale, we get

$$\Psi_Q \approx \frac{1}{2}\partial_z \bar{b}^{-1} \int_{y_s}^{y_t} \overline{\tau_r{}^{-1}|b_{Eq} - b_i|}dy' = \frac{1}{2}\partial_z \bar{b}^{-1} \int_{y_s}^{y_t} \overline{\tau_r^{-1}|b_{Eq} - \langle b_{Eq}\rangle|}dy' , \qquad (2.C4)$$

where $\langle \bar{b}_{Eq}\rangle \equiv \int_{y_s}^{y_t} \overline{\tau_r{}^{-1} b_{Eq}}dy \,/\, \int_{y_s}^{y_t} \overline{\tau_r^{-1}}dy$ is the weighted mean equilibrium buoyancy along the isentrope b_i, and we again used that the net heating over the isentrope b_i vanishes. We thus find that the residual overturning mass flux scales as

$$\Psi_Q \sim \frac{\Delta b_{Eq} l}{\partial_z \bar{b} \tau_r} \qquad (2.C5)$$

where Δb_{Eq} denotes the variation of the equilibrium buoyancy over the isentrope b_i, and l denotes the length of the isentrope between the surface and the tropopause.

APPENDIX D

The Spectral EKE Budget

We showed in Fig. 2-7 that the separation between the scale of the eddies (which scales with the Rhines scale) and the scale of the instability (which scales with the deformation scale) increases as the thermal expansion coefficient is reduced. This suggests that our simulations must display a substantial up-scale transfer of eddy kinetic energy from the scale of the instability to the Rhines scale for small α. To support this conclusion we compute the spectral eddy kinetic energy budget for the two simulations with the largest and smallest thermal expansion coefficients. We calculate the vertically integrated eddy kinetic energy budget in terms of horizontal wavenumbers. The calculation is analog to Koshyk and Hamilton (2001), except that, due to the cartesian geometry underlying our simulations, we use horizontal wavenumbers instead of spherical harmonics. We further separate the EKE and KE of the zonal mean flow, an important distinction for our purposes.

The spectral EKE budget can then be written as

$$\partial_t EKE_K \approx T_{EE} - T_{EM} + T_{PK} - D\,, \tag{2.D1}$$

where

$$EKE_K = \left\langle \int_0^H \frac{1}{2}\left(|u'_K|^2 + |v'_K|^2\right) dz \right\rangle \tag{2.D2}$$

denotes the EKE at the horizontal wavenumber $K = \sqrt{k^2 + l^2}$, with $\langle\rangle$ here denoting a time mean,

$$T_{EE} = \left\langle \int_0^H Re\left[-{u'_K}^*(\mathbf{u}' \cdot \nabla u')_K - {v'_K}^*(\mathbf{u}' \cdot \nabla v')_K\right] dz \right\rangle \tag{2.D3}$$

denotes the spectral eddy-eddy energy transfer,

$$T_{EM} = \left\langle \int_0^H Re\left[{u'_K}^* (\mathbf{u}' \cdot \nabla \overline{u})_K + {v'_K}^* (\mathbf{u}' \cdot \nabla \overline{v})_K + {u'_K}^* (\overline{\mathbf{u}} \cdot \nabla u')_K + {v'_K}^* (\overline{\mathbf{u}} \cdot \nabla v')_K \right] dz \right\rangle \tag{2.D4}$$

denotes the spectral kinetic energy transfer from the eddies to the mean flow,

$$T_{PK} = \left\langle \int_0^H Re\left({w'_K}^* b'_K \right) dz \right\rangle \tag{2.D5}$$

denotes the energy transfer from eddy available potential energy (APE) to eddy kinetic energy, and

$$D = \left\langle \int_0^H Re\left[{u'_K}^* \nu \partial_{zz} u'_K + {v'_K}^* \nu \partial_{zz} v'_K \right] dz \right\rangle + filter \tag{2.D6}$$

denotes dissipation by the explicit vertical viscosity ν and by the numerical filter (Shapiro, 1970). Note that there is some contribution to the energy budget at any given wavenumber by the Coriolis term, because f is not constant with latitude. This term is, however, small in our simulations and is herein ignored.

Fig. 2-12 shows all the terms in the spectral EKE budget for the two simulations with the largest and smallest thermal expansion coefficients $\alpha = 1.44 \times 10^{-2}\mathrm{K}^{-1}$ and $\alpha = 1.6 \times 10^{-4}\mathrm{K}^{-1}$. In both experiments the transfer from eddy APE to EKE peaks at the scale of instability as calculated from the QG instability analysis and shown in Fig. 2-7. For the simulation with the largest thermal expansion coefficient $\alpha = 1.44 \times 10^{-2}\mathrm{K}^{-1}$, this instability scale coincides with the Rhines scale, and thereby with the dominant barotropic eddy scale. The EKE produced at the scale of the instability is therefore dominantly transferred into the mean flow or dissipated in eddies of similar scales. No significant up-scale eddy-eddy transfer is observed, though some energy is transferred to small scales where it is dissipated by the numerical filter. For the simulation with the smallest thermal expansion coefficient $\alpha = 1.6 \times 10^{-4}\mathrm{K}^{-1}$, the instability scale in significantly smaller (by about a factor of 6) than the Rhines scale, which in turn coincides with the dominant barotropic eddy scale. The EKE at this larger scale is maintained by an up-scale energy transfer from the scale of the

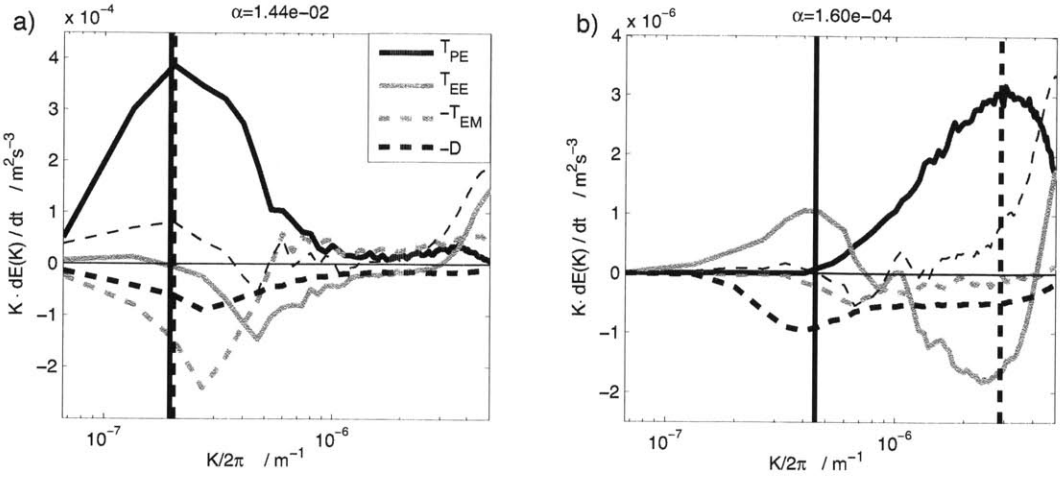

Figure 2-12: **a)** Spectral EKE budget for the simulation with $\alpha = 1.44 \times 10^{-2}\mathrm{K}^{-1}$: Eddy APE to EKE transfer (solid black), EKE transfer due to eddy-eddy interactions (solid grey), mean KE to EKE transfer (dashed grey), and the explicit part of the dissipation (dashed black). The kinetic energy transfer terms have been smoothed by a five-point running mean. The thin dashed black line denotes the residual and includes the dissipation due to the numerical filter, which becomes dominant near the grid-scale. Notice, that the residual, which (next to the numerical filter) arises due to limited statistics and inaccuracy in the calculation of the spectral transfer terms, is small compared to the leading order terms at all relevant wavenumbers away from the grid scale. The vertical black dashed and solid lines denote the Rhines scale and the scale of the instability, respectively, which are shown in figure 2-7 of the main paper. **b)** As (a), but for the simulation with $\alpha = 1.6 \times 10^{-4}\mathrm{K}^{-1}$.

instability to the Rhines scale. The transfer of kinetic energy from the eddies to the mean flow, plays a smaller role in this simulation.

The results presented here support the conclusion presented in the main paper that, while the simulations with large thermal expansion coefficients are marginally critical and do not exhibit a significant up-scale transfer of EKE, the simulations with the smallest thermal expansion coefficients show all aspects of a supercritical state, including a significant up-scale energy transfer which is responsible for setting the scale of the barotropic eddies. The up-scale energy transfer here spans about a factor of six in wavenumber space, which is of similar order though likely somewhat larger than found in the Southern Ocean (e.g Tulloch et al., 2011). Notice that, even though up-scale energy fluxes due to nonlinear eddy-eddy interactions are important

for the dynamics in these states, we do not find a clean "inertial range" over which the energy flux is constant and unaffected by EKE production or dissipation. Such an "inertial range", can be achieved only if the scale separation between the maximum EKE production and dissipation (or transfer to the mean flow) spans several orders of magnitude. Given our computational resources, we cannot run simulations spanning such a wide range of scales, nor does such a limit appear to be relevant for the ocean or the atmosphere.

Chapter 3

The Criticality and the Vertical Structure of the Eddy Diffusivity.

3.1 Introduction

Observations suggest that the time- and zonal-mean state of the extra-tropical atmosphere adjusts itself such that isentropes leaving the surface in the sub-tropics reach the tropopause near the pole, and thus $\xi \equiv \frac{a}{H}s \sim O(1)$, where ξ is the criticality parameter, $a \sim f/\beta$ denotes the planetary radius, which in turn scales with the ratio of the Coriolis parameter f and the planetary vorticity gradient β, H denotes the height of the tropopause, and s denotes the slope of the isentropes. While some numerical studies suggested that the observed adjustment of the extra-tropical atmosphere to O(1) criticalities holds over a wide range of forcings and parameters (e.g. Schneider and Walker, 2006), the previous chapter has shown that more supercritical states can also be obtained, if external parameters are changed sufficiently.

Various theories have been put forward to explain the observed equilibration of the mid-latitude atmosphere to a state of marginal criticality. One line of arguments is based on constraints arising from the zonal momentum budget. The vertically integrated QG zonal momentum budget can be used to derive a balance condition between the eddy fluxes of potential vorticity (PV) in the interior and the eddy fluxes of potential temperature at the surface. Held (1978, 1982) used this constraint

to argue that atmospheric mean states with $\xi \approx 1$ are obtained if eddy PV fluxes decay in the vertical over the depth scale of the troposphere. Using a diffusive closure for the eddy fluxes of PV and surface potential temperature, the QG momentum budget gives a relation between the criticality parameter and the eddy diffusivity. Most importantly the relation shows that the criticality parameter can be finite only if the eddy diffusivity decreases in the vertical (Green, 1970).

Schneider (2004) argued that the results of Green (1970) and Held (1978, 1982) apply only to QG systems, but are not recovered in primitive equations. He finds that, unlike in QG, the zonal momentum budget in primitive equations can be closed assuming that the eddy diffusivity for PV and surface potential temperature is constant in the vertical throughout the whole depth of the troposphere. Moreover, the choice of a vertically constant eddy diffusivity implies that $\xi \approx 1$. A potential problem with this argument is that it is not clear whether the eddy diffusivity is vertically constant in the real troposphere. While Schneider (2004) finds that the eddy diffusivity is approximately vertically constant throughout the troposphere in his idealized simulations, a vertically decreasing eddy diffusivity is found in the more realistic simulation discussed in Plumb and Mahlman (1987). Moreover, Haynes and Shuckburgh (2000) use reanalysis data to show that the eddy diffusivity decreases strongly with height in the real troposphere, though they only discuss diffusivities above the 300 K surface, to avoid isentropes which intersect with the surface. This paper thus aims to re-examine the relation between the criticality parameter and the vertical structure of the eddy diffusivity.

The result obtained by Schneider (2004) is shown to depend crucially upon how eddy PV fluxes are computed along isentropes which intersect the surface. Koh and Plumb (2004) take isentropic averages only over the part of the isentrope that is above the surface. Schneider (2004), instead, uses a different approach, and introduces an extended PV, whose average includes mathematically ill-defined contributions from isentropes below the surface.

Schneider (2005) compares the two approaches, and concludes that the definition of Koh and Plumb (2004) is less useful, because the resulting near-surface PV

gradients are often small and of varying sign (which makes an estimate of the eddy diffusivity problematic). Idealized model results discussed here, instead, show that the eddy fluxes computed with Koh and Plumb's (2004) approach, can be closed diffusively. A down-gradient diffusive closure is also supported by theoretical arguments based on analysis of the PV variance budget. A diffusive closure following the approach proposed by Schneider (2004), on the other hand, generates inconsistent results when applied to our simulations.

We therefore revisit Schneider's (2004) derivation for the relation between the criticality parameter and the vertical structure of the eddy diffusivity, but using the averaging approach advocated by Koh and Plumb (2004). Using this approach, we can extend the QG results for the relation between the criticality parameter and the eddy diffusivity to finite isentropic slopes. In particular, we show that the eddy diffusivity decreases in the vertical for any finite criticality, consistent with results obtained using QG scaling, but not with those of Schneider (2004). The revised scaling relation further shows that criticality parameters much larger than one are possible, if the eddy diffusivity decays only weakly in the vertical. This provides theoretical support for the numerical studies discussed in chapter 2, as well as other studies which have found supercritical mean states in primitive equation models (e.g. Zurita-Gotor, 2008; Zurita-Gotor and Vallis, 2010).

This chapter is organized as follows: in section 3.2 we illustrate the constraint of the momentum budget on the vertical structure of the eddy PV diffusivity, using a simple QG model. In section 3.3, we discuss the two different approaches that have been proposed to close the isentropic zonal momentum budget in primitive equations. In section 3.4, we test the diffusive closures against idealized numerical simulations. In section 3.5, we finally derive a revised condition for the criticality parameter from the vertically integrated isentropic zonal momentum budget. The conclusions are summarized in section 3.6.

3.2 Eddy Diffusivity and Criticality in QG

This study discusses the relation between the criticality parameter and the vertical structure of the eddy diffusivity in the troposphere. The problem is well understood in models using the QG approximation. Schneider (2004), however, pointed out that the relationship may be quite different in primitive equation systems, that allow for steep isentropes which intersect with the surface. In the next few sections we will revisit these arguments and show that the result of QG theory is recovered, if care is taken in computing averages along isentropic surfaces. It therefore seems appropriate to start with a review of the QG results, to set the stage for the rest of the paper.

We will illustrate the QG argument using the arguably simplest configuration: a zonally re-entrant channel composed of 2 separate layers with different density. The QG argument goes back to Green (1970), who discussed the constraint on the vertical structure of the eddy diffusivity in the continuous coordinates case. A discussion of the two-layer case was, to our knowledge, first given by Marshall (1981). The qualitative result from the two-layer model, discussed here, is similar to the continuous QG case.

Ignoring frictional forces, the steady state zonal-mean zonal momentum budget in the two layer QG model can be expressed in terms of a balance between the Coriolis acceleration, acting on the mean flow, and the reynolds stress:

$$f_0 \overline{v_i} = \partial_y \overline{u_i' v_i'}\,, \tag{3.1}$$

where $i = 1, 2$ is the model layer, the overbar denotes a time and zonal mean, and primed quantities denote deviations thereof. Introducing a residual mean flow as $\overline{v_i}^* = \overline{v} + H^{-1}\overline{v_i' h_i'}$, with h_i and H_i denoting the in-situ and mean layer depths, respectively, the momentum budget can be re-written as a balance between the Coriolis acceleration, acting on the residual mean flow, and the eddy flux of PV (e.g. Vallis, 2006):

$$f_0 \overline{v_i}^* = -\overline{v_i' q_i'}\,. \tag{3.2}$$

Here $q_i = \beta y + \zeta_i - f_0 \frac{h_i}{H_i}$ is the QG PV, where β is the planetary vorticity gradient,

ζ_i is the relative vorticity, and f_0 is the Coriolis parameter. Using a diffusive closure for the eddy fluxes of PV, and ignoring the contribution of relative vorticity to the mean PV gradient, we can approximate the residual flow in each layer as

$$\overline{v_i}^* = f_0^{-1}\overline{v_i'q_i'} \equiv -f_0^{-1}D_i\partial_y q_i \approx -D_i(\frac{\beta}{f_0} \mp \frac{s}{H_i}), \tag{3.3}$$

where $s \equiv \partial_y\overline{h_1} = -\partial_y\overline{h_2}$ denotes the slope of the interface. The negative sign in the last term on the R.H.S. of Eq. (3.3) holds for the lower layer (layer 1), where the planetary vorticity and thickness contribution to the PV gradient have opposite sign, while the positive sign holds for the upper layer (layer 2), where the planetary vorticity and thickness contribution to the PV gradient have the same sign. Mass conservation provides the additional constraint that

$$H_1\overline{v_1}^* + H_2\overline{v_2}^* = 0\,. \tag{3.4}$$

Combining Eqns. (3.2) and (3.4) and using the closure in (3.3) yields

$$D_1(\frac{H_1\beta}{f_0} - s) \approx -D_2(\frac{H_2\beta}{f_0} + s)\,. \tag{3.5}$$

This yields a relation between the vertical structure of the eddy diffusivity and the criticality parameter as

$$\xi \sim \frac{fs}{\beta H} \sim \frac{\tilde{D}}{\Delta D}, \tag{3.6}$$

where $H = H_1 + H_2$ denotes the total depth[1], $\tilde{D} \equiv (H_1D_1 + H_2D_2)/H$ is the vertical mean eddy PV diffusivity, and $\Delta D \equiv D_1 - D_2$ is the difference in the diffusivities. Eq. (3.6) states that the relative vertical variation of the eddy diffusivity scales inversely with the criticality parameter. O(1) criticality parameters are associated with vertical variations in D on the same order of D itself, while strongly supercritical states are associated with weak vertical variations in D.

[1]Notice, that the definition of the criticality parameter employed here differs somewhat from the commonly used definition in the two-layer QG model, where the depth scale is generally defined as the layer depth. For a two-layer model with unequally deep layers, the condition for baroclinic instability depends on the depth of the lower layer.

Eq. (3.6) also points towards the condition for baroclinic instability in the two layer model. If we require that baroclinically unstable eddies flux PV down the mean gradient in both layers, i.e. $D_1, D_2 > 0$, Eq. (3.6) implies that $\xi > \frac{H_1}{H}$, which is exactly the necessary criterion for baroclinic instability in this model. This result is apparent if one considers that the condition for baroclinic instability is a reversal of the PV gradients between the two layers. Since the PV flux in the two layers has to balance, and therefore needs to have opposite sign, this is also the necessary condition for a finite down-gradient flux of PV in both layers.

The result from the two layer QG model is qualitatively similar to what is obtained in the continuously stratified QG problem. The latter has been discussed by Green (1970). In section 3.5, we show that a result analogous to Eq. (3.6) can also derived in primitive equations, if the troposphere is divided into two vertical layers. The discussion of the full problem in primitive equations further yields insight about the interpretation of the lower layer in the two layer model, whose depth can be chosen somewhat arbitrarily in the two-layer QG problem, but nevertheless has important implications for the dynamics.

3.3 The Isentropic Zonal Momentum Budget in Primitive Equations

As discussed in Schneider (2004, 2005) and Koh and Plumb (2004), the vertically integrated isentropic zonal momentum budget in primitive equations can be used to relate the meridional mass transport in the troposphere to the eddy fluxes of PV and surface potential temperature. Assuming that the net mass transport vanishes upon integration over the depth of the troposphere, and that the eddy fluxes of PV and surface potential temperature can be described in terms of mean state variables through a closure, one can derive a condition for the criticality of the extra-tropical atmosphere, analog to the QG argument described above. However, before discussing the relation between the criticality parameter and the vertical structure of the eddy

diffusivity in isentropic coordinates, we need an appropriate formulation of the isentropic zonal-mean zonal momentum budget on isentropes which intersect with the surface.

For simplicity, we will assume that both the large-scale mean and eddy flows have a small Rossby number Ro, which is generally a good approximation in the troposphere. Departing from the QG approximation, however, we do not make an assumption for the smallness of the isentropic slope (e.g. Vallis, 2006). The latter is inadequate for studies of the large scale atmospheric circulation, and crucial to understand the differences between the QG results and those presented in Schneider (2004).

For small Ro, the isentropic zonal momentum budget reduces to the geostrophic wind relation

$$fv \approx \partial_x M \,, \tag{3.7}$$

where f is the planetary vorticity, v is the meridional velocity and $M = c_p T + gz$ is the Montgomery streamfunction (c_p denotes the specific heat capacity of air at constant pressure, T is temperature, g is the gravitational acceleration and z is height). The partial zonal derivative ∂_x is taken at constant potential temperature θ. In addition to terms which are higher order in Ro, we neglected the effect of diabatic and frictional forcing in the momentum equation. The full budget is discussed in Schneider (2005) and Koh and Plumb (2004), but the neglected terms are not relevant for the key results presented here.

To derive an equation for the isentropic mass transport, we need to take zonal and temporal averages of the momentum budget along isentropes. This raises the issue of how to define these averages when isentropes intersect the surface. We can introduce a normalized zonal and temporal integral along any isentrope (that may or may not outcrop at some longitude or time) as in Koh and Plumb (2004)

$$\overline{f(\theta,x,y,t)}^{\diamond} \equiv \frac{1}{TL} \iint\limits_{\theta>\theta_s(x,y,t)} f(\theta,x,y,t)\,dx\,dt \tag{3.8}$$

where L is the width of the (zonally re-entrant) domain and the temporal integral is taken over some time period T. For simplicity we use cartesian coordinates but the generalization to spherical coordinates is straightforward. If $f(\theta, x, y, t)$ is continually extended to isentropes below the surface, the normalized integral may for convenience be written as

$$\overline{f(\theta,x,y,t)}^{\diamond} = \frac{1}{TL}\iint \mathcal{H}(\theta-\theta_s)f(\theta,x,y,t)dxdt \equiv \overline{\mathcal{H}(\theta-\theta_s)f(\theta,x,y,t)}\,, \qquad (3.9)$$

where the over-bar denotes the isentropic zonal and temporal mean, and $\mathcal{H}(\theta-\theta_s)$ is the Heaviside function, which guarantees that there are no contributions to the integral from the sub-surface part of an isentrope.

Using the definition in (3.9), the normalized integral of the momentum budget in (3.7) can be written as

$$\overline{\mathcal{H}(\theta-\theta_s)fv} \approx \overline{\mathcal{H}(\theta-\theta_s)\partial_x M}\,. \qquad (3.10)$$

Equation (3.10) is the starting point to illustrate the two different approaches used by Schneider (2004) and Koh and Plumb (2004) in re-writing the mean zonal momentum budget in terms of mean and eddy fluxes of PV.

3.3.1 Two Formulations for Mean and Eddy Fluxes of PV

In order to derive an equation for the isentropic mass transport from the momentum budget in (3.10), we want to express the Coriolis term on the L.H.S. of Eq. (3.10) in terms of thickness weighted mean and eddy fluxes of PV. Upon division by the mean PV, this yields an equation for the thickness weighted velocity, which can be integrated in the vertical to yield the total isentropic mass transport.

Two different approaches have been proposed to separate the term $\overline{\mathcal{H}(\theta-\theta_s)vf}$ into mean and eddy flux terms (see also Schneider, 2005). The approach used in Koh

and Plumb (2004), can be written as

$$\begin{aligned}
\overline{\mathcal{H}(\theta-\theta_s)vf} &= \overline{\left(\frac{\mathcal{H}(\theta-\theta_s)\sigma vf}{\sigma}\right)} \\
&= \overline{\mathcal{H}(\theta-\theta_s)\sigma vP} \\
&= \overline{\rho_\theta}\,\overline{vP}^* \\
&= \overline{\rho_\theta}(\overline{v}^*\overline{P}^* + \overline{\hat{v}\hat{P}}^*), \qquad (3.11)
\end{aligned}$$

where we introduced the isentropic thickness, $\sigma \equiv -g^{-1}\partial_\theta p$, and the planetary PV, $P \equiv \frac{f}{\sigma}$. We further introduced a generalized thickness as $\rho_\theta = \mathcal{H}(\theta-\theta_s)\sigma$ and a generalized thickness weighted zonal average, $\overline{(\,)}^* = \overline{\sigma(\,)}^\diamond/\overline{\sigma}^\diamond = \overline{\rho_\theta(\,)}/\overline{\rho_\theta}$ (see also Andrews, 1983; Juckes et al., 1994). Note, that $\overline{(\,)}^*$ is simply the thickness weighted zonal average, taken over the above-surface part of the isentrope. Deviations from this average are denoted by $\hat{(\,)} \equiv (\,) - \overline{(\,)}^*$.

Schneider (2004, 2005) instead chooses to define

$$\begin{aligned}
\overline{\mathcal{H}(\theta-\theta_s)vf} &\equiv \overline{\left(\frac{\rho_\theta\mathcal{H}(\theta-\theta_s)vf}{\rho_\theta}\right)} \\
&= \overline{\rho_\theta\mathcal{H}(\theta-\theta_s)vP_{ext}} \\
&= \overline{\rho_\theta}\,\overline{\mathcal{H}(\theta-\theta_s)vP_{ext}}^* \\
&= \overline{\rho_\theta}\left(\overline{v_{ext}}^*\overline{P_{ext}}^* + \overline{\hat{v}_{ext}\hat{P}_{ext}}^*\right), \qquad (3.12)
\end{aligned}$$

and introduces an extended planetary PV, $P_{ext} \equiv \frac{f}{\rho_\theta}$ (notice the generalized thickness, ρ_θ, in the denominator), and an extended velocity, $v_{ext} \equiv \mathcal{H}(\theta-\theta_s)v$, defined to exist on isentropes both above and below the surface. Notice, that the first step in (3.12) is mathematically ill-defined, since it implies multiplying and dividing by zero whenever the isentrope is inside the surface and ρ_θ vanishes – it is here taken as a definition for the ill-defined expression on the R.H.S. Furthermore, the extended PV, $P_{ext} \equiv \frac{f}{\rho_\theta}$, is infinite on isentropes inside the surface, and thus both the generalized thickness-weighted average of P_{ext} and $\hat{v}_{ext}\hat{P}_{ext}$ are ill defined. Schneider (2004) evaluates $\overline{P_{ext}}^*$

as

$$\overline{\rho_\theta}^{*}\overline{P_{ext}}^{*} = \overline{\left(\frac{\rho_\theta f}{\rho_\theta}\right)} \equiv f\,, \tag{3.13}$$

i.e. the ratio of ρ_θ in the numerator and ρ_θ in the denominator of Eq. (3.13) is assumed equal to one everywhere, including the part of isentropes below the surface, where $\rho_\theta = 0$.

Schneider (2005) discusses the relative merits of the two formulations used in Schneider (2004), and Koh and Plumb (2004). He argued that the two approaches can be understood as arising from different evaluations of the ill-defined ratio in Eq. (3.13). The formulation of Koh and Plumb (2004) is recovered if the term $\left(\frac{\rho_\theta f}{\rho_\theta}\right)$ is assumed to vanish when isentropes are below the surface, while Schneider's (2004) approach assumes that it is equal to f. Notice, however, that the approach of Koh and Plumb (2004) can instead be derived without making any assumptions for quantities on the sub-surface part of isentropes, as per Eq. (3.11). The problem is that by introducing the generalized quantities P_{ext} and v_{ext}, the extended PV approach requires arbitrary assumptions down the line, to obtain well defined thickness weighted averages.

Taking a different point of view, which we will adopt in the following, the separation into mean and eddy terms in (3.12), together with the definition for the mean extended PV in (3.13), may be regarded as a definition for the extended eddy PV flux $\overline{\hat{v}_{ext}\hat{P}_{ext}}^{*}$. One could then regard (3.12) as a different choice as to how to separate mean and eddy fluxes. The question is whether one can rationalize what the mean and eddy flux terms physically represent in this case, as they are no longer defined as the mean and eddy contributions from a Reynolds decomposition.

The physical meaning of the mean and eddy flux terms becomes particularly important if we want to relate the eddy PV flux to the mean gradient through a diffusive closure, in order to close the momentum budget in terms of mean state variables. Tung (1986) offers support for a diffusive closure for the thickness weighted isentropic eddy PV flux, using small amplitude theory. He does, however, not consider isentropic outcrops, which are crucial for the discussion here. In Appendix A, we

present a general justification for a diffusive closure for the interior eddy PV flux, $\overline{\hat{v}\hat{P}}^*$, based on the PV variance budget, that accounts for isentropic outcrops. We were not able to derive a similar relation for the extended PV variance, since $\overline{\hat{P}^2_{ext}}^*$ is not well defined on outcropping isentropes. Schneider (2004, 2005) justifies his closure showing that the extended eddy flux $\overline{\hat{v}_{ext}\hat{P}_{ext}}^*$ is down the gradient of $\overline{P_{ext}}^*$ in his numerical simulations, which suggests that he may proceed to use a diffusive closure $\overline{\hat{v}_{ext}\hat{P}_{ext}}^* = -D\partial_y\overline{P_{ext}}^*$. However, we will argue below, that such a relationship is not justified in general.

3.3.2 An Equation for the Meridional Mass Transport

In this section we will discuss how the isentropic zonal momentum budget can be transformed into an equation for the meridional isentropic mass transport, following the same approach outlined in Schneider (2004, 2005) and Koh and Plumb (2004). Focussing on the role of isentropic outcrops, we will here analyze the mass transport integrated over the surface layer (SL), which is defined as the layer including all isentropes that intersect the surface at some longitude or time.

Schneider (2005) shows that the mass transport over the SL can be estimated by dividing the zonal momentum equation (3.10) by $\overline{P}^*$ and integrating vertically over the SL. Substituting (3.11) into (3.10), to express the Coriolis term by a thickness weighted mean and eddy flux of PV, dividing by $\overline{P}^*$, and integrating from the surface to the top of the SL, one obtains an estimate for the transport in the SL,

$$\int_{\theta_b}^{\theta i} \overline{\rho_\theta}\,\overline{v}^* d\theta \approx -\underbrace{\int_{\theta_b}^{\theta_i} \frac{\overline{\rho_\theta \hat{v}\hat{P}}^*}{\overline{P}^*} d\theta}_{(1)} - \underbrace{\frac{f}{\overline{P}^*(\overline{\theta}_s)}\overline{v'_s\theta'_s}^s}_{(2)} . \tag{3.14}$$

Here θ_b is the minimum potential temperature over the domain and θ_i is the potential temperature at the top of the SL, the subscript s denotes surface quantities and $\overline{(\,)}^s$ denotes an average along the surface. The surface potential temperature flux term on the R.H.S. of (3.14) represents the bottom form stress, which arises as the boundary contribution from the Montgomery streamfunction term in Eq. (3.10) (see Koh

and Plumb, 2004; Schneider, 2005). The derivation of this term is unambiguous and therefore not repeated in detail here. Equation (3.14) states that the total meridional mass transport between the surface and the isentropic surface θ_i, is driven by isentropic eddy PV fluxes, and the eddy flux of surface potential temperature.

The same equation can be derived using the extended PV approach used by Schneider (2004), who finds that

$$\int_{\theta_b}^{\theta i} \overline{\rho_\theta}\,\overline{v}^*\,d\theta \approx -\underbrace{\int_{\theta_b}^{\theta_i} \frac{\overline{\overline{\rho_\theta}\hat{v}_{ext}\hat{P}_{ext}}^*}{\overline{P_{ext}}^*}d\theta}_{(1)} - \underbrace{\frac{f}{\overline{P_{ext}}^*(\overline{\theta_s})}\overline{v'_s\theta'_s}^s}_{(2)}. \tag{3.15}$$

The total mass transport – the term on the L.H.S. of Eqs. (3.14) and (3.15) – is independent of the approach, but the separation between the contributions associated with the eddy flux of PV, term (1), and the contribution associated with the eddy flux of surface potential temperature, term (2), differs in the two approaches. This can be seen by noting that $\overline{P_{ext}}^*(\overline{\theta_s}) \neq \overline{P}^*(\overline{\theta_s})$. The pre-factor multiplying the eddy flux of surface potential temperature, term (2), thus differs in the two approaches. This difference is absorbed by a corresponding difference in the PV flux contribution, term (1).

Using diffusive closures for the eddy fluxes of interior PV and surface potential temperature, Eq. (3.14) becomes

$$\int_{\theta_b}^{\theta i} \overline{\rho_\theta}\,\overline{v}^*\,d\theta \approx \int_{\theta_b}^{\theta_i} \frac{\overline{\rho_\theta} D\partial_y\overline{P}^*}{\overline{P}^*}d\theta + \frac{f}{\overline{P}^*(\overline{\theta_s})}D_s\partial_y\overline{\theta_s} \tag{3.16}$$

that is the SL mass transports is given by a contribution associated with the interior PV gradient and a contribution associated with the surface potential temperature gradient (describing the form drag on outcropping isentropes). Using instead a diffusive closure for the eddy flux of extended PV, along with a closure for the surface potential temperature flux, Eq. (3.15) becomes

$$\int_{\theta_b}^{\theta i} \overline{\rho_\theta}\,\overline{v}^*\,d\theta \approx \int_{\theta_b}^{\theta_i} \frac{\overline{\rho_\theta} D_{ext}\partial_y\overline{P_{ext}}^*}{\overline{P_{ext}}^*}d\theta + \frac{f}{\overline{P_{ext}}^*(\overline{\theta_s})}D_s\partial_y\overline{\theta_s}. \tag{3.17}$$

One would now like to assume that the eddy diffusivity is a fundamental property of the flow, and thus $D_{ext} = D \approx D_s$ near the surface. However, we will show that the budget in Eq. (3.16) can be closed assuming that $D \approx D_s$ near the surface, but Eq. (3.17) strongly overestimates the near-surface mass transport if we assume that $D_{ext} \approx D_s$.

3.4 Numerical Simulations

We proceed to test the arguments presented in the previous section, and in particular the applicability of diffusive closures for the eddy PV fluxes in the two approaches, in an idealized numerical simulation. The model is set up to limit boundary layer effects that arise from explicit parameterization of boundary layer physics. While the model setup might be a less realistic description of the real atmosphere, it helps to focus exclusively on the dynamics which are the topic of the present paper, and keep any additional physics as simple as possible.

3.4.1 Model Setup

The model and setup is similar to the simulations discussed in chapter 2. We use a hydrostatic, Boussinesq[2] version of the MIT general circulation model (Marshall et al., 1997), in a zonally reentrant β-plane channel configuration. The channel is 15,000 km long, bounded meridionally by side walls at y=$\pm$ 4500km, and vertically by rigid lids at z=H=10.2km and z=0. Differing from the simulations discussed in chapter 2 we use free slip boundary conditions on all boundaries to limit frictional effects. Kinetic energy is removed by a linear Rayleigh drag with a constant drag coefficient of $r = (40\text{days})^{-1}$ acting over the whole domain. We use a linear equation of state with a thermal expansion coefficient of $\alpha = 2.25 \cdot 10^{-4} K^{-1}$. The thermal expansion coefficient is smaller than that of air to obtain a better separation between

[2]Notice, that the theoretical discussions above are for the more general case of a compressible fluid, in direct analogy to the derivations in Schneider (2004) and Koh and Plumb (2004). However, as discussed in chapter 2, the same equations are obtained in the Boussinesq limit.

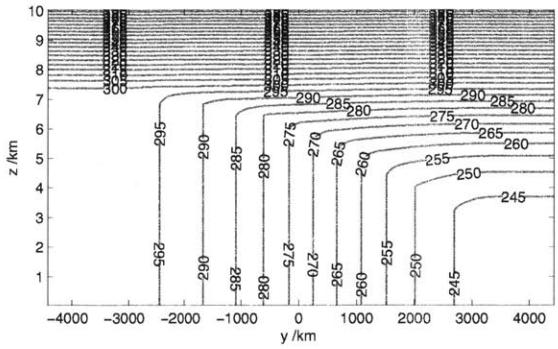

Figure 3-1: Equilibrium potential temperature for thermal restoring in K. (CI: 5K)

the eddy and domain scale and to allow the model to set its criticality (see chapter 2).

The simulations are forced through relaxation to the equilibrium temperature profile shown in Fig. 3-1, which is the radiative convective equilibrium solution of the profile used in the simulations described in chapter 2. It is characterized by a baroclinic zone 7000 km wide, across which the temperature drops by about 55 K. The equilibrium stratification is neutral over the lower part of the domain, while a statically stable equilibrium stratification is prescribed at higher altitudes to mimic the stable radiative-equilibrium profile of the stratosphere. The relaxation time-scale is constant over the domain at $\tau_{int} = 50$ days.

The simulation is spun up until a quasi-steady state is reached. Isentropic diagnostics are calculated from 200 snapshots saved every ten days after the solution is equilibrated.

3.4.2 Results

The equilibrated time- and zonal-mean state of the simulation is shown in Fig. 3-2. Significant baroclinicity is found over most of the domain, with a jet centered around $y = -400km$. The jet is associated with a maximum in baroclinicity, as well as maxima in the barotropic westerly wind and eddy kinetic energy.

Fig. 3-3 shows the three terms that appear in the zonal momentum budget as per Eq. (3.14). The integral is taken from the surface to the top of the SL, defined to

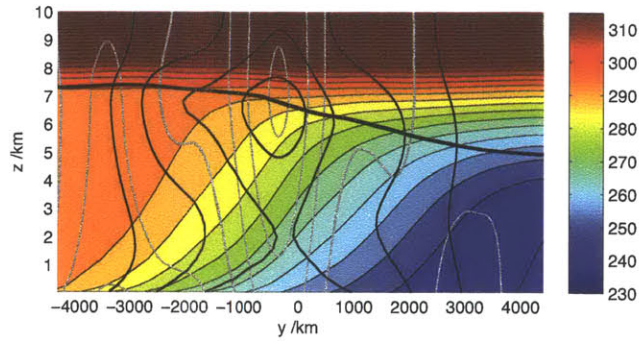

Figure 3-2: Time- and zonal-mean fields of potential temperature (color shading - CI: 5 K), EKE (thin black lines - CI: 2 m^2s^{-2}), zonal wind (gray lines - CI: 1 ms^{-1}), and the tropopause height, defined as the height at which $\frac{d\theta}{dz} = 10^{-2}Km^{-1}$ (thick black line).

include all isentropes up to the 95% quantile of potential temperature values found at the surface, along a latitude circle. The budget is shown only for the SL, because that's where we expect differences in the averaging approaches (all approaches are equivalent aloft, where there are no isentropes that intersect the surface). The continuos grey lines show the total SL isentropic mass flux,

$$F_{tot} = \int_{\theta_b}^{\theta i} \overline{\rho_\theta}\, \overline{v}^* d\theta \,. \tag{3.18}$$

The dotted black lines show the sum of the mass fluxes associated with the eddy PV flux and the surface potential temperature flux. Using the averaging approach of Koh and Plumb (2004), these are

$$F_{\overline{\hat{v}\hat{P}}^*} \equiv -\int_{\theta_b}^{\theta_i} \frac{\overline{\rho_\theta \hat{v}\hat{P}}^*}{\overline{P}^*} d\theta \quad \text{and} \quad F_{\overline{v_s'\theta_s'}} \equiv -\frac{f}{\overline{P}^*(\overline{\theta_s})} \overline{v_s'\theta_s'}^s \tag{3.19}$$

The budget derived in Eq. (3.14) predicts that

$$F_{tot} \approx F_{\overline{\hat{v}\hat{P}}^*} + F_{\overline{v_s'\theta_s'}} \,. \tag{3.20}$$

Fig. 3-3 (a) shows that this relation is satisfied by the numerical simulation. We find that most of the SL mass transport is associated with the surface contribution

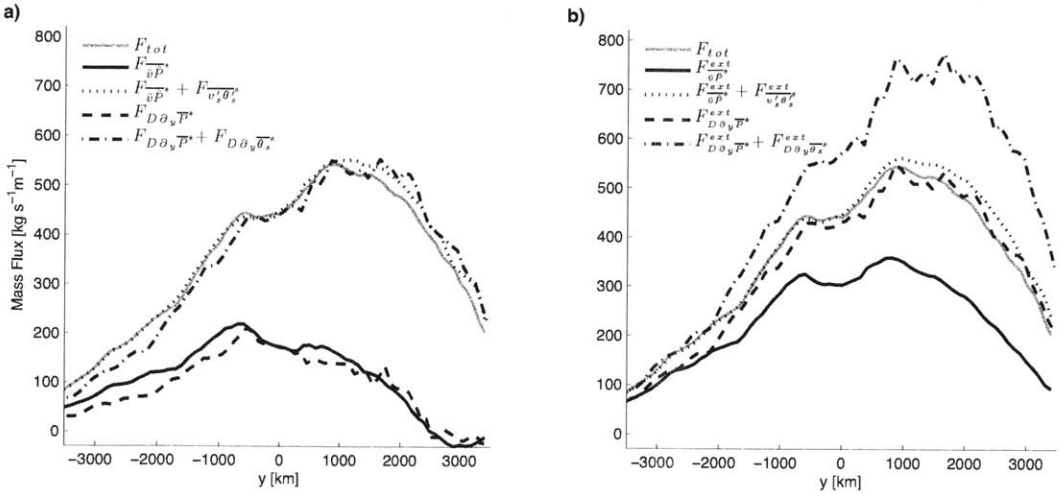

Figure 3-3: SL mass fluxes over the baroclinically forced zone. Shown is the total mass transport integrated vertically over the SL, its contribution due to eddy PV and surface potential temperature flux, as well as estimates of the respective fluxes resulting from a diffusive closure using the surface eddy diffusivity (see legend). Figure a) shows results using the interior PV approach for the separation of SL mass fluxes into a contribution from the eddy PV flux and surface potential temperature fluxes, and figure b) shows results using the extended PV approach. The SL is here defined as including all isentropes up to the 95% quantile of the surface potential temperature.

$F_{\overline{v'\theta'_s}}$, with a smaller (but significant) contribution from the interior eddy PV flux component $F_{\overline{\hat{v}\hat{P}}^*}$.

Alternatively we can separate the eddy mass flux components according to the extended PV approach of Schneider (2004), given in Eq. 3.15,

$$F_{tot} \approx F^{ext}_{\overline{\hat{v}\hat{P}}^*} + F^{ext}_{\overline{v'_s\theta'_s}}, \tag{3.21}$$

where

$$F^{ext}_{\overline{\hat{v}\hat{P}}^*} \equiv -\int_{\theta_b}^{\theta_i} \frac{\overline{\overline{\rho_\theta}\hat{v}_{ext}\hat{P}_{ext}}^*}{\overline{P_{ext}}^*} d\theta \quad \text{and} \quad F^{ext}_{\overline{v'_s\theta'_s}} \equiv -\frac{f}{\overline{P_{ext}}^*(\overline{\theta_s})}\overline{v'_s\theta'_s}^s \tag{3.22}$$

The extended eddy PV flux $\overline{\hat{v}_{ext}\hat{P}_{ext}}^*$ is defined as the residual between the total PV flux $\overline{vP}^*$ and the mean advection of the generalized PV $\overline{v_{ext}}^*\overline{P_{ext}}^*$, as discussed

in section 3.3.1. The mass flux budget in Eq. (3.21) is similarly confirmed by the model simulations (Fig. 3-3b). Compared to the budget in Fig. 3-3 b, the total mass transport has a larger contribution from the extended eddy PV flux term, and a correspondingly smaller contribution from the eddy flux of surface potential temperature. In fact it can be shown easily that $F^{ext}_{\overline{v'_s\theta'_s}} \approx \frac{1}{2}F_{\overline{v'_s\theta'_s}}$, by comparing Eqs. (3.19) and (3.22), but realizing that

$$\overline{P}^*(\overline{\theta}_s) = \frac{\overline{f\mathcal{H}(\overline{\theta}_s - \theta_s)}}{\overline{\rho_\theta}(\overline{\theta}_s)} \approx \frac{1}{2}\frac{f}{\overline{\rho_\theta}(\overline{\theta}_s)} = \frac{1}{2}\overline{P_{ext}}^*(\overline{\theta}_s)\,, \tag{3.23}$$

because the mean surface potential temperature is well approximated by its median value, hence $\overline{\mathcal{H}(\overline{\theta}_s - \theta_s)} \approx \frac{1}{2}$. Since the total mass transport is independent of the averaging approach, a similar but opposite difference exists between the eddy PV flux contributions $F_{\overline{v}\overline{\hat{P}}^*}$ and $F^{ext}_{\overline{v}\overline{\hat{P}}^*}$.

We now test diffusive closures for the eddy fluxes of PV using the two approaches. We calculate the eddy diffusivity from the surface potential temperature flux/gradient relationship as[3]

$$D_s \equiv -\overline{v'_s\theta'_s}^s / \partial_y \overline{\theta_s}^s\,. \tag{3.24}$$

Using this definition, the diffusive closures for the mass transport associated with the surface eddy flux of potential temperature,

$$F_{D\partial_y\overline{\theta_s}^s} \equiv \frac{f}{\overline{P}^*(\overline{\theta}_s)} D_s \partial_y \overline{\theta}_s \quad \text{and} \quad F^{ext}_{D\partial_y\overline{\theta_s}^s} \equiv \frac{f}{\overline{P_{ext}}^*(\overline{\theta}_s)} D_s \partial_y \overline{\theta}_s\,, \tag{3.25}$$

reproduce by construction the corresponding flux terms $F_{\overline{v'\theta'_s}}$ and $F^{ext}_{\overline{v'\theta'_s}}$.

Schneider (2004) argues that a diffusive closure holds also for the eddy PV flux, with the same eddy diffusivity D_s, as one ought to expect if eddies mix all tracers at the same rate, and if this mixing rate varies little over the depth of the SL. This is

[3]Notice, that the surface eddy diffusivity is here calculated using the actual surface potential temperature flux. Following the full derivation shown in Schneider (2004, 2005), or Koh and Plumb (2004), the surface term in Eqs. (3.14) and (3.15) should generally be described by the *geostrophic* eddy flux of surface potential temperature. In the presented simulation, where the Rossby number is small, and no enhanced surface drag is used, the difference between the full eddy flux and the geostrophic eddy flux is negligible.

tested by computing

$$F_{D\partial_y\overline{P}^*} \equiv \int_{\theta_b}^{\theta_i} \frac{\overline{\rho_\theta} D_s \partial_y \overline{P}^*}{\overline{P}^*} d\theta \quad \text{and} \quad F^{ext}_{D\partial_y\overline{P}^*} \equiv \int_{\theta_b}^{\theta_i} \frac{\overline{\rho_\theta} D_s \partial_y \overline{P_{ext}}^*}{\overline{P_{ext}}^*} d\theta \,. \tag{3.26}$$

For the interior PV approach, we find that the PV flux and therefore the full SL mass transport is described reasonably well by the diffusive closure (Fig. 3-3a), suggesting that the PV flux in the SL can be described as a diffusive flux, with an eddy diffusivity similar to that for surface potential temperature. However, with the extended PV approach, we find that the eddy PV flux, and therefore the total SL mass flux is considerably overestimated by the diffusive closure. Interestingly, the diffusive approximation for the extended PV flux contribution $F^{ext}_{D\partial_y\overline{P}^*}$ alone is a better approximation of the total SL mass transport F_{tot} (Fig. 3-3b). This result can be explained in terms of the different approaches taken to treat outcropping isentropes, as discussed in the following.

3.4.3 Explaining the Results

The difference between the SL mass balance in the two approaches can be understood by re-writing the extended PV flux and gradient, in terms of the interior PV contributions, and contributions associated with fluxes and gradients of surface potential temperature. Using again that $F^{ext}_{\overline{v'_s\theta'_s}} \approx \frac{1}{2} F_{\overline{v'_s\theta'_s}}$, we can show that (see Appendix B for a more detailed derivation):

$$F^{ext}_{\overline{\hat{v}\hat{P}}^*} \approx F_{\overline{\hat{v}\hat{P}}^*} + \frac{1}{2} F_{\overline{v'_s\theta'_s}} \,, \tag{3.27}$$

In the extended PV formulation of the mass budget (Eq. 3.21), about *half* of the surface potential temperature flux contribution to the isentropic mass transport is thus absorbed into the extended PV flux term.

However, the diffusive closure for the flux associated with the extended PV gradient contains the contribution associated with the interior PV gradient, plus the *full* contribution associated with the surface potential temperature gradient (see Ap-

pendix B for a derivation):

$$F^{ext}_{D\partial_y\overline{P}^*} \approx F_{D\partial_y\overline{P}^*} + F_{D\partial_y\overline{\theta_s}^s} \,. \tag{3.28}$$

If the interior eddy PV flux near the surface can be closed with a diffusivity similar to that for surface potential temperature (as confirmed in our simulation), a similar closure for the extended eddy PV flux thus automatically overestimates the flux. Consistent with the numerical results shown in Fig. (3-3), a comparison of Eqs. (3.28) and (3.20) suggests that the diffusive closure for the flux associated with the extended PV, is by itself an approximation for the full SL mass transport.

Before returning to the implications of our findings for the criticality parameter, we remark that the numerical results discussed here have been confirmed in a whole suite of simulations, using a similar idealized setup but with differing parameters and restoring profiles — the results hold as long as the system does not become convective, in which case the transformation into isentropic coordinates fails. Results from these simulations will be reported in the next two chapters, where we discuss their implications for our understanding of the equilibration of the extra-tropical troposphere.

Schneider (2005) argues that in his simulations a diffusive closure for the extended eddy PV flux is better justified than for the eddy flux of interior PV, since the gradients of the latter are generally weak and vary on small scales in the SL. While this makes it impractical to estimate an eddy diffusivity from a flux-gradient relationship for the interior PV, it does not necessarily mean that the integrated SL momentum budget cannot be closed with a diffusive closure for the eddy flux of interior PV. Instead, if the eddy flux of interior PV is similarly weak, the integrated momentum budget can still be closed (and in fact becomes rather independent of the exact choice for the interior PV diffusivity). We have looked at some example simulations which are in this limit.

In cases where both the eddy flux and gradient of interior PV are very weak, the extended eddy PV flux appears to be well defined and down-gradient, as both the flux

and the gradient are dominated by the surface potential temperature contribution (see Eqs. 3.27 and 3.28). This might explain why Schneider (2005) comes to the conclusion that the extended PV approach is more suitable for a closure, based on the empirical evidence that the extended PV gradient in the SL is typically large, and accompanied by a down-gradient eddy flux. However, as discussed above, the mass transport associated with the extended eddy PV flux in this case is over-estimated by a factor of two, if it is closed with an eddy diffusivity similar to that of surface potential temperature. This becomes crucial in the derivation of a relation between the criticality parameter and the vertical structure of the eddy diffusivity, as will be discussed in section 3.5.

For the extended eddy PV flux closure to correctly represent the SL mass budget, a very weak interior PV gradient would still have to be associated with a strong eddy flux of interior PV. This may have happened in some of the simulations analyzed by Schneider (2005). However, we surmise that such situations may as well be explained by non-conservative boundary layer effects, which can cause both interior PV and surface potential temperature to behave little like conservative tracers. This problem, however, cannot generally be salvaged by re-defining the zonal average; instead, a simple diffusive closure may just no longer be appropriate in such a case. In chapter 4 we discuss a wider range of numerical simulations as well as observational data, which provide further support for the closure advocated here.

3.5 The Integrated Momentum Budget and the Criticality

Schneider (2004) derives a condition for the state of the extra-tropical atmosphere by integrating the isentropic mass flux balance (3.14) to the top of the troposphere θ_t. He further makes a diffusive closure for both the extended eddy PV flux $\overline{\hat{v}_{ext}\hat{P}_{ext}}^{*}$ and the surface potential temperature flux $\overline{v_s'\theta_s'}^{s}$, with the same vertically constant eddy diffusivity. We showed above that this is generally not expected to hold. Instead,

we argued that a diffusive closure for the eddy flux of interior PV, as defined in Koh and Plumb (2004), is better supported by our numerical simulations, and can be justified by physical arguments. We will therefore repeat the derivation of Schneider (2004), but using diffusive closures for the interior eddy PV fluxes $\overline{\hat{v}\hat{P}}^*$ and surface potential temperature flux $\overline{v'_s\theta'_s}^s$. We find that, except in the limit case of infinite supercriticality, the momentum balance cannot be satisfied with a vertically constant eddy diffusivity, consistent with theories based on the QG approximation (Green, 1970). We then discuss how the revised momentum balance can be used to derive a "criticality" condition, or more generally a scaling relation between the criticality parameter and the vertical structure of the eddy diffusivity.

3.5.1 The Vertically Integrated Isentropic Momentum Budget

If the integration in the mass balance equation (3.14) is taken out all the way up to the tropopause, and it is assumed that the mass transport above the troposphere is negligible, one gets

$$\int_{\theta_b}^{\bar{\theta}_t} \frac{\overline{\rho_\theta \hat{v}\hat{P}}^*}{\overline{P}^*} d\theta \approx -\frac{f}{\overline{P}^*(\overline{\theta}_s)} \overline{\tilde{v}'_s\theta'_s}^s . \tag{3.29}$$

Assuming a diffusive closure for the eddy flux of PV and surface potential temperature then yields

$$-\int_{\theta_b}^{\bar{\theta}_t} \frac{\overline{\rho_\theta} D \partial_y \overline{P}^*}{\overline{P}^*} d\theta \approx \frac{f}{\overline{P}^*(\overline{\theta}_s)} D_s \partial_y \overline{\theta}_s . \tag{3.30}$$

While we found in the previous section that D may be assumed similar to D_s within the SL, we now use Eq.(3.30) to show that D is expected to vary throughout the depth of the entire troposphere, generally decreasing from D_s.

The thickness weighted mean PV can be approximated as $\overline{P}^* \approx \frac{\Pi f}{\overline{\rho_\theta}}$, and thus

$$\partial_y \overline{P}^* \approx \frac{\overline{P}^*}{f}\beta + \frac{\overline{P}^*}{\Pi}\partial_y \Pi - \frac{\overline{P}^*}{\overline{\rho_\theta}}\partial_y \overline{\rho_\theta} . \tag{3.31}$$

Equation (3.30) then becomes

$$-\int_{\theta_b}^{\bar{\theta}_t} D\left(\frac{\overline{\rho_\theta}}{f}\beta - \partial_y\overline{\rho_\theta}\right) d\theta - \int_{\theta_b}^{\bar{\theta}_t} D\frac{\overline{\rho_\theta}}{\Pi}\partial_y\Pi\, d\theta \approx D_s\frac{\overline{\rho_\theta}(\overline{\theta_s})}{\Pi(\overline{\theta_s})}\partial_y\overline{\theta_s}\,. \tag{3.32}$$

The second term on the L.H.S. of Eq. (3.32) can be approximated as

$$\begin{aligned}
-\int_{\theta_b}^{\bar{\theta}_t} D\frac{\overline{\rho_\theta}}{\Pi}\partial_y\Pi\, d\theta &= -\int_{\theta_b}^{\bar{\theta}_t} D\frac{\overline{\rho_\theta}}{\Pi}\overline{\partial_y\mathcal{H}(\theta-\theta_s)}\, d\theta \\
&= D_s\overline{\left(\frac{\overline{\rho_\theta}(\theta_s)}{\Pi(\theta_s)}\partial_y\theta_s\right)} \\
&\approx D_s\frac{\overline{\rho_\theta}(\overline{\theta_s})}{\Pi(\overline{\theta_s})}\partial_y\overline{\theta}_s\,,
\end{aligned} \tag{3.33}$$

which leaves us with

$$\overline{-\int_{\theta_b}^{\bar{\theta}_t} D\left(\frac{\rho_\theta}{f}\beta - \partial_y\rho_\theta\right) d\theta} \approx 0\,. \tag{3.34}$$

Equation (3.34) states that the diffusive flux associated with the planetary vorticity gradient and the generalized thickness gradient has to integrate to zero over the depth of the troposphere.

Comparison of Eq. (3.32) to Eq. (11) in Schneider (2004) shows that the first integral on the L.H.S is similar in the two approaches, but Schneider (2004) does not include the second integral on the L.H.S, which appears due to the factor Π in the definition of the thickness weighted mean PV. This term balances the surface contribution on the R.H.S. of Eq. (3.32). Schneider (2004) therefore remains with an additional surface potential temperature gradient contribution on the R.H.S. of Eq. (3.34). This additional term allows him to balance the momentum budget with a vertically constant eddy diffusivity. According to Eq. (3.34), however, this is generally not possible. This can be seen by noting that the second term in the integral in Eq. (3.34) approximately integrates to zero, if D is assumed vertically constant:

$$\overline{\int_{\theta_b}^{\bar{\theta}_t} D\partial_y\rho_\theta\, d\theta} = -Dg^{-1}(\partial_y|_\theta\overline{p}(\overline{\theta}_t) - \partial_y\,\overline{p_s}^s) \approx 0\,. \tag{3.35}$$

As justified in Schneider (2004), we here assumed that both the isentropic "slope"

at the tropopause $\partial_y|_\theta \overline{p}(\overline{\theta}_t)$, and the surface pressure gradient,$\partial_y \overline{p_s}^s$, are negligible. The first term in the integral in Eq. (3.34), however, is positive definite. As in the QG model, we thus find that the eddy diffusivity D can generally not be vertically constant.

3.5.2 A Scaling Relation for the Criticality Parameter

Eq. (3.34) can be used to obtain a scaling relation between the criticality and the vertical structure of the eddy diffusivity. As argued above, the momentum budget cannot generally be satisfied if the eddy diffusivity is assumed vertically constant. Instead, we expect the eddy diffusivity to be large near the surface and decay towards the tropopause (Plumb and Mahlman, 1987; Haynes and Shuckburgh, 2000).

To derive a scaling argument for the vertical structure of the eddy diffusivity, we separate the integral of the mass transport in Eq. (3.34) into two parts, above and below some level $\theta_1(y)$, which yields

$$\overline{D_1 \int_{\theta_b}^{\theta_1} \left(\frac{\rho_\theta}{f}\beta - \partial_y \rho_\theta \right) d\theta} = -\overline{D_2 \int_{\theta_1}^{\theta_t} \left(\frac{\rho_\theta}{f}\beta - \partial_y \rho_\theta \right) d\theta}\,, \tag{3.36}$$

where we defined bulk diffusivities D_1 and D_2 for the two layers, which formally can be described as weighted vertical averages of the eddy diffusivity over the respective layer. We further assume that the lower layer is chosen such that it includes the entire "surface layer", which, at any given latitude, comprises all isentropes that intersect with the surface at some time or longitude. We thus require that $\mathcal{H}(\theta_1 - \theta_s) = 1$ at all times and longitudes. Ignoring again contributions due to the isentropic "slope" at the tropopause, $\partial_y|_\theta \overline{p}(\overline{\theta}_t)$, and the surface pressure gradient, $\partial_y \overline{p_s}^s$, we then find that

$$D_1 \left(\frac{(\overline{p}(\theta_1) - \overline{p_s}^s)\beta}{f} - \partial_y|_\theta \overline{p}(\theta_1) \right) \approx -D_2 \left(\frac{(\overline{p}(\overline{\theta}_t) - \overline{p}(\theta_1))\beta}{f} + \partial_y|_\theta \overline{p}(\theta_1) \right). \tag{3.37}$$

Equation (3.37) is the generalization of the two layer QG relation in Eq. (3.5), where layer thicknesses have been replaced by the corresponding pressure ranges, and the

isentropic slope becomes $\partial_y|_\theta \overline{p} \approx \overline{\partial_z p}\, \partial_y|_\theta \overline{z}$. As in the QG problem, the mass fluxes in the two layers can be written in terms of the PV diffusivity multiplied by the sum of a contribution associated with the layer-integrated planetary vorticity gradient, β, and a contribution associated with the thickness gradient in each layer, which in turn is given by the isentropic slope at the interface.

As in the QG case, Eq. (3.37) can be used to derive a scaling relation for the criticality parameter as

$$\xi \sim \frac{fs}{\beta H} \sim \frac{\tilde{D}}{\Delta D}, \tag{3.38}$$

where $\tilde{D} \equiv \left((\overline{p_s}^s - \overline{p}(\theta_1))D_1 + (\overline{p}(\theta_1) - \overline{p}(\overline{\theta}_t))D_2\right) / (\overline{p_s}^s - \overline{p}(\overline{\theta}_t))$ denotes the vertical mean of the eddy diffusivity, $\Delta D \equiv D_1 - D_2$, $s \equiv \partial_y|_\theta \overline{z}(\theta_1)$, and $H \equiv -\overline{\partial_p z}(\theta_1)\,(\overline{p_s}^s - \overline{p}(\overline{\theta}_t))$. The scaling relation in Eq. (3.38) is analog to the two-layer QG result in Eq. (3.6).

Notice, that we had to require that the lower layer shall include the entire surface layer. Apart from that requirement, Eq. (3.38) can technically be derived for any choice of the height of the layer interface. However, the bulk diffusivities D_1 and D_2 represent poorly defined layer averages if the weighting factor, $(\rho_\theta / f\beta - \partial_y \rho_\theta)$, takes on large positive and negative values within a single layer. The sign of this factor is given by the sign of the extended PV gradient, and is typically negative throughout the SL, due to the dominant contribution associated with the isentropic outcrops. An adequate choice of the layer interface is thus given by the first level above the SL where the PV gradient becomes positive. Schneider (2005) finds that this is typically just above the SL; in the simulation discussed here, the sign change occurs somewhat higher than the top of the SL.

Relation (3.38) shows that vertical variations in the eddy diffusivity over the troposphere may be small (compared to its mean value) only if $\xi \gg 1$, which is in agreement with the fact that eddies tend to be more barotropic in the limit of large supercriticalities. If, on the other hand, the criticality is of order one, vertical variations in the eddy diffusivity are expected to be on the same order as the eddy diffusivity itself. This is in agreement with the numerical simulation discussed in

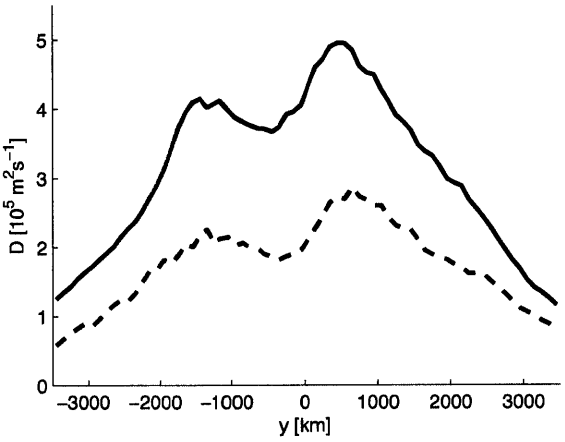

Figure 3-4: Surface (solid) and upper-tropospheric (dashed) eddy diffusivity. The surface eddy diffusivity is calculated form a flux-gradient relationship of surface potential temperature as in Eq. (3.24). The upper tropospheric eddy diffusivity is calculated as an effective bulk eddy diffusivity integrated from the first level above the SL where the PV gradients becomes positive, θ_1, to the top of the troposphere as $D_{UT} = \int_{\theta_1}^{\bar{\theta}_t} \frac{\overline{\rho_\theta \hat{v}\hat{P}^*}}{\overline{P}^*} / \int_{\theta_1}^{\bar{\theta}_t} \frac{\overline{\rho_\theta}\partial_y \overline{P}^*}{\overline{P}^*} d\theta$. Notice, that both quantities are independent of the definition of PV fluxes and gradients on near-surface isentropes.

section 3.4. A rough estimate for the criticality in the simulation can be obtained from Fig. 3-2. With $a = \frac{f}{\beta} = 6250\,\mathrm{Km}$, we have $\xi = \frac{a}{H} s \approx 2$, which is in qualitative agreement with the observed upper tropospheric eddy diffusivity being approximately 50% smaller than the eddy diffusivity near the surface (see Fig 3-4). An extensive series of numerical simulations supporting the scaling relation (3.38) will be discussed in chapter 4.

The argument for the relationship between the criticality and the vertical structure of D is closely related to the analysis by Held (1978, 1982), who argues that the criticality parameter needs to be close to one, if the depth of the tropopause is set by the depth scale of the baroclinic eddies, and therefore equals the vertical scale over which the eddy diffusivity decays. This is likely to be the case in the present atmosphere and for a considerable range of parameters around the present state, which would explain why the criticality of the atmosphere is O(1), and is reported to be rather insensitive to changes in the external forcing in numerical simulations (Schneider, 2004; Schneider and Walker, 2006). However, the previous chapter has shown

that supercritical mean states are possible if one forces the system to be very different from today's atmosphere. According to relation (3.38) such states are possible if the eddy diffusivity decays only weakly over the depth of the troposphere. The scaling relation in (3.38) by itself, is not a predictive theory for the criticality. Such a theory would require an independent prediction for the vertical structure in D.

3.6 Conclusions

We used the isentropic zonal momentum budget of the troposphere, to derive a scaling relation, which links the criticality parameter to the vertical structure of the eddy diffusivity (Eq. 3.38). We found that the criticality parameter scales as the ratio of the vertical decay of the eddy diffusivity over the depth of the troposphere, to the vertical mean of the eddy diffusivity. Marginally critical states are expected if the eddy diffusivity decays from its surface value to about zero in the upper troposphere, that is if the relative vertical variations of the eddy diffusivity are O(1). Supercritical states are predicted if the eddy diffusivity varies only weakly in the vertical. Subcritical states would require the eddy diffusivity to decrease rapidly over a scale much smaller than the depth of the troposphere.

This result is in contrast to that of Schneider (2004), who argued that, in primitive equations, marginally critical states are obtained with an eddy diffusivity that is vertically constant throughout the whole depth of the troposphere, while strongly supercritical states are impossible. The difference stems from the different approaches taken to compute averages along isentropes in the surface layer. We use a closure for the interior eddy PV flux as defined in Koh and Plumb (2004), which can be justified by analysis of the PV variance budget and is supported by idealized numerical simulations. Schneider (2004) instead uses a closure for an extended eddy PV flux, which includes contributions from isentropes below the surface. We argue that this closure over-represents the surface layer mass transport associated with the form drag on outcropping isentropes.

With our approach, the relation between the criticality and the vertical structure

of the eddy diffusivity is a direct extension of Green's (1970) result based on QG theory. Differences from the QG results are only quantitative in nature, and arise due to the finite isentropic slope and intersections of isentropes with the ground. Schneider's (2004) result instead does not reduce to the QG result, even in the limit of small isentropic slopes.

The revised scaling relationship has important implications for the macroturbulent equilibration of an atmosphere. In particular, the criticality parameter is no longer constrained to one. Both marginally critical and strongly supercritical states are possible, if the magnitude and vertical structure of the eddy diffusivity can change. Theories for the eddy diffusivity are therefore needed to predict the response of the criticality parameter to changes in external parameters.

A number of additional effects important for the real atmosphere have been ignored in this study. For example, complex boundary layer dynamics and moisture both introduce sources and sinks of PV, raising questions about whether diffusive closures for the eddy PV fluxes hold, especially near the surface. Our work should be seen as a step in a hierarchy of studies. We extended results from QG theory to an idealized primitive equation system. Next we will need to connect our scaling for the extra-tropical adjustment to more realistic settings. This is left for future work.

APPENDIX A

The PV Variance Budget and the Closure Problem

We want to relate the eddy PV flux to mean quantities in terms of a diffusive closure, which assumes that eddy PV fluxes are directed down the mean PV gradient. In the following we present justification for such a closure using the interior PV approach, based on the PV variance budget.

An equation for the thickness weighted zonal mean PV

We start with the adiabatic potential vorticity equation in isentropic coordinates (e.g. Vallis, 2006)

$$\partial_t P + \mathbf{u}\cdot\nabla_\theta P = -rP \tag{3.A1}$$

where ∇_θ denotes the horizontal nabla operator, with derivatives taken along isentropes, and $\mathbf{u}$ denotes the horizontal velocity vector. Dissipation is here represented by a simple linear Rayleigh sink term, but other dissipation mechanisms would lead to qualitatively similar results, as long as they tend to reduce the PV variance (see also Plumb, 1979). Taking the generalized thickness weighted isentropic average of (3.A1), and re-arranging terms, yields

$$\partial_t\overline{P}^* - \overline{\frac{P}{\overline{\rho_\theta}}\partial_t\rho_\theta} + \overline{\frac{\rho_\theta P}{\overline{\rho_\theta}^2}}\partial_t\overline{\rho_\theta} + \frac{1}{\overline{\rho_\theta}}\nabla_\theta(\overline{\rho_\theta}\,\overline{\mathbf{u}}^*\overline{P}^*) + \frac{1}{\overline{\rho_\theta}}\nabla_\theta\overline{\rho_\theta\hat{\mathbf{u}}\hat{P}} - \overline{\frac{P}{\overline{\rho_\theta}}\nabla_\theta\cdot(\mathbf{u}\rho_\theta)} = -r\overline{P}^* \,. \tag{3.A2}$$

We can now use the (adiabatic) thickness equation

$$\partial_t\rho_\theta + \nabla_\theta\cdot(\mathbf{u}\rho_\theta) = 0\,, \tag{3.A3}$$

which can be shown to hold similarly for the generalized thickness[4] ρ_θ, to cancel the

[4]The conservation equation for the generalized thickness (3.A3) can be derived from the conservation equations for thickness $\partial_t\sigma + \nabla_\theta\cdot(\mathbf{u}\sigma) = 0$ (e.g. Andrews et al., 1987) and the thermodynamic equation for surface potential temperature $\partial_t\theta_s + \mathbf{u}\cdot\nabla\theta_s = 0$.

second and the last terms on the L.H.S. of (3.A2). If we further use the isentropic average of (3.A3) to rewrite the third term on the L.H.S. of (3.A2) as $\frac{\overline{\rho_\theta P}}{\overline{\rho_\theta}^2}\partial_t\overline{\rho_\theta} = \frac{\overline{P}^*}{\overline{\rho_\theta}}\partial_t\overline{\rho_\theta} = -\frac{\overline{P}^*}{\overline{\rho_\theta}}\nabla_\theta\cdot(\overline{\rho_\theta}\,\overline{\mathbf{u}}^*)$, we arrive at

$$\partial_t\overline{P}^* + \overline{\mathbf{u}}^*\cdot\nabla_\theta\overline{P}^* + \frac{1}{\overline{\rho_\theta}}\nabla_\theta\cdot(\overline{\rho_\theta\hat{\mathbf{u}}\hat{P}}) = -r\overline{P}^*\,. \tag{3.A4}$$

An equation for PV variance

Subtracting Eq. (3.A4) from (3.A1), we obtain an equation for the PV perturbations $\hat{P} = P - \overline{P}^*$,

$$\partial_t\hat{P} = -\mathbf{u}\cdot\nabla_\theta\hat{P} - \hat{\mathbf{u}}\cdot\nabla_\theta\overline{P}^* + \frac{1}{\overline{\rho_\theta}}\nabla_\theta\cdot(\overline{\rho_\theta\hat{\mathbf{u}}\hat{P}}) - r\hat{P}\,. \tag{3.A5}$$

To derive a variance equation, we multiply both sides by $\rho_\theta\hat{P}$ and average, which after some algebra yields

$$\frac{1}{2}\partial_t\overline{\rho_\theta\hat{P}^2} - \frac{1}{2}\overline{\hat{P}^2\partial_t\rho_\theta} = -\frac{1}{2}\nabla_\theta\cdot(\overline{\rho_\theta\mathbf{u}\hat{P}^2}) + \frac{1}{2}\overline{\hat{P}^2\nabla_\theta\cdot(\rho_\theta\mathbf{u})} - \overline{\rho_\theta\hat{\mathbf{u}}\hat{P}}\cdot\nabla_\theta\overline{P}^* - r\overline{\rho_\theta\hat{P}^2} \tag{3.A6}$$

The thickness equation (3.A3) implies that the second term on the L.H.S. and the second term on the R.H.S. cancel. For a zonally re-entrant channel, the budget simplifies to

$$\frac{1}{2}\partial_t(\overline{\rho_\theta}\,\overline{\hat{P}^2}^*) = -\frac{1}{2}\partial_y(\overline{\rho_\theta}v\overline{\hat{P}^2}^*) - \overline{\rho_\theta}\overline{\hat{v}\hat{P}}^*\partial_y\overline{P}^* - r\overline{\rho_\theta}\overline{\hat{P}^2}^* \tag{3.A7}$$

Note, that the triple correlation is included in the flux term (i.e. the first term on the R.H.S.), which describes the flux of PV variance associated with the total meridional velocity $v = \overline{v}^* + \hat{v}$. If the turbulence is sufficiently homogeneous, such that the meridional advection of variance can be ignored, we find that in a statistically steady state

$$\overline{\hat{v}\hat{P}}^*\partial_y\overline{P}^* = -r\overline{\hat{P}^2}^*\,. \tag{3.A8}$$

Since the R.H.S. of (3.A8) is negative definite, the thickness weighted eddy PV flux has to be down the thickness weighted mean gradient. If the turbulence is not homo-

geneous, and the meridional advection of PV variance is a dominant contribution, a local down-gradient closure is not defensible, though the eddy PV flux still needs to be down-gradient in a domain-averaged sense.

APPENDIX B

Relations between the Interior and Extended PV Fluxes and Gradients in the SL

We here want to show how the mass transport associated with the extended eddy PV flux, can be written in terms of the mass transport associated with the eddy flux of interior PV, plus roughly *half* of the mass transport associated with the surface eddy potential temperature flux. The extended PV gradient, instead can be written in terms of the interior PV gradient, plus a contribution associated with the *full* eddy PV gradient.

The extended eddy PV flux contribution to the mass transport can be re-written by subtracting Eq. (3.20) from (3.21), which yields

$$\begin{aligned} F^{ext}_{\overline{\hat{v}\hat{P}^*}} &= F_{\overline{\hat{v}\hat{P}^*}} + F_{\overline{v'_s\theta'_s}} - F^{ext}_{\overline{v'_s\theta'_s}} \\ &\approx F_{\overline{\hat{v}\hat{P}^*}} + \frac{1}{2}F_{\overline{v'_s\theta'_s}}, \end{aligned} \tag{3.B1}$$

where for the last step we used that $F^{ext}_{\overline{v'_s\theta'_s}} \approx \frac{1}{2}F_{\overline{v'_s\theta'_s}}$, because $\overline{P_{ext}}^*(\overline{\theta_s}) \approx 2\overline{P}^*(\overline{\theta_s})$, as shown in Eq. (3.23).

Using that[5] $\overline{P_{ext}}^* = \Pi^{-1}\overline{P}^*$, where we defined $\Pi(\theta) \equiv \overline{\mathcal{H}(\theta - \theta_s)}$, we find that the estimated mass transport associated with the extended PV gradient, on the other

[5]Note, that $\overline{P_{ext}}^* \equiv \frac{f}{\overline{\rho\theta}}$, while $\overline{P}^* \equiv \frac{\overline{\mathcal{H}(\theta-\theta_s)f}}{\overline{\rho\theta}} = \Pi\,\overline{P_{ext}}^*$

hand, becomes

$$
\begin{aligned}
F^{ext}_{D\partial_y\overline{P}^*} &= \int_{\theta_b}^{\theta_i} \frac{\overline{\rho_\theta} D_s \partial_y \overline{P_{ext}}^*}{\overline{P_{ext}}^*} d\theta \\
&= \int_{\theta_b}^{\theta_i} \frac{\overline{\rho_\theta} D_s \partial_y \overline{P}^*}{\overline{P}^*} d\theta - \int_{\theta_b}^{\theta_i} \overline{\rho_\theta} \Pi^{-1} D_s \partial_y \Pi \, d\theta \\
&= \int_{\theta_b}^{\theta_i} \frac{\overline{\rho_\theta} D_s \partial_y \overline{P}^*}{\overline{P}^*} d\theta + \overline{\int_{\theta_b}^{\theta_i} \frac{f}{\overline{P}^*} D_s \delta(\theta - \theta_s) \partial_y \theta_s \, d\theta} \\
&\approx \int_{\theta_b}^{\theta_i} \frac{\overline{\rho_\theta} D_s \partial_y \overline{P}^*}{\overline{P}^*} d\theta + \frac{f}{\overline{P}^*(\overline{\theta_s})} D_s \partial_y \overline{\theta_s}^s \qquad \text{(3.B2)} \\
&= F_{D\partial_y\overline{P}^*} + F_{D\partial_y\overline{\theta_s}^s} \, .
\end{aligned}
$$

APPENDIX C

Comparison to "PV Sheet" Formulations

The extended PV, P_{ext} defined by Schneider (2004) has similarities to the "PV-sheet" formulation that is commonly used to avoid non-homogeneous boundary conditions in QG dynamics (Bretherton, 1966). Extensions of this formulation to primitive equations have been proposed by Andrews (1983) and Schneider et al. (2003). The formulation in Andrews (1983) uses an isentropic coordinate formulation and describes isentropes which intersect with the surface as closing in an infinitesimal surface sheet. The relation of the approaches discussed above, to such a PV sheet formulation will be addressed here.

The total isentropic mass transport (i.e. the L.H.S. of Eq. 3.14), is unaltered whether or not we assume that isentropes intersect the surface or close in an infinitesimal sheet just above the surface, since the geostrophic velocity is continuous (and thus finite) in this sheet and its thickness is by construction infinitesimal. Since the explicit surface potential temperature flux contribution on the R.H.S. of Eq. (3.14) vanishes if isentropes are assumed to close in an infinitesimal sheet above the surface, this contribution has to be absorbed by the PV flux contribution. The isentropic mass budget (3.14) then reduces to

$$\int_{\theta_b}^{\theta i} \overline{\rho_\theta}\,\overline{v}^*\,d\theta \approx -\int_{\theta_b}^{\theta_i} \frac{\overline{\overline{\rho_\theta}\hat{v}\hat{P}}^*}{\overline{P}^*}\,d\theta\,. \tag{3.C1}$$

The thickness weighted average of PV in the PV sheet is well defined if we first construct a scenario in which isentropes close in a finite sheet above the surface, in which case $\overline{P}^* = f/\overline{\sigma}$, and then take the limit in which the thickness of this sheet goes to zero, i.e. $\sigma = 0$ on isentropes within the sheet. The thickness defined this way thus becomes analog to the generalized thickness $\rho_\theta = \mathcal{H}(\theta - \theta_s)$ as defined above (but with θ_s now denoting the potential temperature just above the surface

sheet). Consequentially, the thickness weighted PV becomes similar to the extended PV defined above, since $\overline{P}^* \rightarrow f/\overline{\rho_\theta} = \overline{P_{ext}}^*$.

The eddy PV flux $\overline{\hat{v}\hat{P}}^*$, however, does not reduce to the expression $\overline{\hat{v}_{ext}\hat{P}_{ext}}^*$, since the geostrophic velocity is continuous in the surface sheet[6], while v_{ext} was defined to be zero on the "sub-surface" part of the isentrope. This explains the difference between the SL mass transport associated with the eddy flux $\overline{\hat{v}\hat{P}}^*$ in the PV sheet limit, which by construction contains the full "surface" contribution, and the SL mass transport associated with $\overline{\hat{v}_{ext}\hat{P}_{ext}}^*$, which contains only about half of the surface contribution (Eq. (3.27)).

If we use the diffusive closure for the PV flux in the PV sheet limit: $\overline{\hat{v}\hat{P}}^* = -D\partial_y\overline{P}^*$, Eq. (3.C1) becomes

$$\int_{\theta_b}^{\theta i} \overline{\rho_\theta}\,\overline{v}^* d\theta \approx \int_{\theta_b}^{\theta_i} \frac{\overline{\rho_\theta} D\partial_y \overline{P}^*}{\overline{P}^*} d\theta \rightarrow \int_{\theta_b}^{\theta_i} \frac{\overline{\rho_\theta} D\partial_y \overline{P_{ext}}^*}{\overline{P_{ext}}^*} d\theta\,. \tag{3.C2}$$

Unlike in the extended PV approach used in Schneider (2004), Eq. (3.C2) together with Eq. (3.B3), yields the same result as is obtained using a closure for the eddy flux of interior PV and surface potential temperature.

[6]Note that, since the pressure gradient in an infinitesimal surface sheet is similar to the surface pressure, the geostrophic velocity would be continuous into the sheet but vary somewhat within the sheet, due to the varying density. These variations are on the order of $\frac{\rho^{-1}-\rho_s^{-1}}{\rho_s^{-1}} = \frac{\theta-\theta_s}{\theta_s}$, where the index s here denotes values just above the surface sheet. Since the potential temperature θ in the surface sheet takes on all surface potential temperature values over the regarded domain, the geostrophic velocities over the whole depth of the surface sheet can be assumed similar to the velocity just above the sheet if $\frac{\Delta\theta_s}{\theta_S} \ll 1$, where $\Delta\theta_s$ denotes the horizontal surface potential temperature variation over the domain. The geostrophic velocity in the surface sheet is exactly equal to the geostrophic surface velocity if the Boussinesq approximation is valid.

Chapter 4

The Vertical Structure of the Eddy Diffusivity – Observations and Numerical Results.

4.1 Introduction

It is commonly held that turbulent eddies equilibrate the extra-tropical atmosphere by fluxing PV and surface potential temperature down their mean gradient. As first shown by Green (1970), the structure of theses eddy fluxes is constrained by the vertically integrated quasi-geostrophic (QG) zonal momentum budget. If the eddy fluxes of PV and surface buoyancy can be expressed by a diffusive closure, this constraint yields a relation between the equilibrated zonal mean state, and the vertical structure of the eddy PV diffusivity over the depth of the troposphere. The result suggests that, for any finite criticality parameter, ξ, the eddy diffusivity needs to decay in the vertical, over the depth of the troposphere. Marginally critical states (i.e. $\xi \approx 1$), as observed in the Earth's extra-tropics, are obtained if the eddy diffusivity decays from its surface value to about zero near the tropopause.

Schneider (2004) argued that the zonal momentum budget in full primitive equations returns a different relation than in QG. Unlike in QG, he finds that marginally

critical states are obtained with an eddy diffusivity that is vertically constant throughout the whole depth of the troposphere, while strongly supercritical states are argued to be impossible (Schneider and Walker, 2006). The result of Schneider (2004), however, was questioned in the previous chapter, where we instead argued that primitive equations and QG are equivalent, if isentropic averages are defined appropriately.

We derived a relation between the criticality parameter and the vertical structure of the eddy diffusivity as

$$\frac{\tilde{D}}{\Delta D} \sim \xi, \tag{4.1}$$

where $\tilde{D}$ denotes a vertical mean of the tropospheric eddy diffusivity of PV, and ΔD denotes a bulk difference between the eddy diffusivities in the lower and upper troposphere. Eq. (4.1) states that mean states close to marginal criticality (i.e. $\xi \approx 1$) require the eddy diffusivity to decay strongly over the depth of the troposphere. Strongly supercritical states could instead have eddy diffusivities approximately constant throughout the whole depth of the troposphere.

This chapter analyzes the vertical structure of the eddy PV diffusivity in the troposphere. Since Earth's extra-tropics are in a state near marginal criticality, Eq. (4.1) requires that the eddy diffusivity decays substantially over the depth of the troposphere. This is confirmed by re-analysis data, which shows that the extra-tropical eddy diffusivity of PV and surface potential temperature, decays from large values near the surface, to almost zero near the tropopause.

To test the scaling relation in Eq. (4.1) more quantitatively, and to analyze its general implications for the turbulent equilibration of a baroclinic flow, we further analyze a series of idealized numerical simulations, with varying Coriolis parameters f and planetary vorticity gradients β. The simulations quantitatively confirm the proposed scaling relation between the criticality parameter and the vertical structure of the eddy diffusivity. However, they also show that this relation does not pose an obvious constraint on the possible values of the criticality parameter. We show that the vertical structure of the eddy diffusivity does vary a lot for particular choices of f and β, thus allowing similarly large variations in the criticality parameter.

This chapter is organized as follows. In section 4.2, we present an analysis of the isentropic eddy diffusivities of PV from re-analysis data. In section 4.3, we discuss the results of a series of numerical simulations, which exhibit strongly varying criticality parameters. The results of the simulations are used to quantitatively test the relation between the criticality parameter and the vertical structure of the eddy diffusivity in Eq. (4.1). Some concluding remarks are presented in section 4.4.

4.2 Observations

In this section we analyze the vertical structure of the eddy diffusivity in the extra-tropical atmosphere. Haynes and Shuckburgh (2000) estimated tropospheric and lower stratospheric passive tracer diffusivities, using the effective diffusivity diagnostic proposed by Nakamura (1996). Their results suggest that the extra-tropical eddy diffusivity decays strongly between the 300K surface and the tropopause. This is in qualitative agreement with the prediction of Eq. (4.1), which for Earth's atmosphere predicts a strong overall decrease in the eddy diffusivity over the depth of the troposphere. Unfortunately, the analysis of Haynes and Shuckburgh (2000) does not extend below the 300K surface, and thus misses a significant part of the extra-tropical lower troposphere.

We here want to estimate the eddy diffusivity of PV and of surface potential temperature directly from the ratio of the eddy flux to the mean gradient in the ERA-40 reanalysis. The theoretical arguments for the relation between the vertical structure of the eddy diffusivity and the criticality of the equilibrated mean state generally assume that the eddy diffusivity of surface potential temperature is similar to the PV diffusivity near the surface. This is to be expected if the eddy diffusivity can be regarded as a fundamental property of the flow, which is independent of the conserved tracer, and has been confirmed in numerical simulations in chapter 4. The PV diffusivity in the upper troposphere, however, can be strongly different from the near surface diffusivity, as will be shown below.

The thickness weighted mean PV, $\overline{P}^*$, and eddy PV flux, $\overline{\hat{v}\hat{P}}^*$, are calculated

as proposed by Koh and Plumb (2004). $P \equiv (f + \zeta)/(g^{-1}\partial_\theta p)$ is the isentropic PV, where $\zeta = \partial_x v - \partial_y u$ is the relative vorticity, with derivatives taken along θ surfaces. $\overline{()}^* \equiv \overline{\rho_\theta()}/\overline{\rho_\theta}$ denotes an isentropic time- and zonal-average, weighted by the generalized thickness, $\rho_\theta \equiv -\mathcal{H}(\theta - \theta_s)g^{-1}\partial_\theta p$, and $\hat{()}$ denotes deviations from the generalized thickness weighted average. $\mathcal{H}(\theta - \theta_s)$ is the Heaviside function, and θ_s is the surface potential temperature. The Heaviside function in the definition of the generalized thickness weighted average takes care that averages are taken only over regions where the isentrope is above the ground.

A problem that arises when calculating isentropic diagnostics from atmospheric data is the frequent occurrence of statically unstable stratification in the planetary boundary layer. A dynamically meaningful coordinate transformation from pressure coordinates into isentropic coordinates requires that $\theta(p)$ be monotonic. To avoid this problem, we here ignore the lowest 10 model levels[1] of the re-analysis data, which comprise about the lowest kilometer above the surface and contain virtually all occurrences of negative $\partial_p\theta$. Averages on isentropes which intersect with this boundary layer are treated as discussed above, but with the surface potential temperature θ_s being replaced by the potential temperature at the top of this layer.

Figure 4-1 shows the thickness weighted isentropic eddy PV flux and gradient as a function of latitude and θ, calculated from all-year averages over the period from 1982 to 2001. PV fluxes are mostly negative, while the PV gradient is mostly positive throughout the troposphere and lower stratosphere, in agreement with the notion of generally down-gradient eddy fluxes. While PV fluxes are down-gradient in a bulk averaged sense, up-gradient PV fluxes are observed locally around the subtropical jet (this has recently been observed also by Birner, personal communication). The vertical structure of the PV gradients in the extra-tropical troposphere reveals low values in the lower troposphere and maxima near the tropopause. The eddy fluxes, on the other hand remain more constant throughout the troposphere, so that the eddy diffusivity decreases towards the upper troposphere and tropopause region.

[1]The model uses a hybrid coordinate system. The pressure at the top of the 10th model level is given as $p = 3850.91$ Pa$+0.847375 \times p_s$, where p_s denotes the local surface pressure.

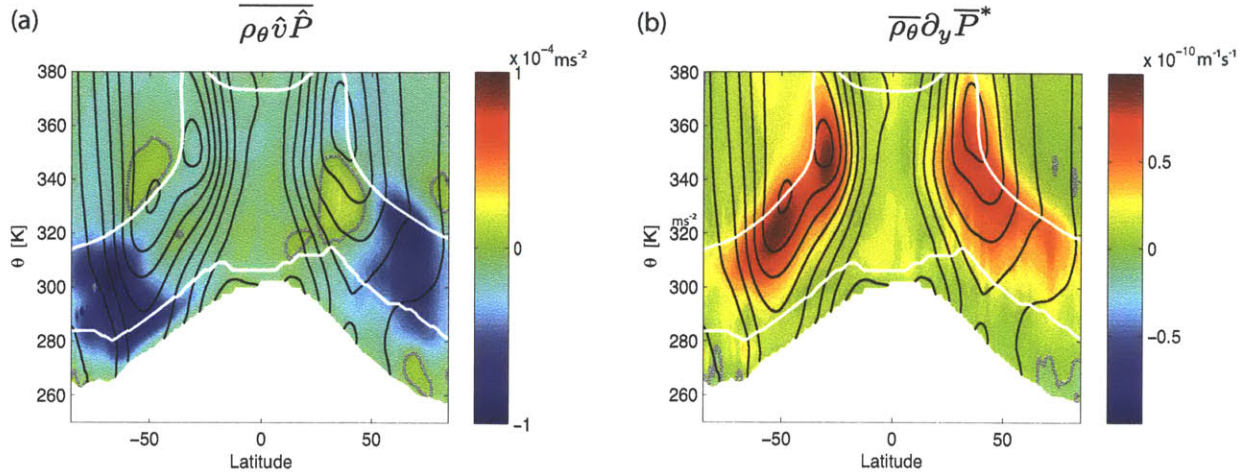

Figure 4-1: **(a)** Thickness weighted isentropic PV fluxes, $\overline{\rho_\theta \hat{v}\hat{P}}$, from the ERA-40 reanalysis (color shading). The grey contours denote zero PV flux. The black contours show the zonal mean zonal wind. The white lines indicate the top of the surface layer (here defined by the 95% quantile of potential temperature at the top of the boundary layer) and the tropopause (defined by a lapse rate of $dT/dz = 2K/km$). **(b)** As (a), but with the color shading showing the thickness weighted isentropic PV gradient, $\overline{\rho_\theta}\partial_y\overline{P}^*$.

The vertical decrease in the eddy diffusivity is confirmed by figure 4-2, which shows the isentropic eddy PV diffusivity, calculated as

$$D = \frac{\overline{\hat{v}\hat{P}}^*}{\partial_y \overline{P}^*} . \tag{4.2}$$

We find large vertical variability in the eddy diffusivity over the depth of the tropopause, with a strong overall vertical decrease between the surface layer and the tropopause, in the extra-tropics. This is in agreement with the predictions of chapter 3.

For comparison, we also estimate the near-surface eddy diffusivity of potential temperature, as

$$D_s \equiv \frac{\overline{v'\theta'}^s}{\partial_y \overline{\theta}^s}, \tag{4.3}$$

where $\overline{()}^s$ denotes an average along the first model level above the boundary layer, as defined above. The results shown in figure 4-2 support the notion that the extra-tropical near-surface eddy diffusivity of potential temperature is of similar magnitude

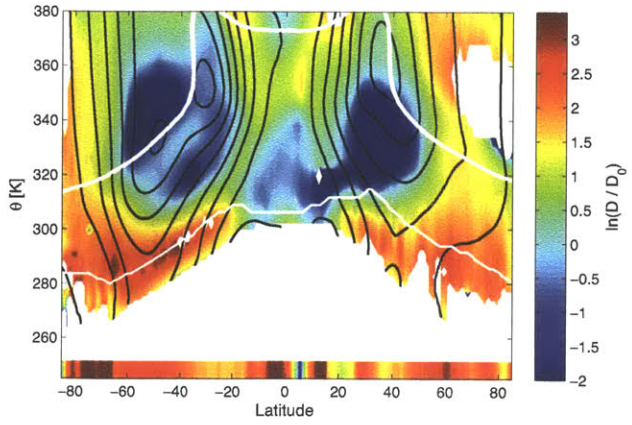

Figure 4-2: Estimate of the isentropic eddy PV and near surface potential temperature diffussivities from ERA-40 reanalysis data. The near-surface eddy diffusivity of potential temperature is represented by the bar at the bottom. The figure is cut of below the 5% quantile of the near-surface potential temperature (defined as the potential temperature at the top of the removed boundary layer) and the thin white line shows the 95% quantile of the near-surface potential temperature. The thick white line denotes an estimate of the tropopause (here calculated as the level where the stratification reaches $-2K/km$). Notice that the colorbar is logarithmic, with the normalization, $D_0 = 3.24 \times 10^5$, chosen as in Haynes and Shuckburgh (2000). The colorbar is saturated in the dark blue regions, over which the eddy diffusivity is small and mostly negative.

as the PV diffusivity in the surface layer. Notice that the eddy PV diffusivity varies significantly throughout the depth of the surface layer, and becomes poorly defined towards its bottom (which comprises potential temperature values which are only rarely found at the given latitude). The mean PV diffusivity over the surface layer, however, agrees well with the near-surface eddy diffusivity of surface potential temperature, everywhere outside of the tropics and latitudes with large topography (not shown).

The results in figure 4-2 are qualitative similar to the effective diffusivities computed by Haynes and Shuckburgh (2000), though there are also some notable differences. In particular, the eddy PV diffusivity calculated from the flux/gradient ratio shows regions of weakly negative diffusivities associated with the PV flux reversals near the subtropical jets. The effective diffusivity calculated by Haynes and Shuckburgh (2000) shows small values in the regions of the subtropical jets, but it is by

definition always positive. Furthermore, the regions of vanishingly small eddy PV diffusivities seem to extend further downwards into the troposphere than the effective diffusivity minima reported in Haynes and Shuckburgh (2000). Notice, that it is the actual PV diffusivity, as calculated here, which is relevant for the theoretical arguments discussed above. To what extent this is equivalent to Nakamura's (1996) effective diffusivity remains unclear.

4.3 Numerical Simulations

We now test the scaling relation in Eq. (4.1) by analyzing a series of numerical simulations with strongly varying criticality parameters. We use an idealized β-plane channel configuration, which allows us to vary the Coriolis parameter f and the planetary vorticity gradient β separately and without changing the size of the domain. Notice, that on a spherical planet, f and β are related through the planetary scale. However, it is the dynamical scale $a \equiv f/\beta$, which goes into the definition of the criticality parameter, $\xi \sim a/Hs$, and thus determines the characteristics of the flow. Exploring various combinations of f and β, thus proves to be an efficient way to greatly vary the criticality parameter of the equilibrated mean state, and thus test the theoretical arguments discussed above.

4.3.1 Model Setup

The model and setup is similar to the one discussed in chapter 3: a zonally reentrant β-plane channel, 15,000 km long, bounded meridionally by side walls at y=$\pm$ 4500km, and vertically by a rigid lid at z=H=10.2km and a flat bottom at z=0. Free slip boundary conditions are used on all boundaries, and kinetic energy is removed by a linear Rayleigh drag with a constant drag coefficient of $r = (50\text{days})^{-1}$ throughout the domain. We use a linear equation of state with a thermal expansion coefficient of $\alpha = 3.6 \cdot 10^{-4} K^{-1}$, i.e. $b = g\alpha(\theta - \theta_0)$, where b is buoyancy, θ_0 a reference potential temperature, and g the acceleration of gravity. The thermal expansion coefficient used here is larger than that in chapter 3 and was chosen to resemble the

thermal expansion of air. The simulations are forced through relaxation to the same equilibrium temperature profile used in chapter 3 (figure 3-1). The relaxation time-scale is $\tau_s = 14$ days at the surface and decreases exponentially, with an e-folding depth of 500 m, to an interior value of $\tau_{int} = 50$ days. The simulations are spun up until a quasi-steady state is reached. Diagnostics are calculated over at least 500days after equilibration is reached, which guarantees that the presented results are not affected by stochastic variability.

The setup was chosen to provide an idealized testbed to test the discussed theory, and avoids various possibly complicating effects, as for example compressibility and the parameterization of boundary layer and convective processes. While these effects can have a quantitative influence on the proposed relations, the qualitative results presented here should carry over to more realistic setups. A detailed analysis of the roles of these neglected processes should be the subject to future studies.

4.3.2 General Results

We performed a total of 11 simulations with Coriolis parameters $f_0 = 1, 2, 4, 8 \times 10^{-4}\mathrm{s}^{-1}$ and planetary vorticity gradients $\beta = 0.8, 1.6, 3.2 \times 10^{-11}\mathrm{m}^{-1}\mathrm{s}^{-1}$. This allows for a total of 12 possible combinations of f_0 and β. Only the combination $f_0 = 1 \times 10^{-4}\mathrm{s}^{-1}$, $\beta = 3.2 \times 10^{-11}\mathrm{m}^{-1}s^{-1}$ was omitted, since the resulting Coriolis parameter $f = f_0 + \beta y$ would change sign within the domain.

The first question to address is whether or not eddies maintain a marginally critical equilibrium state, $\xi \approx 1$, for all choices of f and β. Before looking at all simulations, we focus on two illustrative cases: one using parameters characteristic of Earth's mid-latitudes: $f_0 = 1 \times 10^{-4}\mathrm{s}^{-1}$, $\beta = 1.6 \times 10^{-11}\mathrm{m}^{-1}\mathrm{s}^{-1}$, and one using a much faster rotation rate, but less curvature: $f_0 = 8 \times 10^{-4}\mathrm{s}^{-1}$, $\beta = 0.8 \times 10^{-11}\mathrm{m}^{-1}\mathrm{s}^{-1}$. Figure 4-3 shows snapshots of surface potential temperature as well as the equilibrated time- and zonal-mean state for both simulations. In the simulations with Earth-like parameters, eddies equilibrate the system in a way that qualitatively resembles the extra-tropical atmosphere in many aspects. In particular, we find that the isentropic slope is such that the criticality parameter is around 1, i.e. $s \sim \beta H / f_0$. The simulation develops a

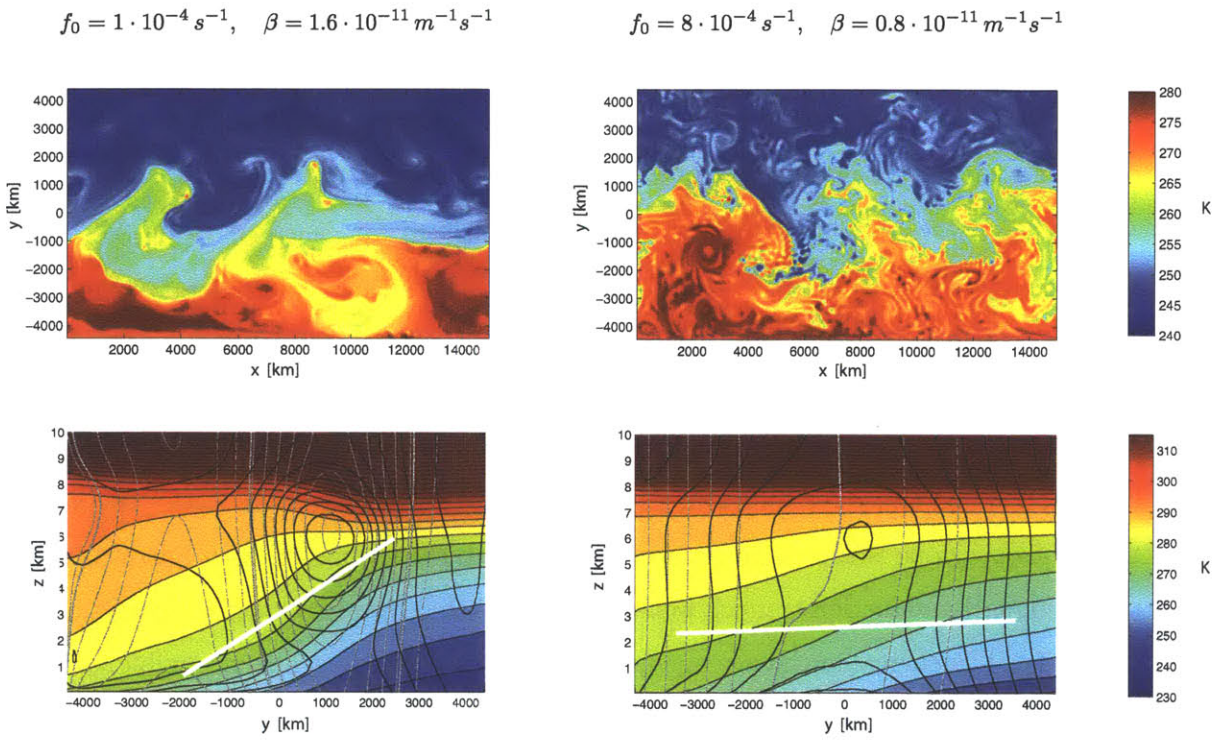

Figure 4-3: Top: Snapshots of surface potential temperature from the simulations with $f = 1 \times 10^{-4}\mathrm{s}^{-1}$, $\beta = 1 \times 10^{-11}\mathrm{m}^{-1}\mathrm{s}^{-1}$ and $f = 8 \times 10^{-4}\mathrm{s}^{-1}$, $\beta = 0.8 \times 10^{-11}\mathrm{m}^{-1}\mathrm{s}^{-1}$. Bottom: Time- and zonal-mean cross-sections for the same two simulations. Colors show potential temperature, gray lines show the zonal wind (CI: 5 ms^{-1}, and 2 ms^{-1}, for $f = 1 \times 10^{-4}\mathrm{s}^{-1}$, $\beta = 1 \times 10^{-11}\mathrm{m}^{-1}\mathrm{s}^{-1}$, and $f = 8 \times 10^{-4}\mathrm{s}^{-1}$, $\beta = 0.8 \times 10^{-11}\mathrm{m}^{-1}\mathrm{s}^{-1}$, respectively), and thin black lines show EKE (CI: $30\mathrm{m}^2\mathrm{s}^{-2}$ and $10\mathrm{m}^2\mathrm{s}^{-2}$, respectively). The thick white lines denote the characteristic isentropic slope expected if $\xi = 1$.

Table 4.1: Criticality parameters for all performed simulations.

	$f_0 = 1 \times 10^{-4}$	$f_0 = 2 \times 10^{-4}$	$f_0 = 4 \times 10^{-4}$	$f_0 = 8 \times 10^{-4}$
$\beta = 3.2 \times 10^{-11}$	/	1.2	2.0	4.0
$\beta = 1.6 \times 10^{-11}$	0.9	1.5	2.5	5.5
$\beta = 0.8 \times 10^{-11}$	1.2	2.0	3.8	8.8

very pronounced westerly jet. As in the extra-tropical atmosphere, isentropic slopes are enhanced in the center of the jet and are somewhat weaker outside.

The simulation with $f_0 = 8 \times 10^{-4}\text{s}^{-1}$, $\beta = 0.8 \times 10^{-11}\text{m}^{-1}\text{s}^{-1}$, instead, equilibrates to a strongly supercritical mean state. Notice, that the dynamical planetary scale, $a \equiv f/\beta$, is here increased by a factor of 16 relative to the Earth-like case. A marginally critical state would thus require either that the characteristic slope of the isentropes be decreased by a factor of 16, or the tropopause height be increased by a similar amount. As shown in figure 4-3, this is clearly not the case. While the isentropic slope is somewhat reduced compared to the simulation with Earth-like parameters, the reduction is much weaker than predicted by adjustment to marginal criticality. The change in the average height of the troposphere is also negligible.

Criticality parameters for all simulations are estimated as,

$$\xi \equiv \frac{f_0}{\beta H} \frac{\langle \partial_y \theta \rangle}{\langle \partial_z \theta \rangle}, \tag{4.4}$$

where $\langle ( ) \rangle$ denotes a horizontal average over the baroclinically forced region -3500 km $< y <$ 3500km, taken at the fixed level $z = 2$km (which roughly corresponds to the average height of the layer interface used to calculate bulk diffusivities below). Due to the relatively strong constraint put on the tropopause height by the restoring profile, variations in the latter are negligible over the regarded set of simulations. For simplicity, we set $H = 7.5$km in Eq. (4.4) for all simulations. The criticality parameters vary between 0.9 (for $f_0 = 1 \times 10^{-4}\text{s}^{-1}$, $\beta = 1.6 \times 10^{-11}\text{m}^{-1}\text{s}^{-1}$) and 8.8 (for $f_0 = 8 \times 10^{-4}\text{s}^{-1}$, $\beta = 0.8 \times 10^{-11}\text{m}^{-1}\text{s}^{-1}$), and are summarized in table 4.1.

As discussed in chapters 1 and 2, the criticality parameter has important implica-

tions for the characteristics of the turbulent flow. In particular, criticality parameters larger than one are associated with strongly non-linear flows, which produce a significant up-scale energy transfer, resulting in eddies much larger than the scale of the linearly most unstable mode (Held and Larichev, 1996). As discussed in Appendix B, an analysis of the spectral energy budget confirms these properties for the simulations presented in this study. The simulation with Earth-like rotational parameters reveals only a small difference between the scale of the instability and the scale of the most energetic eddies. However, this scale separation increases approximately linearly with the criticality parameter, demonstrating the increasing role of nonlinear eddy-eddy interactions.

4.3.3 The Criticality Parameter and the Vertical Structure of the Eddy Diffusivity

Next we analyze the structure of the eddy diffusivity in our model simulations, with the ultimate goal of testing the relation between the criticality parameter and the vertical structure of the eddy diffusivity derived in chapter 3. We start by focusing on the same two illustrative cases: the marginally critical Earth-like simulation, using $f_0 = 1 \times 10^{-4}\mathrm{s}^{-1}$, $\beta = 1.6 \times 10^{-11}\mathrm{m}^{-1}\mathrm{s}^{-1}$, and the strongly supercritical simulation, using $f_0 = 8 \times 10^{-4}\mathrm{s}^{-1}$, $\beta = 0.8 \times 10^{-11}\mathrm{m}^{-1}\mathrm{s}^{-1}$.

Figure 4-4 shows the isentropic eddy PV fluxes and PV gradients as a function of latitude and θ, for the two model simulations. In the upper troposphere, the PV fluxes are mostly negative, while the PV gradients are mostly positive. Below, the PV fluxes are generally weaker and mostly positive, while the PV gradients are mostly negative[2]. Overall the PV fluxes tend to be down the mean gradient, though the spacial structure of the fluxes and gradients, particularly for the more Earth-like, marginally critical simulation, with $f_0 = 1 \times 10^{-4}\mathrm{s}^{-1}$ and $\beta = 1.6 \times 10^{-11}\mathrm{m}^{-1}s^{-1}$,

[2]The weakly negative PV gradients in the lower troposphere are associated with a slight flattening of the isentropes near the surface. The flattening of the near surface isentropes in the simulations, which differs from Earth's atmosphere, could be avoided by a further reduction of the thermal restoring time-scale near the surface. We here refrain from further reducing the near-surface restoring time-scale to ensure that PV behaves approximately like a conserved quantity over the whole domain.

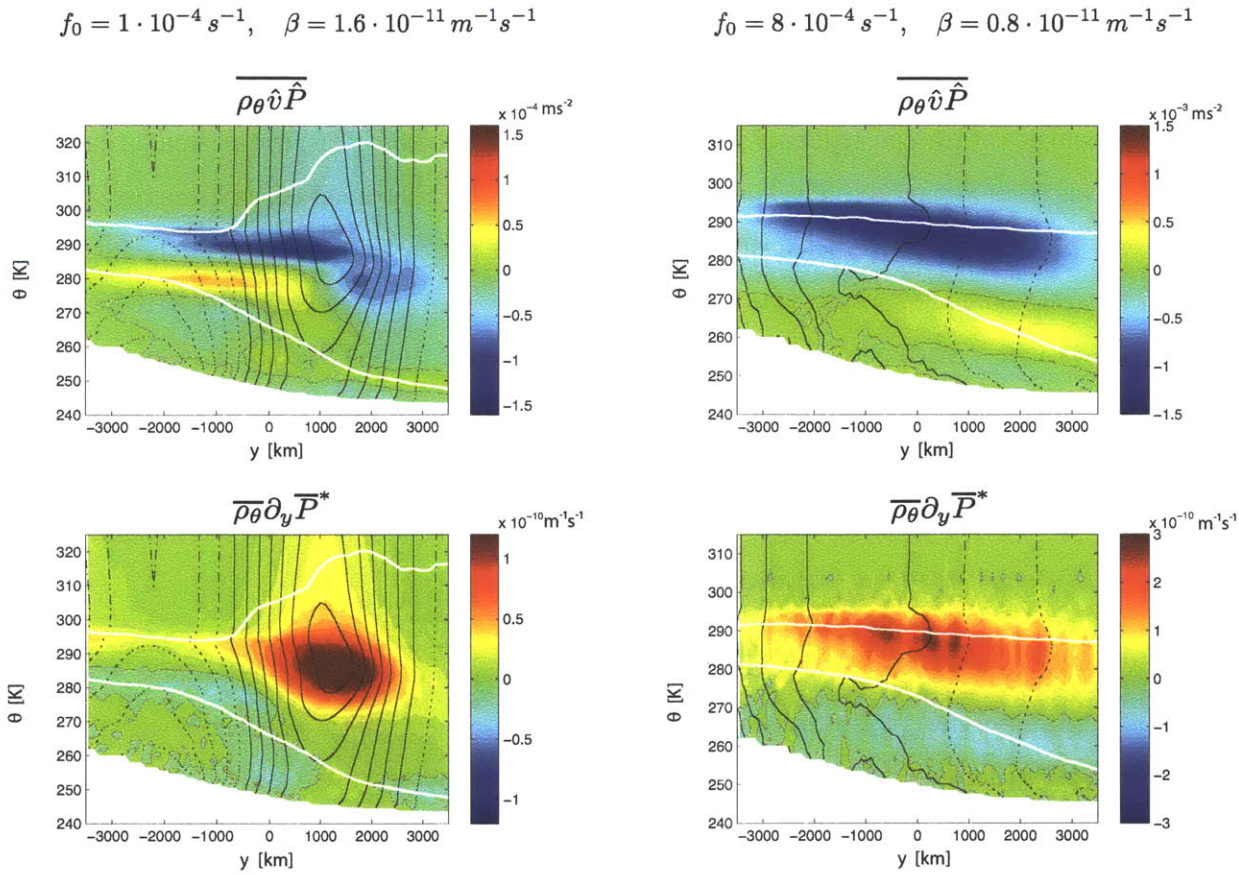

Figure 4-4: Top: Thickness weighted eddy PV flux for the simulations with $f = 1 \times 10^{-4}\mathrm{s}^{-1}$, $\beta = 1 \times 10^{-11}\mathrm{m}^{-1}\mathrm{s}^{-1}$ and $f = 8 \times 10^{-4}\mathrm{s}^{-1}$, $\beta = 0.8 \times 10^{-11}\mathrm{m}^{-1}\mathrm{s}^{-1}$. Bottom: Corresponding PV gradient for the same two simulations. Grey lines mark the zero contours of the PV fluxes and gradients. The black lines show the thickness weighted zonal-mean wind $\overline{u}^*$ (CI: 5 ms^{-1}, and 2 ms^{-1}, for $f = 1 \times 10^{-4}\mathrm{s}^{-1}$, $\beta = 1 \times 10^{-11}\mathrm{m}^{-1}\mathrm{s}^{-1}$, and $f = 8 \times 10^{-4}\mathrm{s}^{-1}$, $\beta = 0.8 \times 10^{-11}\mathrm{m}^{-1}\mathrm{s}^{-1}$, respectively). The white lines indicate the top of the surface layer (defined by the 95% quantile of surface potential temperature), and the "tropopause", used as the top of the upper layer. The "tropopause" is here defined such that it includes 85% of the northward return flow at any given latitude. Notice that, for the simulation with $f = 1 \times 10^{-4}\mathrm{s}^{-1}$, $\beta = 1 \times 10^{-11}\mathrm{m}^{-1}\mathrm{s}^{-1}$, this "tropopause" is not very well defined in the northern part of the domain, since the total mass transport is very low. The bulk diffusivities shown in figures 4-5 and 4-6, however, are not very sensitive to the exact choice for the top of the upper layer.

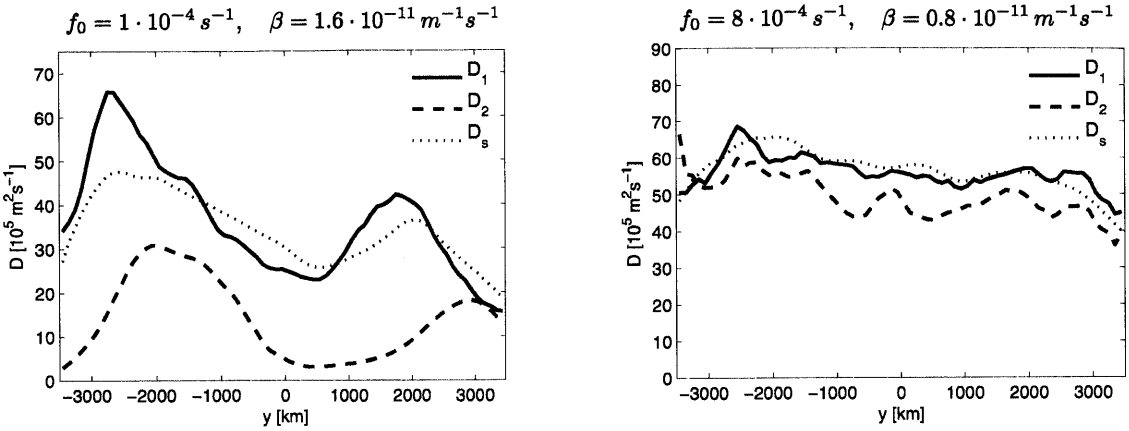

Figure 4-5: Eddy diffusivities for the simulations with $f = 1 \times 10^{-4}\text{s}^{-1}$, $\beta = 1 \times 10^{-11}\text{m}^{-1}\text{s}^{-1}$ (left), and $f = 8 \times 10^{-4}\text{s}^{-1}$, $\beta = 0.8 \times 10^{-11}\text{m}^{-1}\text{s}^{-1}$ (right). The solid lines show the bulk eddy diffusivity in the lower troposphere and the dashed lines show the bulk eddy diffusivity in the upper troposphere. For comparison, the dotted line shows the eddy diffusivity of surface potential temperature. As found in chapter 4, the latter is overall similar to the bulk diffusivity in the lower layer. All diffusivities have been smoothed by a 500km running mean.

shows some differences. Most markedly, this simulation reveals a locally very strong PV gradient near the maximum of the zonal jet, which is not reflected by a similar peak in the PV fluxes. This implies a very weak eddy diffusivity near the jet center, in agreement with the notion that zonal jets can act as diffusivity barriers (e.g. Ferrari and Nikurashin, 2010, and references therein).

The generally weak PV gradients in the lower troposphere make it difficult to define a local diffusivity from a PV flux/gradient relationship. Nevertheless, we can define bulk diffusivities for the lower and upper troposphere, which are calculated from the vertically integrated eddy PV fluxes and gradients in each layer, as discussed in Appendix A. Notice, that the bulk diffusivity for the lower troposphere here further includes a contribution associated with the eddy flux and gradient of surface potential temperature, which is similar to the PV sheet contribution in continuous QG (Bretherton, 1966).

Figure 4-5 shows the bulk eddy diffusivities in the upper and lower troposphere, for

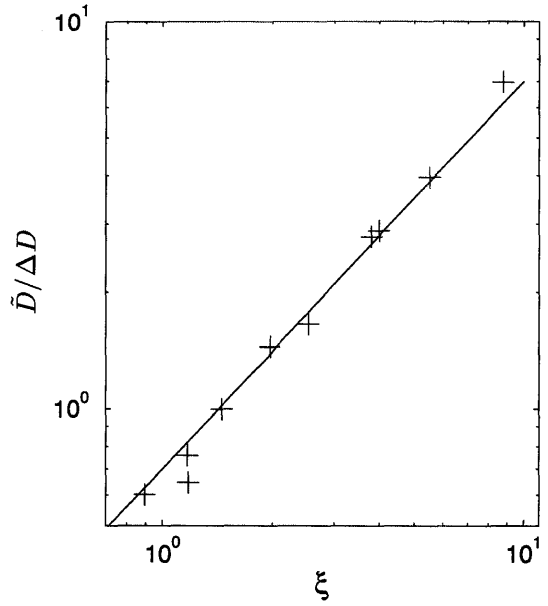

Figure 4-6: The ratio of the vertical mean of the eddy diffusivity to it's vertical decrease, $\tilde{D}/\Delta D$, against the criticality parameter, ξ. Each marker represents one simulation. The black line denotes $\tilde{D}/\Delta D = 0.7\xi$.

the Earth-like simulation with $f_0 = 1 \times 10^{-4}\mathrm{s}^{-1}$ and $\beta = 1.6 \times 10^{-11}\mathrm{m}^{-1}\mathrm{s}^{-1}$, as well as for the most supercritical simulation with $f_0 = 8 \times 10^{-4}\mathrm{s}^{-1}$, $\beta = 0.8 \times 10^{-11}\mathrm{m}^{-1}\mathrm{s}^{-1}$. In agreement with the prediction of Eq. (4.1), we see that in the Earth-like case, where $\xi \sim 1$, the eddy diffusivity decreases strongly between the lower and upper troposphere. For the simulation with $f_0 = 8 \times 10^{-4}\mathrm{s}^{-1}$ and $\beta = 0.8 \times 10^{-11}\mathrm{m}^{-1}\mathrm{s}^{-1}$, on the other hand, the eddy diffusivity in the lower and upper troposphere is quite similar, in agreement with the criticality parameter being much larger than one.

We can test the prediction of the scaling law in Eq. (4.1) more quantitatively. Figure 4-6 shows the ratio $\tilde{D}/\Delta D$, calculated from horizontal averages[3] of the bulk diffusivities in each layer, against the criticality parameter ξ, for all simulations. The results are in good agreement with the proposed scaling relation.

[3]As for the estimate of the criticality parameter, averages are taken over the baroclinically forced region between $-3500km < y < 3500km$. To avoid large contributions from locations where the PV gradient becomes very small, we here use harmonic averages of the eddy diffusivity. This yields somewhat less noisy results than the use of arithmetic averages, but does not affect the overall picture.

4.4 Conclusions

We used re-analysis data to show that the eddy PV diffusivity in the extra-tropical atmosphere decreases substantially over the depth of the troposphere. This decrease is in qualitative agreement with the scaling argument proposed in chapter 3 (Eq. 4.1), which suggests that mean states with O(1) criticality parameters require a vertical decrease of the eddy diffusivity of the same order as the diffusivity itself.

The scaling relation, which connects the criticality parameter to the vertical structure of the eddy diffusivity, is further supported quantitatively by a series of numerical simulations, using an idealized primitive equation model. Marginally critical mean states are associated with an eddy diffusivity that strongly decays in the vertical over the depth of the troposphere, while strongly supercritical mean states can have an eddy diffusivity that stays almost constant over the full depth of the troposphere.

Our results further show that the criticality parameter is not constrained to be O(1) in a turbulently equilibrated primitive equation system. Instead, numerical simulations, with varying Coriolis parameters f and planetary vorticity gradients β, equilibrate into states with a wide range of criticality parameters, spanning about an order of magnitude. The vertical structure of the eddy diffusivity adjusts accordingly, and it is unclear in how far the latter may be predicted without prior knowledge of the criticality parameter of the equilibrated state. In the next chapter, we will instead argue that the criticality parameter can be predicted using an argument for the magnitude of the eddy diffusivity in the lower troposphere, which is more easily predicted than its vertical structure.

In agreement with 2-layer quasi-geostrophic turbulence theory (Held and Larichev, 1996), the changes in the criticality parameter are associated with strong changes in the non-linear flow characteristics. States with criticality parameters close to one are associated with only weakly non-linear flows, where the dominant eddy scale is close to the scale of the most linearly unstable mode. Strongly supercritical states in turn are associated with highly nonlinear flows, which exhibit eddies much larger than the scale of the instability, maintained by an inverse energy cascade. This is in agreement

with the results of chapter 2, where we first showed support for the applicability of this theory to multi-level primitive equation models.

APPENDIX A

The Vertical Structure of the Eddy Diffusivity in Primitive Equations

In chapter 3 we showed that the primitive equation isentropic zonal momentum budget can be used to derive a relation between the vertical structure of the eddy diffusivity and the criticality parameter. For the purpose of deriving a scaling relation, the troposphere is divided into two layers, separated by a potential temperature $\theta = \theta_1$, which may be a function of latitude. The level separating these two layers is assumed to be above the surface layer, which, at any given latitude, is defined to include all isentropes which intersect with the surface at some time or longitude. We thus have that $\overline{\mathcal{H}(\theta_1 - \theta_s)} = 1$, where θ_s is the surface potential temperature and $\mathcal{H}$ the Heaviside function.

It is useful to introduce the bulk diffusivities D_1 and D_2, for each layer, defined as the ratio between a weighted integral of the eddy flux of PV and the weighted integral of the PV gradient. For the upper layer, D_2 is defined as

$$D_2 = \int_{\theta_1}^{\theta_t} \frac{\overline{\rho_\theta \hat{v} \hat{P}}^*}{\overline{P}^*} d\theta \Big/ \int_{\theta_1}^{\theta_t} \frac{\overline{\rho_\theta} \partial_y \overline{P}^*}{\overline{P}^*} d\theta \,, \tag{4.A1}$$

where θ_t denotes the potential temperature at the tropopause. The lower layer diffusivity, D_1, includes an additional contribution from the eddy flux and gradient of surface potential temperature, and can be written as

$$D_1 = \int_{\theta_{min}}^{\theta_1} \frac{\overline{\rho_\theta \hat{v} \hat{P}}^* + \delta(\theta - \overline{\theta}_s) f \overline{v' \theta'}^s}{\overline{P}^*} d\theta \Big/ \int_{\theta_{min}}^{\theta_1} \frac{\overline{\rho_\theta} \partial_y \overline{P}^* + \delta(\theta - \overline{\theta}^s) f \partial_y \overline{\theta}^s}{\overline{P}^*} d\theta \,, \tag{4.A2}$$

where θ_{min} denotes the minimum potential temperature in the domain, $\overline{(\,)}^s$ denotes the zonal average along the surface, and $(\,)'$ indicates deviations thereof. The surface

contribution in the lower layer is analog to the "surface PV sheet", which can be used to treat inhomogeneous boundary conditions in a continuously stratified QG model (Bretherton, 1966). Notice, however, that this surface contribution affects all isentropes within the SL.

With these definitions, we derived a scaling relation for the criticality parameter as

$$\xi \sim \frac{fs}{\beta H} \sim \frac{\tilde{D}}{\Delta D}. \tag{4.A3}$$

Here $\Delta D \equiv D_1 - D_2$ is the difference in the eddy diffusivity between the two layers, and $\tilde{D}$ denotes the vertical mean of the eddy diffusivity, which for a Boussinesq fluid (as used in the discussed simulations) becomes $\tilde{D} \equiv (\overline{z}(\theta_1)D_1 + (\overline{z}(\theta_t) - \overline{z}(\theta_1))D_2)/H$, where $H = \overline{z}(\theta_t)$ and we assumed a flat bottom at $z = 0$. The scaling relation in Eq. (4.A3) is a direct generalization of the QG results discussed by Green (1970) and Marshall (1981).

Notice, that apart from the requirement that the lower layer shall include the entire surface layer, Eq. (4.A3) can technically be derived for any choice of the layer interface θ_1. However, the bulk diffusivities D_1 and D_2 are poorly defined layer averages if the generalized PV gradient (defined to include the contribution from the surface potential temperature gradient) takes on large positive and negative values within a single layer. As proposed in chapter 3, we thus here define the layer interface as the first isentropic level above the surface layer (for practical purposes defined as the layer where $\overline{\mathcal{H}(\theta - \theta_s)} < 0.95$) where the PV gradient becomes positive. This level typically separates layers of equatorward mass transport from layers of poleward mass transport. The top of the upper layer, θ_t, is here defined such that it includes 85% of the northward return flow at any given latitude. This threshold was chosen to give rough agreement with the average height of the tropopause as found from a stratification condition. The general results presented in this paper, however, do not depend on the exact choice of this threshold.

Finally, it should be noted that, consistent with the theoretical arguments, the PV in the numerical simulations is approximated by the planetary PV, $P = f/(g^{-1}\partial_\theta p)$.

One exemption to this is the inclusion of the curvature of the barotropic mean flow in the calculation of the PV gradient (i.e. we use an effective planetary vorticity gradient $\beta^* = \beta + \partial_{yy}\overline{u_t}$). While the latter has little influence on the domain wide averages, it can have a significant effect locally in simulations which develop a strong jet. All additional neglected contributions to the full PV flux and gradient are generally smaller.

APPENDIX B

Turbulent flow Characteristics

The criticality parameter is related to characteristics of the turbulent flow itself. Held and Larichev (1996) argue that the flow field in marginally critical mean states is expected to be dominated by weakly non-linear eddies with a scale close to that of the fastest growing linearly unstable mode (which in turn is on the same order as the Rossby radius of deformation). Large criticality parameters, on the other hand, are expected to be associated with strongly turbulent flows. The dominant eddy scale in the turbulent flow regime scales with the Rhines scale L_R, which in turn becomes much larger than the scale of the most unstable mode, by a factor which is on the same order as the criticality parameter. While eddy kinetic energy (EKE) is still produced near the Rossby radius of deformation, non-linear eddy-eddy interactions produce an up-scale energy transfer to the Rhines scale.

The relation between the criticality parameter and the characteristics of the turbulent flow can be tested by analysis of the spectral EKE budget. We again want to focus on the simulation with Earth-like parameters ($f_0 = 1 \times 10^{-4} s^{-1}$, $\beta = 1.6 \times 10^{-11} m^{-1} s^{-1}$), as well as the most supercritical simulation ($f_0 = 8 \times 10^{-4} s^{-1}$, $\beta = 0.8 \times 10^{-11} m^{-1} s^{-1}$). Figure 2 shows the spectral conversion of eddy available potential energy to eddy kinetic energy (EKE), as well as the spectral dissipation of EKE, for both cases. The eddy energy conversion rate is calculated from the cospectrum between the eddy vertical velocity and potential temperature, as

$$T_{PK} = -\alpha \, \Re \left(\hat{w'}^* \, \hat{\theta'} \right) \tag{4.B1}$$

where α is the thermal expansion coefficient, $\hat{()}$ denotes the horizontal fourier transform of the respective variable, and $()^*$ denotes the complex conjugate. Due to the use of a constant linear drag, the eddy kinetic energy dissipation is simply proportional

to the eddy kinetic energy itself, and can be calculated as

$$D = -\frac{r}{2}\Re\left(|\hat{u'}|^2 + |\hat{v'}|^2\right), \tag{4.B2}$$

where | | denotes the absolute value. In both cases, spectral energy transfer rates are calculated in 2 dimensional spectral space at each vertical level, and are afterwards integrated in the vertical, and along circles of constant total horizontal wavenumber.

We also computed the scale of the fastest growing baroclinically unstable mode and the Rhines scale. The wavelength of the most unstable mode is calculated solving the QG linear stability analysis, as in Smith (2007), based on the meridional planetary QGPV gradient, averaged over the baroclinically forced region between $-3500km < y < 3500km$. The Rhines wavelength is calculated as

$$L_R \equiv 2\pi EKE_t^{1/4}\beta^{-1/2}, \tag{4.B3}$$

where EKE_t denotes the barotropic EKE.

The spectral EKE budgets, together with the scales of the most unstable mode and the Rhines scales, for the two simulations, are shown in figure 4-7. In both simulations, the transfer from availalable potential energy to EKE peaks near the wavelength of the most unstable mode as calculated from the QG instability analysis. For the simulation with Earth like parameters, this instability scale is on the same order as the Rhines scale and the dominant barotropic eddy scale. Only a small up-scale energy transfer is observed. This is in agreement with the expected characteristics for a flow near marginal criticality. For the strongly supercritical simulation with $f_0 = 8 \times 10^{-4}s^{-1}$ and $\beta = 0.8 \times 10^{-11}m^{-1}s^{-1}$, the transfer from availalable potential energy to EKE again peaks near the wavelength of the most unstable mode. The latter, however, is now more than an order of magnitude smaller than the Rhines scale, which in turn again coincides with the dominant barotropic eddy scale. The EKE (and associated dissipation) at this much larger scale must be maintained by a strong up-scale energy flux due to eddy-eddy interactions.

The different characteristics of the turbulent flow are also evident in the different

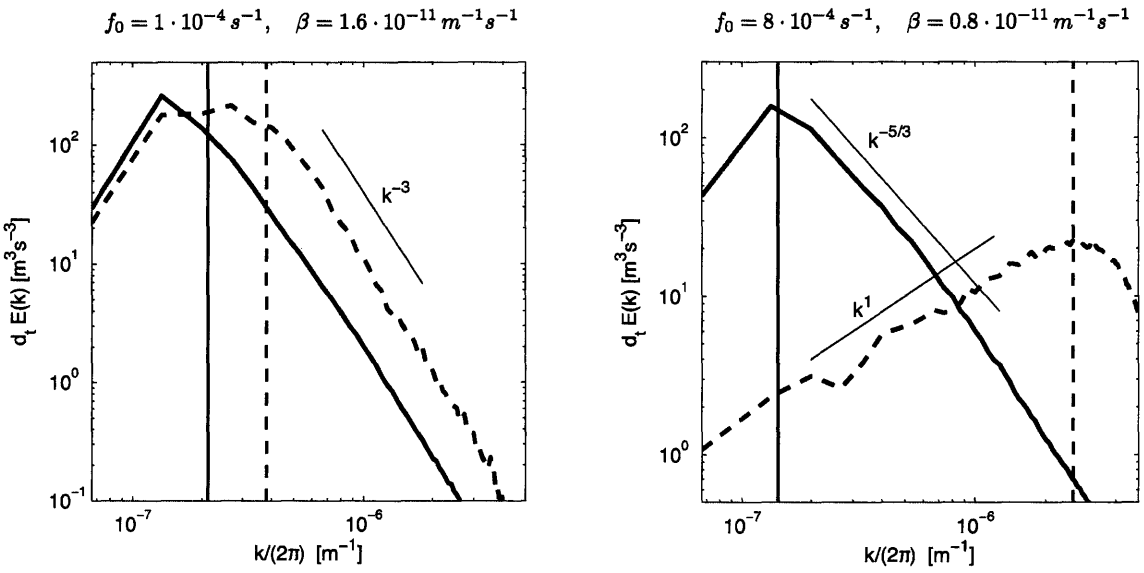

Figure 4-7: Spectral EKE production and dissipation for the simulations with $f = 1 \times 10^{-4}\mathrm{s}^{-1}$, $\beta = 1 \times 10^{-11}\mathrm{m}^{-1}\mathrm{s}^{-1}$ (left), and $f = 8 \times 10^{-4}\mathrm{s}^{-1}$, $\beta = 0.8 \times 10^{-11}\mathrm{m}^{-1}\mathrm{s}^{-1}$ (right). Shown is the eddy APE to EKE transfer (dashed), and the EKE dissipation (solid), which is here directly proportional to the EKE itself (due to the use of a linear drag). The vertical dashed and solid lines denote estimates of the wavelength of the most unstable mode and the Rhines scale, respectively (see text).

slopes of the EKE spectra in figure 4-7. The EKE spectrum in the Earth-like simulation falls off as $\sim k^{-3}$ at scales smaller than the dominant eddy scale, as observed in the atmosphere (e.g. Boer and Shepherd, 1983). The EKE in the strongly supercritical simulations, instead, falls of less steeply, with a slope close to $k^{-5/3}$, which is the slope predicted by QG turbulence theory for the inverse energy cascade range (e.g. Rhines, 1979).

Chapter 5

Equilibration of the Thermal Structure by Adiabatic Eddy Fluxes

5.1 Introduction

In this chapter we return to the problem of predicting how large-scale turbulent eddy fluxes equilibrate the mean state of an atmosphere. As discussed previously, one line of arguments, about how eddy fluxes set the atmospheric mean state, is based on the assumption that the extra-tropical atmosphere always adjusts to O(1) criticality parameters. This notion has been supported by a series of numerical simulations presented in Schneider (2004) and Schneider and Walker (2006), which show that the atmospheric mean state consistently equilibrates in such a way that $\xi \approx 1$, for a wide range of forcings and parameters.

In chapters 2 and 4 we have, however, found that this is not generally the case. In chapter 2 we obtained criticality parameters between 1 and 4 in an idealized primitive equation system, in which the thermal expansion coefficient was varied to obtain properties resembling Earth's extra-tropical atmosphere as well as properties resembling more closely the Southern Ocean. In chapter 4 we obtained a range of criticality

parameters covering a full order of magnitude, by changing the Coriolis parameter, f, and the planetary vorticity gradient β, in a similar numerical model.

In chapters 3 and 4 we have argued why the theoretical argument for adjustment to marginal criticality, proposed by Schneider (2004), is not generally expected to hold. We revised Schneider's arguments to derive a scaling relation between the criticality parameter and the vertical structure of the eddy diffusivity. The latter, however, does not pose an obvious constraint for the criticality parameter, since it was shown that the vertical structure of the eddy diffusivity can change strongly in response to changes in external parameters. Any constraint for the criticality parameter thus requires an understanding of how turbulent fluxes depend on changes in the external parameters, as well as changes in the equilibrated mean state itself.

We will here follow an argument first made by Held (2007), to derive a scaling relation for the criticality parameter, from the balance between the radiative forcing and the adiabatic eddy fluxes, similar to the relation derived in chapter 2. This scaling relation predicts the weak dependence of ξ to changes in the radiative restoring, observed in previous studies. However, it also shows that the criticality parameter can change strongly in response to changes in other external parameters, such as the planetary size and rotation rate. The scaling relation is confirmed by the series of numerical simulations with varying f and β, first discussed in chapter 4 .

The scaling relation for the criticality parameter is then extended to obtain a constraint for both the meridional temperature gradient and the static stability. The criticality parameter is directly related to the isentropic slope, which in turn gives the ratio of the meridional temperature gradient to the static stability, $\xi \sim a/H\, s \sim a\partial_y\overline{\theta}/(H\partial_z\overline{\theta})$. A condition for both the meridional temperature gradient and static stability can then be derived from the thermodynamic budget; if eddy heat fluxes are approximately adiabatic, the net heating along any isentrope must to vanish. This provides an additional constraint on the position of the isentropes, which can be used to derive a scaling relation for the meridional temperature gradient and static stability, given the criticality parameter and radiative equilibrium temperature profile.

This paper is organized as follows: in section 5.2, we discuss the setup and some

basic results from the numerical simulations. In section 5.3 we discuss scaling laws for the criticality parameter, and test them against the numerical simulations. In section 5.4, we derive and test an argument to retrieve both the horizontal temperature gradient and vertical stratification. A discussion of the results and their implications, is given in section 5.5.

5.2 Numerical Simulations

The numerical simulations discussed primarily in this chapter are the ones described in chapter 4. The model domain is a zonally-reentrant, β-plane channel. The β-plane configuration, where the Coriolis parameter is given as $f = f_0 + \beta y$, allows us to easily vary f and β separately and without changing the size of the domain. As shown in chapter 4, this proves to be an efficient way to greatly vary the criticality parameter of the equilibrated mean state.

Radiative forcing is represented through relaxation to the equilibrium temperature profile shown in figure 3-1. The relaxation time-scale is $\tau_s = 14$ days at the surface and decreases exponentially, with an e-folding depth of 500 m, to an interior value of $\tau_{int} = 50$ days. Free slip boundary conditions are used on all boundaries, and kinetic energy is removed by a linear Rayleigh drag with a constant drag coefficient of $r = (50\text{days})^{-1}$ throughout the domain. For further details about the model the reader is referred to chapter 4.

The series includes 11 simulations, using Coriolis parameters $f_0 = (1, 2, 4, 8) \times 10^{-4}$ s^{-1}, and planetary vorticity gradients $\beta = (0.8, 1.6, 3.2) \times 10^{-11}$ $\text{m}^{-1}\text{s}^{-1}$. As discussed in chapter 4 the simulations equilibrate to a wide range of criticality parameters. A criticality parameter close to one is obtained for parameters characteristic for Earth's mid-latitudes: $f_0 = 1 \times 10^{-4}\text{s}^{-1}$, $\beta = 1.6 \times 10^{-11}\text{m}^{-1}\text{s}^{-1}$, while the criticality parameter increases by an order of magnitude for the largest Coriolis parameter and weakest curvature: $f_0 = 8 \times 10^{-4}\text{s}^{-1}$ and $\beta = 0.8 \times 10^{-11}\text{m}^{-1}\text{s}^{-1}$.

In chapter 2 we showed that an alternative way to obtain supercritical states is to decrease the thermal expansion coefficient from atmosphere-like values to ocean-

like values. A set of simulations with varying thermal expansion coefficients, α, was described in chapter 2, and will also be used in this chapter. There are some differences between the simulations of chapter 2 and those of chapter 4 discussed above. Most notably, the radiative equilibrium profile is statically unstable in the lower troposphere, and frictional drag acts only in a viscous surface Ekman layer (see chapter 2 for more details). However, none of these differences is crucial for the arguments discussed below.

5.3 Scaling Arguments for the Criticality Parameter

The simulations described above showed that strongly supercritical states can be achieved in primitive equation models, in particular if the Coriolis parameter, f, and planetary vorticity gradient β are varied independently. This seems to contradict previous numerical studies which found that $\xi \lesssim 1$ over a wide range of parameters (Schneider, 2004; Schneider and Walker, 2006). It is therefore necessary to revisit scaling arguments for the criticality parameter, in order to understand how it depends on external parameters, and in particular on f and β.

In this section we derive a scaling argument for the criticality parameter, similar to that proposed in chapter 2. Instead of using isentropic coordinates, as in chapter 2, we present a derivation in cartesian coordinates, which largely follows the arguments by Held (2007), and Zurita-Gotor and Vallis (2009, 2010). The principle idea is that the isentropic slope, and thus the criticality parameter, is set through a balance between the radiative forcing and the eddy heat flux. In combination with a diffusive scaling argument for the magnitude of the eddy fluxes, this constrains the equilibrated mean state.

All arguments are presented for a Boussinesq fluid with a linear equation of state, as used in the numerical simulations. Eddy fluxes and gradients of buoyancy in this case are linearly proportional to eddy fluxes and gradients of potential temperature:

$\overline{v'b'} = g\alpha\,\overline{v'\theta'}$, and $\nabla\bar{b} = g\alpha\,\nabla\theta$, where overbars denote time- and zonal-averages, and primes denote deviations thereof. While all equations are expressed in terms of buoyancy, for better readability, we will use the term heat fluxes interchangeably for buoyancy fluxes in the discussions. All results can be easily generalized to an ideal gas, if the height coordinate is replaced by pressure.

5.3.1 Relating the criticality parameter to the eddy diffusivity

The zonal momentum budget, and thermodynamic equation, are now used to derive a relation between the criticality parameter, the radiative forcing, and the eddy diffusivity. Using the QG approximation, and ignoring frictional forces, the zonal momentum budget can be written as

$$f\overline{v}^{\dagger} = -\overline{v'q'}, \tag{5.1}$$

where $\overline{v}^{\dagger} = \partial_z\Psi^{\dagger}$ is the residual meridional velocity, with $\Psi^{\dagger} = \int_0^z \overline{v}dz' - \overline{v'b'}/\bar{b}_z$ denoting the residual overturning streamfunction, and $q \approx f + \zeta + f_0\partial_z(b/b_{0z})$ is the QG PV, with b_{0z} denoting the background stratification, and $\zeta = \partial_x v - \partial_y u$ the relative vorticity. Using a down-gradient closure for the eddy flux of PV, i.e. $\overline{v'q'} = -D\partial_y\overline{q}$, and neglecting the relative vorticity contribution to the PV gradient, which is a reasonable approximation on the planetary scale, we find that

$$\overline{v}^{\dagger} \approx D(\beta/f - \partial_z s)\,, \tag{5.2}$$

where $s = \partial_y\bar{b}/\partial_z\bar{b}$ denotes the isentropic slope. For strongly supercritical mean states, where the contribution of the first term on the R.H.S. of Eq. (5.2) can be neglected, and the eddy diffusivity can be approximated as vertically constant (see chapter 3), integration of Eq. (5.2) yields that

$$\Psi^{\dagger} \approx Ds\,. \tag{5.3}$$

Eq. (5.3) is commonly used to parameterize the eddy driven overturning circulation in ocean models (Gent and McWilliams, 1990). It is typically motivated in terms of a closure for the horizontal eddy buoyancy flux $\overline{v'b'} = -D\partial_y\bar{b}$. Using this closure, Eq. (5.3) can be derived without any assumption for the supercriticality of the mean state. This derivation is also used in Held (2007) and Zurita-Gotor and Vallis (2009, 2010). We here use a derivation based on a diffusive closure for the eddy PV flux, since eddy buoyancy fluxes are typically primarily along isentropes, i.e. "skew", rather than down-gradient. Indeed, the closure in Eq. (5.3), together with the assumption that the eddy buoyancy flux is directed along isentropes, implies that the vertical eddy heat flux is up-gradient, since $\overline{w'b'} = s\overline{v'b'} = -Ds\partial_y\bar{b} = Ds^2\partial_z\bar{b}$. The interpretation of D as a buoyancy "diffusivity" is therefore inappropriate. For marginally critical mean states, where the planetary vorticity gradient β modifies the PV gradient significantly, and the PV diffusivity has strong vertical structure, the physical motivation of Eq. (5.3) thus remains less clear. The empirical results presented below, however, support the use of (5.3) even in this limit.

Assuming that the eddy fluxes are primarily adiabatic, the time- and zonal-mean buoyancy budget can be approximated as

$$J(\Psi^\dagger, \bar{b}) \approx -\bar{\dot{b}}\,, \tag{5.4}$$

where $J(A, B) = \partial_y A\partial_z B - \partial_z A\partial_y B$ denotes the Jacobian in the y-z plane, and $\dot{b}$ denotes the diabatic (radiative) forcing (e.g. Plumb and Ferrari, 2005, and references therein). Notice that we are not using the QG approximation for the thermodynamic budget here. As discussed in chapter 2, the planetary scale atmospheric dynamics are well described by the QG approximation, but the thermodynamic budget cannot be described adequately using the QG equations, which imply zero net vertical heat transport across any given level.

Eq. (5.4) shows that advection by the residual overturning circulation has to balance the radiative forcing. Choosing some level z_1, such that it separates levels of net warming (below) and net cooling (above), the heat transport across this level

needs to balance the cooling above this level. Integrating horizontally, we find that

$$\Psi^{\dagger}(y_1, z_1) L \partial_y \bar{b} \sim QHL\,, \tag{5.5}$$

where $\Psi^*(y_1, z_1)$ denotes the maximum residual overturning transport across the level z_1. $L\partial_y \bar{b}$ denotes the buoyancy difference between the upwelling and downwelling branches of the eddy-driven overturning circulation, $Q = -\frac{1}{HL}\int_{z_1}^{z_t}\int_{y_{min}}^{y_{max}} \bar{\dot{b}}\, dy\, dz$ denotes the average radiative cooling in the upper troposphere, and $H = z_t - z_1$ is the depth scale of the upper troposphere. In practice, cooling typically dominates over more than half of the troposphere, and we may, for scaling purposes, assume that H is on the same order as the total depth of the troposphere. We notice, however, that this assumption could be problematic when considering the response to changes in the vertical structure of the radiative forcing, in which case the vertical extent of the levels of net warming and cooling may change independently from the tropopause height.

Combining Eqs. (5.3) and (5.5) yields

$$s \sim \frac{QH}{D\partial_y \bar{b}} \tag{5.6}$$

A scaling for the average radiative cooling, Q, is derived by assuming that the radiative forcing can be described as a restoring to a radiative equilibrium buoyancy, b_{eq}, over a time-scale τ, $\dot{b} = (b - b_{eq})/\tau$. We then find that

$$Q \sim \frac{(\partial_z \bar{b} - \partial_z b_{eq})H}{\tau}\,. \tag{5.7}$$

A particularly intuitive result is obtained if the thermal forcing can be approximated as a restoring towards a statically neutral state, i.e. if $\partial_z b_{eq} = 0$. In this case, combining Eqs. (5.6) and (5.7) yields

$$s \sim \frac{H}{\sqrt{\tau D}} \tag{5.8}$$

Equation (5.8) states that the length of an isentrope, from the surface to the tropopause, $l_{isen} \sim s^{-1}H$, scales with the length scale $l_{diff} \sim \sqrt{\tau D}$, which denotes the distance over which diffusive fluxes homogenize a tracer over the time-scale given by the radiative restoring τ.

Equation (5.8) can easily be transformed into a scaling relation for the criticality parameter. Using that $\xi \sim s\,a/H$, where $a \equiv f/\beta$, we obtain that

$$\xi \sim \frac{a}{\sqrt{\tau D}}. \tag{5.9}$$

The criticality parameter thus is given simply by the ratio of the dynamical planetary scale, $a \sim f/\beta$, to the diffusive length scale, $l_{diff} \sim \sqrt{\tau D}$.

5.3.2 Comparison to Numerical Results

Before proceeding to relate the eddy diffusivity, D, to the mean state itself, we test the scaling relation in Eq. (5.9) against numerical simulations. We estimate criticality parameters for all performed simulations as in chapter 4:

$$\xi \equiv \frac{f_0/\beta\langle\partial_y b\rangle}{H\langle\partial_z b\rangle}, \tag{5.10}$$

where $\langle\,\rangle$ denotes a horizontal average, taken over the baroclinically forced region between -3500 km $< y <$ 3500km, at the fixed level $z =$ 2km. Variations in the tropopause height are negligible across our simulations, because the height is largely set by the restoring profile, and we can set $H =$ 7km for all simulations. The criticality parameter varies by about an order of magnitude over the simulations, ranging from about $\xi \approx 1$ for the simulation with Earth-like rotational parameters, $f_0 = 1 \times 10^{-4}s^{-1}$, $\beta = 1.6 \times 10^{-11}m^{-1}s^{-1}$, to about $\xi \approx 10$ for the simulation with $f_0 = 8 \times 10^{-4}s^{-1}$, $\beta = 0.8 \times 10^{-11}m^{-1}s^{-1}$.

Eddy diffusivities are estimated from a flux-gradient relationship of surface buoyancy (skew fluxes vanish at the surface, and the potential temperature diffusivity is

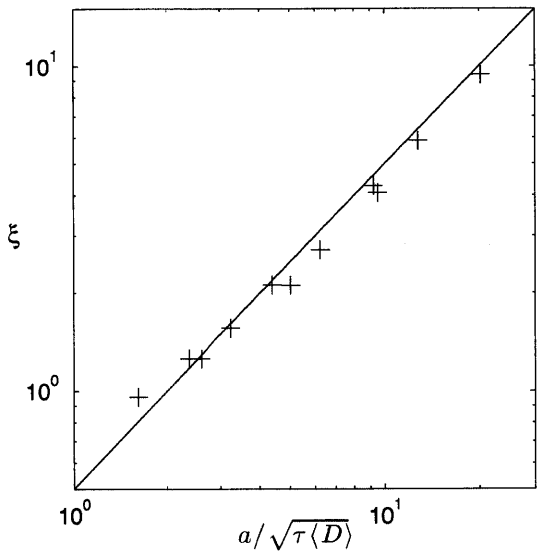

Figure 5-1: Criticality parameter, ξ, against the scaling in Eq. (5.9), for simulations with various combinations of Coriolis parameters $f = 1, 2, 4, 8 \times 10^{-4}\mathrm{s}^{-1}$ and planetary vorticity gradients $\beta = 0.8, 1.6, 3.2 \times 10^{-11}\mathrm{m}^{-1}\mathrm{s}^{-1}$. The black line shows $\xi = 0.5\, a/\sqrt{\tau\langle D\rangle}$. ξ is calculated as in Eq. (5.10), and $\langle D\rangle$ is calculated as in Eq. (5.11), and averaged over the width of the baroclinically forced region, between -3500km< y <3500km.

expected to most closely represent the PV diffusivity):

$$D = -\frac{\overline{v_s' b_s'}}{\partial_y \bar{b}_s}. \tag{5.11}$$

The overbar denotes a time- and zonal-average, and primed quantities denote deviations from this average. The index s here denotes quantities evaluated at the lowest model level.

The scaling relation in Eq. (5.9) is tested in figure 5-1. We find that it successfully reproduces the domain-averaged criticality parameter of the equilibrated mean state over the whole range of simulations. Notice, that the scaling relation in Eq. (5.9) depends on evaluation of the eddy diffusivity, D. A closed scaling relation for the equilibrated mean state, requires that D is expressed in terms of the mean state and external parameters. This is done next by using an argument for the eddy dynamics (in addition to their thermodynamics).

5.3.3 A Scaling Relation For the Criticality Parameter

An expression for the eddy diffusivity that has proven useful in previous studies (e.g. Zurita-Gotor and Vallis, 2010; Jansen and Ferrari, 2012), was proposed by Held and Larichev (1996). They argued that in steady state, the conversion of mean available potential energy to eddy available potential energy is balanced by a flux of kinetic energy towards larger scale. Assuming that the eddy mixing length scales with the Rhines scale, $L_\beta \sim \sqrt{V/\beta}$, where V denotes a characteristic barotropic eddy velocity, Held and Larichev (1996) derive that

$$D \sim L_\beta V \sim \beta \xi^3 L_d^3, \tag{5.12}$$

where $L_d \sim (\partial_z \bar{b}^{1/2})H/f$, denotes the Rossby radius of deformation. The argument was derived assuming $\xi \gg 1$, but reduces to traditional arguments based on linear instability theory in the marginally critical limit. It was also empirically shown to hold for simulations with O(1) criticality parameters[1] (Held and Larichev, 1996).

Interestingly, the scaling for D in Eq. (5.12) does not depend on the Coriolis parameter f. While the criticality parameter is proportional to the Coriolis parameter f, the deformation radius is proportional to f^{-1}. The eddy diffusivity D is thus not directly dependent on changes in f. Together with Eq. (5.8) this implies that the isentropic slope, rather than the criticality parameter, is insensitive to changes in f. This is indeed in general agreement with the numerical results discussed in chapter (4).

Inserting Eq. (5.12) into Eq. (5.9) yields a scaling for the criticality parameter,

$$\xi \sim (f\tau_r)^{-1/5} \left(\frac{L_d}{a}\right)^{-3/5}. \tag{5.13}$$

[1]Notice, that other scaling arguments for the eddy diffusivity could be derived, for example by equating the conversion of mean to eddy available potential energy, to the frictional dissipation of EKE. Such a scaling argument would yield results qualitatively similar to the ones presented here. With the numerical simulations discussed in this study, it is hard to distinguish which of these arguments is more appropriate. In general, the most appropriate scaling argument for the eddy diffusivity may depend on the exact situation considered (see also Thompson and Young, 2007).

Eq. (5.13) is a specialized version of the scaling relation in Eq. (2.31) of chapter 2, for the case in which restoring acts to a statically neutral mean state. The derivation of Eq. (2.31) in chapter 2 assumed that the upper-level radiative cooling scales as $Q \sim \tau_r^{-1} \Delta\theta_{eq}$. Due to the neutral restoring profile assumed here, we instead know that (in a domain averaged sense) $Q \sim \tau_r^{-1} \partial_z \theta H$. Equation (5.9) is thus recovered by replacing $\Delta\theta_{eq}$ in Eq. (2.31) with $H\partial_z\theta$. Eq. (5.13) tells us that the criticality parameter decreases as the normalized deformation scale, L_d/a, increases. In addition, the criticality parameter is weakly dependent on the normalized restoring timescale, τ_r/f.

Eq. (5.13) gives us an estimate for the criticality parameter within a constant O(1) factor. Inserting typical values for Earth's atmosphere suggests that this constant factor is just somewhat larger than one. With a restoring timescale on the order of 50 days, i.e. $\tau_r \approx 4 \times 10^6$ s, and $f \approx 10^{-4}$ s^{-1}, we obtain $(f\tau_r)^{-1/5} \approx 0.3$. The deformation scale L_d on Earth is smaller than the planetary radius, a, by about a factor of 3 to 6, which yields $(L_d/a)^{-3/5} \approx 2$ - 3. With a constant factor between 1 and 2, the scaling relation in Eq. (5.13) thus yields the observed criticality parameter of about 1 for Earth's extra-tropics. In how far the scaling relation in Eq. (5.13) is truly valid for Earth's extra-tropical atmosphere, however, remains unclear. Notice that a strict derivation of Eq. (5.13) required us to assume large criticality parameters, as well as to ignore several processes, in particular those associated with moisture, which may be important in the equilibration of Earth's extra-tropical troposphere.

The relation in Eq. (5.13) further tells us that O(1) criticality parameters may be expected in most dry numerical simulations of atmospheres on a sphere. Since the first factor in Eq. (5.13) appears with a power of 1/5, one order of magnitude variation in this factor would require variations in the planetary rotation rate or radiative restoring timescale by 5 orders of magnitude, which is outside the range typically explored in simulations of planetary atmospheres. Variations in the deformation scale are possible, but in practice are limited by numerical constraints: The deformation scale must be significantly smaller than the scale of the planet, and well resolved by the numerical grid scale. With a typical horizontal resolution of 1°, this allows for

at most one order of magnitude in variations of L_d/a, thus allowing for variations in ξ only up to about a factor of 4. This is about the range of criticality parameters obtained in chapter 2.

In a β-plane channel model, as used for this study, strongly supercritical states are obtained more easily, since the dynamical planetary scale $a \equiv f/\beta$ can be increased without increasing the size of the domain. This allows us to readily set up simulations with $L_d/a << 1$. Notice, however, that we do not decrease a below the width of the channel to avoid changes in the sign of f that would introduce equatorial dynamics effects which are not of interest here. If the deformation scale is required to be smaller than the domain size, we are thus still restricted to $L_d/a < 1$. Criticality parameters much smaller than one can thus only be obtained if τ_r is many orders of magnitude larger than the pendulum day, $4\pi/f$.

5.3.4 Comparison to Numerical Results

Figure 5-1 shows that the criticality parameter, ξ, as estimated from the whole set of numerical simulations, follows the scaling relation in Eq. (5.13). Variations in ξ are due dominantly to the changes in the normalized deformation scale L_d/a. As f is increased, the deformation scale is reduced, while the dynamical planetary scale $a \equiv f/\beta$ is increased. The ratio between the two scales thus decreases strongly as f is increased. A reduction of the planetary vorticity gradient β further reduces the normalized deformation scale, by increasing a.

To isolate the dependence of the criticality parameter on the externally prescribed parameters f and β, it is instructive to re-write Eq. (5.13) as

$$\xi \sim (\tau_r^2 H^6 \partial_z b^3)^{-1/10} \frac{f}{\beta^{3/5}} . \tag{5.14}$$

As indicated above, ξ is linearly dependent on f (while the isentropic slope itself is independent on f). This is a direct consequence of the eddy diffusivity being independent of f, according to the scaling in Eq. (5.12). In the simulations discussed here, the pre-factor, $(\tau_r^2 H^6 \partial_z b^3)^{-1/10}$, in Eq. (5.14) varies much less than f and β.

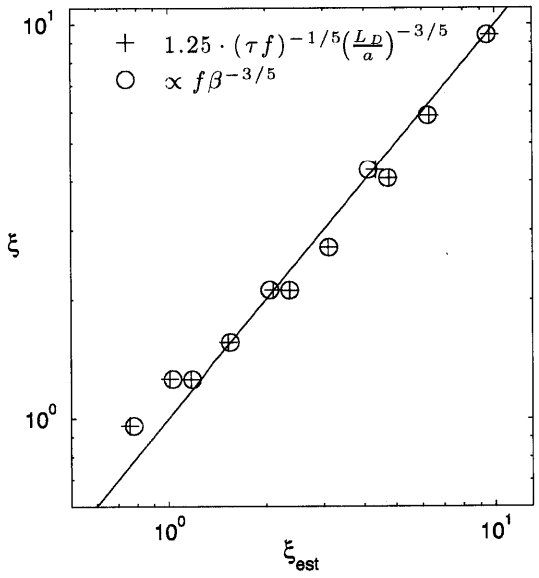

Figure 5-2: Criticality parameter, ξ, against the estimate from the scaling in Eq. (5.13), for simulations with various combinations of Coriolis parameters f and planetary vorticity gradients β (plusses). Circles indicate the estimated variations in ξ due to only the direct dependence on f and β (see Eq. 5.14). In both cases, the proportionality constant was chosen to match the data.

Consistently, figure 5-1, shows that the criticality parameter scales to leading order as $\xi \propto f\beta^{-3/5}$.

Notice that changes in the Coriolis parameter, f, strongly affect the characteristics of the flow, even though they only weakly modify the eddy diffusivity and the thermal mean state. The reason is that as f increases, the deformation scale decreases strongly. The Rhines scale, and with it the dominant eddy scale, however, remains approximately constant. In agreement with the increasing criticality parameter, we thus observe an increase in the inverse energy cascade range, between the deformation scale and the Rhines scale (Held and Larichev, 1996). This change in the turbulent flow characteristics of the simulations was discussed in chapter 4.

5.3.5 Implications for the Sensitivity to Changes in Thermal Forcing

We have shown that the criticality parameter can take on a wide range of values, if external parameters are varied. However, previous studies have found a weak dependence of the criticality parameter to changes in the forcing. In particular, Schneider (2004) and Schneider and Walker (2006) report large cancellations between changes in the bulk static stability, $H\langle\partial_z\theta\rangle$, and changes in the the re-scaled horizontal temperature gradient, $a\langle\partial_y\theta\rangle$, over series of simulations with strongly varying radiative equilibrium equator-to-pole temperature gradients. While both the re-scaled temperature gradient and bulk stability changed strongly over the range of simulations, the criticality parameter, which is given by the ratio of these two quantities, stayed close to one over the entire range of simulations.

A qualitatively similar result is found in the simulations in chapter 2. The simulations used a Boussinesq fluid with a linear equation of state $b = \alpha(\theta - \theta_0)$, and strongly varying thermal expansion coefficient, α. Since the radiative equilibrium potential temperature was held constant throughout all the simulations, changes in the thermal expansion coefficient directly translate into similar changes in the radiative equilibrium buoyancy contrasts (both vertical and horizontal).

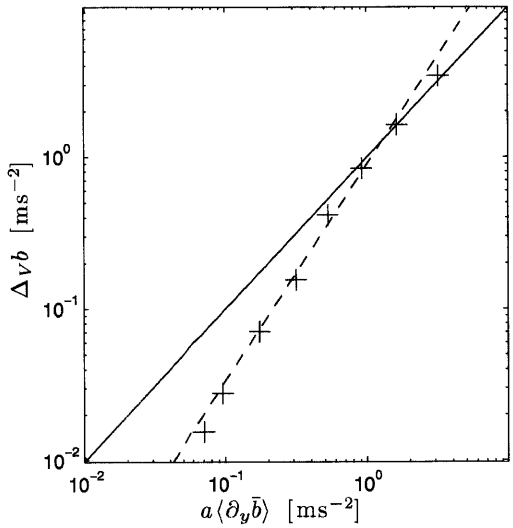

Figure 5-3: Bulk static stability, $\Delta_v\bar{b}$, against the re-scaled horizontal buoyancy gradient, $f_o/\beta\partial_y\bar{b}$, for the simulations in Jansen and Ferrari (2012), with varying thermal expansion coefficients. The solid line indicates $\Delta_v\bar{b} = a\langle\partial_y\bar{b}\rangle$. The dashed line denotes $\Delta_v\bar{b} \propto (a\langle\partial_y\bar{b}\rangle)^{10/7}$

Figure 5-3 shows the re-scaled horizontal buoyancy gradient $a\langle\partial_y\bar{b}\rangle$ against the bulk static stability $\Delta_v b \equiv H\langle\partial_z\bar{b}\rangle$ for the series of simulations discussed in chapter 2. Averages are taken as discussed in section 5.3.2. We observe a large cancellation between changes in the horizontal buoyancy gradient and the bulk static stability, leading to only moderate changes in the criticality parameter. While the criticality parameter changed significantly, by about a factor of 4, this needs to be contrasted to changes in the buoyancy gradients by about two orders of magnitude.

The result in figure 5-3 can be understood in terms of the scaling relation in Eq. (5.14). Noting that f, β and τ_r were held constant and changes in the tropopause height, H, are negligible compared to those in the buoyancy gradient and static stability, the expression in Eq. (5.14) gives a relationship between $\Delta_v b$ and $a\langle\partial_y b\rangle$. Using that $\xi \sim a\langle\partial_y b\rangle/\Delta_v b$, and $L_d \propto \Delta_v b^{-1/2}$, rearrangement of Eq. (5.14) yields

$$\Delta_v b \propto (a\langle\partial_y b\rangle)^{10/7}. \tag{5.15}$$

The relation in Eq. (5.15) was first derived by Held (2007). It states that any

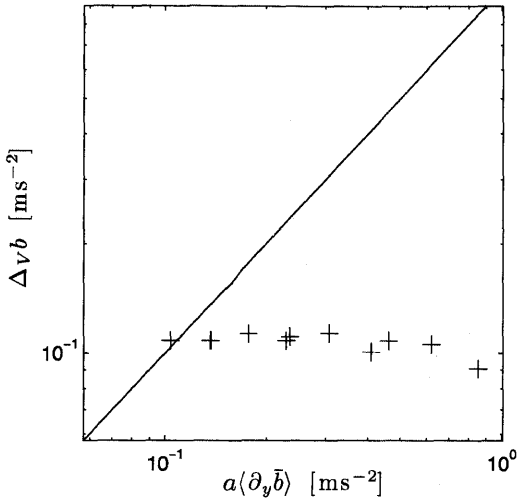

Figure 5-4: As figure 5-3, but for the series of simulations with varying rotational parameters f and β.

change in the horizontal buoyancy gradient is expected to be associated with a similar, but somewhat larger, change in the bulk static stability. Figure (5-3) shows that the relation in Eq. (5.15) successfully predicts the relation between the bulk static stability and the meridional buoyancy gradient in the simulations of chapter 2. A more detailed discussion of the dependence of the criticality parameter to changes in the forcing, for a wide variety of thermal forcing characteristics, is given by Zurita-Gotor and Vallis (2010).

Notice, however, that the result in Eq. (5.15) holds only if the parameter varied is the radiative equilibrium buoyancy contrast. The strong cancellation between changes in the re-scaled meridional buoyancy gradient and bulk static stability, and thus the weak sensitivity of the criticality parameter, does not hold for other parameter variations. Figure 5-4 shows that there is no cancellation between changes in the bulk static stability and the re-scaled horizontal buoyancy gradient[2] for the series of simulations with varying f and β. While the re-scaled horizontal buoyancy gradient

[2]Notice, that in this series of simulations the variation in the re-scaled horizontal buoyancy gradient, $a\langle\partial_y b\rangle$, is dominated by the changes in $a \equiv f/\beta$. The relation between the bulk static stability, $\Delta_v b$, and the horizontal buoyancy gradient itself, $\langle\partial_y b\rangle$, in this case also does not reveal any cancellation between the two quantities (not shown).

varies by about an order of magnitude, the bulk static stability is rather insensitive to changes in f and β. We will return to this result in the next section.

5.3.6 The Role of Frictional Drag

The scaling arguments discussed in this section employ Held and Larichev's (1996) scaling relation for the eddy diffusivity. This relation relies on the implicit assumption that the frictional drag acting on the eddies is small, with the majority of the kinetic energy being dissipated in the mean flow. Thompson and Young (2007) recently questioned this assumption, showing that frictional drag can strongly effect the eddy diffusivity. Thompson and Young (2007) analyze a series of numerical simulations using a two-layer QG model with linear drag in the lower layer. They find that the scaling relation proposed by Held and Larichev (1996)[3] provides a reasonable fit to their simulations only in the limit of large criticality parameters and weak frictional drag. The break-down of the scaling relation in the marginally critical limit is to be expected, since the character of the instability in the two-layer model changes dramatically near marginal criticality. The role of the frictional drag at high criticalities, however, deserves further attention.

As discussed in Thompson and Young (2007), the damping effect of the frictional drag on the eddies can be characterized by the ratio between the inverse Eady growth rate, L_d/U, and the frictional damping time-scale τ_{fric}. They find that frictional drag strongly modifies the Held and Larichev (1996) scaling relation in the supercritical regime if $(L_d/U)/\tau_{fric} \gtrsim 0.5$, where U is the baroclinic mean shear velocity, L_d is the deformation scale, and τ is the frictional damping timescale for a barotropic mode[4].

[3]Thompson and Young (2007) compare their results to the scaling relation of Lapeyre and Held (2003), which attempts to generalize the results of Held and Larichev (1996) to the marginally critical limit in the two-layer model. Due to the large difference between the behavior of the two-layer model and our continuously stratified model near marginal criticality, we here focus on the strongly supercritical limit, where the scaling relation in Lapeyre and Held (2003) reduces to the one in Held and Larichev (1996).

[4]Notice that the definition of the deformation scale used in this thesis differs by a factor of 2π from the definition used in Thompson and Young (2007). In addition, U here denotes the total shear velocity between the upper and lower troposphere, which corresponds to about twice the shear velocity defined in Thompson and Young (2007), where U is defined as half the velocity jump at the layer interface.

To compare our simulations with the study by Thompson and Young (2007), we need to estimate the ratio $(L_d/U)/\tau_{fric}$. In the parameter regime characteristic for Earth's atmosphere, we find shear velocities and deformation scales of $U \approx 10\,\mathrm{m/s}$ and $L_d \approx 2000\,\mathrm{km}$. The frictional damping time-scale in the simulations described in this chapter is prescribed directly as $\tau_{fric} = 50$ days^{-1}. This yields $(L_d/U)/\tau_{fric} \approx 0.05$, which is one order of magnitude smaller than the value at which frictional drag became leading order in Thompson and Young (2007). The Eady growth rate does not depend on f and β and therefore its value does not vary much across the simulations presented in this chapter and is about 2-4 days. Since the frictional damping time-scale is held constant at 50 days, this suggests that all simulations are in a regime where frictional drag has little effect on the eddies. The simulations discussed in chapter 2 with varying thermal expansion coefficient show somewhat larger variations in the Eady growth rate, but it does not exceed $\approx$5 days. Frictional dissipation in these simulations is given by a laminar Ekman layer, with a viscosity of $\nu_z = 10^{-1}\mathrm{m}^2\mathrm{s}^{-1}$. The frictional damping time-scale for a barotropic flow in this case can be computed as $\tau_{fric} \approx H\delta_{Ek}/\nu_z$, where H is the depth scale of the flow (here $H \approx 10\,\mathrm{km}$) and $\delta_{Ek} \equiv (2\nu_z/f)^{1/2}$ is the depth of the Ekman layer. For the parameters used in the simulations described in chapter 2 this yields $\tau_{fric} \approx 50$ days^{-1}. The ratio $(L_d/U)/\tau_{fric}$ thus remains well within the regime where Thompson and Young (2007) find reasonable agreement with the scaling relation of Held and Larichev (1996).

The limit of strong frictional drag discussed by Thompson and Young (2007) thus is not relevant to the simulations in this study, nor does it seem likely to apply to Earth's atmosphere. Nevertheless it is important to note that the scaling relations derived in this chapter hold only in the limit of small friction and are likely to break down in the presence of strong friction. In practice this is probably relevant for eddies in the ocean, where the inverse EKE cascade is understood to be strongly modified by frictional drag. We will return to this issue in chapter 6, where we discuss the relevance of our results to the Southern Ocean.

Finally it should be noted that in the limit of very weak frictional drag, the energy level in the barotropic mean flow can grow so much that the mean shear can strongly

affect the eddies via a mechanism similar to the "barotropic governor" discussed by James and Gray (1986). This is likely to explain at least part of the observed deviation from the Held and Larichev (1996) scaling in the marginally critical limit of the simulations discussed in chapter 2.

5.4 The Meridional Temperature Gradient and Stratification

Much of the work in this and previous studies (e.g. Zurita-Gotor, 2008; Zurita-Gotor and Vallis, 2010) has been focussed on the criticality parameter, which provides a constraint for the relation between the meridional temperature gradient and the bulk static stability. However, for practical purposes, we want to predict not just the criticality parameter, but both the static stability and meridional temperature gradient. In this section, we will argue that the scaling laws discussed above can be extended to predict both quantities independently. The argument is based on the assumption that eddies primarily redistribute heat only along isentropes, and that the radiative equilibrium solution is known. The total radiative heating and cooling along any isentrope then has to vanish. Knowledge of the criticality parameter, and thus the slope of the isentropes, then constrains also their positioning in the domain and thereby the full thermal structure.

5.4.1 Theory

We here derive constraints for the horizontal buoyancy gradient and bulk stability. As in section 5.3, we want to assume that eddy fluxes are adiabatic, such that the heat transport can be expressed in terms of a residual overturning circulation $\Psi^{\dagger}$. The vertical heat transport by this residual overturning circulation has to compensate the imbalance in the radiative forcing between the lower and upper troposphere. If the radiative forcing can be written in terms of a restoring condition, we can insert Eq.

(5.7) into Eq.(5.5), which yields

$$\Psi^{\dagger}(y_1, z_1)\Delta_h \bar{b} \sim \frac{(\partial_z \bar{b} - \partial_z b_{eq})H^2 L}{\tau}, \tag{5.16}$$

where $\Delta_h \bar{b}$ denotes the horizontal buoyancy contrast between the upwelling and downwelling branches of the eddy-driven overturning circulation, which is assumed to scale with the meridional gradient times the width of the baroclinic zone, $\Delta_h \bar{b} \sim -L\partial_y \bar{b}$.

The same argument can be made for the horizontal heat transport across the latitude y_1, which is found to scale as

$$\Psi^{\dagger}(y_1, z_1)\Delta_v \bar{b} \sim \frac{(\partial_y \bar{b} - \partial_y b_{eq})L^2 H}{\tau}, \tag{5.17}$$

where we defined a bulk static stability, $\Delta_v b$, as the vertical buoyancy contrast between the upper (poleward) and lower (equatorward) branch of the residual overturning circulation, which is assumed to scale with the vertical stratification times the tropopause height, $\Delta_v b \sim H\partial_z \bar{b}$.

Combining Eqs. (5.16) and (5.17) yields:

$$-\partial_y \bar{b}(\partial_y \bar{b} - \partial_y b_{eq})L^2 \approx \partial_z \bar{b}(\partial_z \bar{b} - \partial_z b_{eq})H^2 . \tag{5.18}$$

Notice that Eqs. (5.16) and (5.17) are scaling relations, which hold up to approximately constant O(1) factors. Accordingly, Eq. (5.18) may in general be assumed to hold only to within a constant O(1) factor. Instead of explicitly including a pre-factor in Eq. (5.18), we here absorbed the latter into the length scale, L, which is assumed to scale with the width of the baroclinic zone up to an O(1) factor. Empirically, we will show below that that this factor is close to one.

As in section 5.3, we make the simplifying assumption that the forcing can be approximated by a restoring acting towards an equilibrium buoyancy profile which is statically neutral in the troposphere, i.e. $\partial_z b_{eq} = 0$. This assumption simplifies the algebra, but it can easily be relaxed. The full case, allowing for non-zero $\partial_z b_{eq}$ is discussed in Appendix A.

Re-arrangement of Eq. (5.18) then yields

$$\Delta_h \bar{b} \approx \frac{\Delta_h b_{eq}}{1 + \hat{s}^{-2}}, \tag{5.19}$$

where $\Delta_h b_{eq} \equiv -L\partial_y b_{eq}$ denotes the horizontal buoyancy contrast in radiative equilibrium, and $\hat{s} = \Delta_h \bar{b}/\Delta_v \bar{b} \sim s\, L/H$ denotes the isentropic slope, normalized by the aspect ratio of the baroclinic domain. Eq. (5.19) shows that the horizontal buoyancy contrast $\Delta_h \bar{b}$ can be expressed as a function of its radiative equilibrium value and the normalized isentropic slope. The normalized isentropic slope, in turn, is directly related to the criticality parameter as $\hat{s} \sim \xi L/a$. For a spherical planet, where $L \sim a$, $\hat{s}$ in fact scales directly with the criticality parameter. In our numerical simulations where the "planetary scale", a, is varied independently of the width of the baroclinic zone, L, the normalized slope and the criticality parameter can be different. However, knowledge of the criticality parameter implies knowledge of the normalized isentropic slope, and vice versa.

Eq. (5.19) can also be used to infer the bulk static stability, which follows by dividing both sides of the equation by $\hat{s}$:

$$\Delta_v \bar{b} \approx \frac{\Delta_h b_{eq}}{\hat{s} + \hat{s}^{-1}}. \tag{5.20}$$

The bulk static stability, like the horizontal buoyancy contrast, can be expressed in terms of the radiative equilibrium horizontal buoyancy contrasts and the normalized isentropic slope.

It is worthwhile to consider the behavior of the horizontal buoyancy contrast and bulk stability in some special cases. In the limit of steep isentropic slopes, $\hat{s} \gg 1$, we find that $\Delta_h \bar{b} \approx \Delta_h b_{eq}$. Changes in the eddy diffusivity in this limit would thus modify the isentropic slope (or criticality) primarily via changes in the stratification, which to leading order becomes $\Delta_v \bar{b} \approx \hat{s} \Delta_h b_{eq}$. As shown in the Appendix, this result is not altered by the existence of a vertical gradient in the radiative equilibrium profile.

Possibly more relevant for the equilibration of the extra-tropical atmosphere is the behavior around $\hat{s} \approx 1$. Eq. (5.20) suggests that the normalized bulk static stability,

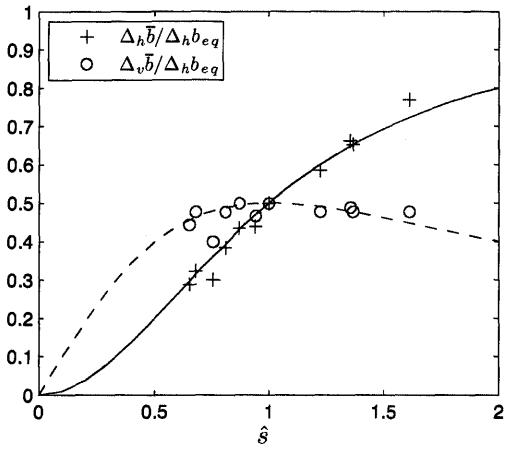

Figure 5-5: Horizontal buoyancy contrast, $\Delta_h\bar{b}$ (plusses), and bulk stability $\Delta_v\bar{b}$ (circles), normalized by the radiative equilibrium horizontal buoyancy contrast Δb_{eq}, as a function of the normalized isentropic slope $\hat{s}$, for the series of simulations with varying rotational parameters f and β. The grey lines show the theoretical predictions using Eqs. (5.19) and (5.20), for the normalized horizontal buoyancy contrast (solid), and for the bulk stability (dashed). As discussed in the text, the reference scale for the width of the baroclinic zone was chosen as $L = 8000$km, to best match the numerical results.

$\Delta_v\bar{b}/\Delta_h b_{eq}$, has a maximum at $\hat{s} \approx 1$, and will thus be weakly sensitive to changes in the isentropic slope. This implies that a change in the eddy diffusivity, for a fixed radiative equilibrium buoyancy contrast, $\Delta_h b_{eq}$, is expected to modify the isentropic slope primarily via changes in the horizontal buoyancy gradient, keeping the bulk stability roughly constant. Equivalently, changes in the equilibrium buoyancy contrast, $\Delta_h b_{eq}$, are expected to cause a directly proportional change in the bulk stability, keeping $\Delta_v\bar{b}/\Delta_h b_{eq}$ roughly constant. As shown in the Appendix, the addition of a vertical gradient in the radiative equilibrium buoyancy contrast modifies this result only quantitatively, by shifting the exact position of the maximum in $\Delta_v\bar{b}/\Delta b_{eq}$.

5.4.2 Comparison to Numerical Results

In the following subsection, we test the predictions of the scaling relations in Eqs. (5.19) and (5.20) against numerical simulations. Figure 5-5 shows the normalized horizontal buoyancy contrast, $\Delta_h\bar{b}/\Delta_h b_{eq}$, and bulk stability $\Delta_v\bar{b}/\Delta_h b_{eq}$, as a func-

tion of the normalized isentropic slope $\hat{s}$, for the simulations with varying f and β, discussed above. The average bulk stability, $\Delta_v b = H\langle\partial_z \bar{b}\rangle$, and horizontal buoyancy gradient, $\langle\partial_y \bar{b}\rangle$, are calculated as described in section 5.3.2. As discussed above, a degree of freedom exists for the exact choice of the length scale, L, which is used in the computation of the horizontal buoyancy contrast $\Delta_h b \equiv L\langle\partial_y \bar{b}\rangle$. A good fit to the numerical simulations is obtained by choosing L= 8000km. This is somewhat larger than the with of the baroclinically forced region (7000km wide), but somewhat smaller than the full width of the domain (9000km wide).

We see that the scaling relations in Eqs. (5.19) and (5.20) predict well the variations in the horizontal buoyancy contrast and bulk stability, associated with changes in the isentropic slope. In particular we find that changes in the slope are here associated mostly with changes in the horizontal buoyancy contrast, while the bulk stability stays relatively constant. This is in agreement with Eq (5.20), which predicts that the bulk stability has a maximum at a normalized slope $\hat{s} = 1$. Since $\hat{s}$ here varies only between about 0.7 and 1.6, the bulk stability stays close to this maximum value.

While the simulations with varying rotational parameters f and β exhibit a large range of criticality parameters (spanning about one order of magnitude), these variations are dominantly associated with changes in the "planetary scale", $a \equiv f/\beta$. The simulations cover only a much smaller range of normalized isentropic slopes (spanning about a factor of 2). To explore the behavior for a larger range of isentropic slopes, we can return to the simulations of chapter 2, where changes in the criticality parameter are achieved by variations in the thermal expansion coefficients. Since a is held constant in these simulations, changes in the criticality parameter translate directly into similar changes in the normalized isentropic slope, $\hat{s} \sim \xi L/a$.

Figure 5-6 shows the normalized horizontal buoyancy contrast, $\Delta_h \bar{b}/\Delta_h b_{eq}$, and bulk stability $\Delta_v \bar{b}/\Delta_h b_{eq}$, as a function of the normalized isentropic slope $\hat{s}$, for the simulations in chapter 2. Notice, that these simulations use a restoring condition to a buoyancy profile which is statically unstable, a generalization which we did not include in the derivation of Eqs. (5.19) and (5.20). Nevertheless, we see that the simulations qualitatively follow the scalings derived above. In particular, we observe the decrease

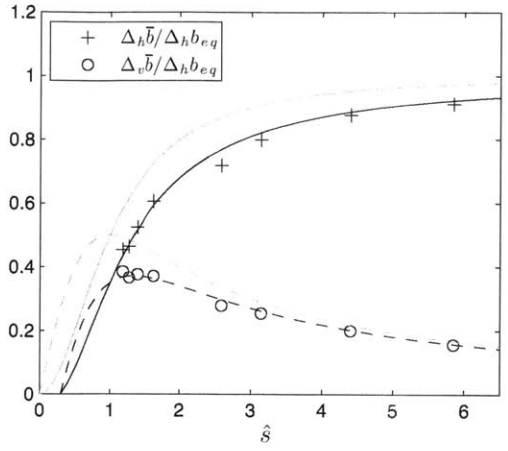

Figure 5-6: As in figure 5-5, but for the simulations in chapter 2, with varying thermal expansion coefficients. The grey lines show the theoretical predictions using Eqs. (5.19) and (5.20), which do not consider thermal restoring to a statically unstable radiative equilibrium state. The black lines show the predictions using Eqs. (5.A1) and (5.A2), with $\Delta_v b_{eq}/\Delta_h b_{eq} = -0.3$ (see Appendix A).

of the bulk stability for large normalized slopes, as the horizontal buoyancy contrast asymptotes its radiative equilibrium value. To quantitatively reproduce the results in these simulations we need to include the negative stratification of the radiative equilibrium profile. This is discussed in Appendix A.

5.4.3 Predicting the Normalized Isentropic Slope from External Parameters

In section 5.3 we derived a scaling relation expressing the criticality parameter in terms of the normalized radiative rstoring timescale $\tau_r f$ and the normalized deformation radius L_d/a. While this represents a closed relation for the mean state, it does not yet give us a fully predictive scaling for the criticality parameter in terms of only external parameter, since $L_d \propto \sqrt{\partial_z \overline{b}}$ is itself a mean state variable, determined by the turbulent equilibration. For simulations with varying rotational parameters, f and β, it was found that changes in the static stability are negligible, such that the full scaling relation for the criticality parameter can to first order be reduced to its dependence on the externally prescribed parameters f and β. However, the weak

variation in the static stability for the considered set of simulations was itself a result of the numerical simulations and was predicted only by the additional scaling relation for the bulk static stability discussed in this section.

Combining the scaling relations for the crtiticality parameter in section 5.3 with the one for the bulk static stability discussed in this section, we can derive a fully closed expression for the criticality parameter or isentropic slope in terms of external parameters. This scaling relation is best written in terms of an equation for the normalized isentropic slope $\hat{s}$, which can be expressed as a function of only one non-dimensional parameter. As mentioned above, the criticality parameter can then be easily obtained, using that $\xi \sim \hat{s}a/L$. If the equation for the normailzed isentropic slope is plugged into the relations in Eqs. (5.19) and (5.20), we further obtain direct predictors for the meridional buoyancy gradient and static stability.

For simplicity we will again assume radiative restoring to a statically neutral buoyancy profile. The full case for radiative restoring to statically stable or unstable profiles is derived in Appendix 5.5. Eq. (5.13) can be used to obtain a scaling relation for the isentropic slope as

$$\hat{s} \sim \frac{L}{a}(f\tau_r)^{-1/5}\left(\frac{\Delta_v \bar{b} H}{f^2 a^2}\right)^{-3/10} . \tag{5.21}$$

Substituting Eq. (5.20) for $\Delta_v \bar{b}$ in Eq. (5.21) and rearranging terms yields

$$\hat{s}(\hat{s} + \hat{s}^{-1})^{-3/10} = \gamma , \tag{5.22}$$

where γ is a non-dimensional parameter which can be expressed as

$$\gamma = c\frac{L}{a}(f\tau_r)^{-1/5}\left(\frac{\Delta_h b_{eq} H}{f^2 a^2}\right)^{-3/10} = c\frac{L\beta^{2/5}}{\tau^{1/5}\Delta_h b_{eq}^{3/10} H^{3/10}} , \tag{5.23}$$

with c an O(1) constant (found to be ≈ 0.9 in our simulations).

Eq. (5.22) implies that $\hat{s} = f(\gamma)$, where the function f is obtained by inversion of Eq. (5.22). $f(\gamma)$ is linear near $\hat{s} = 1$ and converges towards $f(\gamma) \sim \gamma^{10/7}$ for $\hat{s} \gg 1$ and $f(\gamma) \sim \gamma^{10/13}$ for $\hat{s} \ll 1$. Together with Eqs. (5.19) and (5.20), this suggests

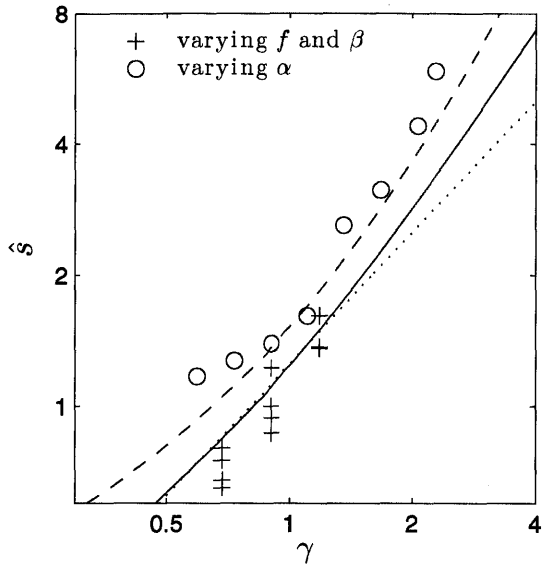

Figure 5-7: The normalized isentropic slope, $\hat{s}$, against the non-dimensional parameter γ (Eq. 5.23). Plusses denote results from the series of numerical simulations with varying f and β, and circles show results from the simulations of chapter 2, with varying thermal expansion coefficient, α. The constant factor in the definition of γ was set to $c = 0.9$ for all simulations. The solid line shows the theoretical prediction of Eq. (5.22) (i.e. assuming $\Delta_v b = 0$), as appropriate for the series of simulations with varying f and β, while the dashed line denotes the theoretical predictions of Eq. (5.B2) with $\Delta_v b_{eq}/\Delta_h b_{eq} = -0.3$, as appropriate for the series of simulations with varying thermal expansion coefficient, α. The dotted line shows a linear slope for reference. (Note that the axes are logarithmic.)

that changes in the the thermal mean state of the system are entirely determined by changes in the parameter γ in Eq. (5.23).

The relation in Eq. (5.22) is tested in figure 5-7. Notice, that γ is independent of the Coriolis parameter, f, suggesting that the isentropic slope is approximately independent of f. Figure 5-7 supports that $\hat{s}$ indeed varies only very little with the Coriolis parameter, considering that the latter is here varied by a factor of 8. Nevertheless there are some variations in $\hat{s}$ with changing f, which are not predicted by the scaling relation. These changes are small compared to the changes in the criticality parameter shown in figure 5-2 (which all else being equal is linearly proportional to f), but become more evident when focussing on the isentropic slope. The response of

$\hat{s}$ to changes in β is in overall agreement with the weak sensitivity predicted by the scaling.

To more adequately predict the isentropic slope in the simulations discussed in chapter 2 with varying thermal expansion coefficient, we need to take into account the effect of the radiative restoring to a statically unstable state. As discussed in Appendix 5.5, the normalized isentropic slope $\hat{s}$ is then determined by a family of functions depending on γ, as well as the ratio between the radiative equilibrium horizontal buoyancy contrast and bulk static stability: $\Delta_v b_{eq}/\Delta_h b_{eq}$. For $\Delta_v b_{eq}/\Delta_h b_{eq} \to 0$ we return to the result in Eq. (5.22). Once the effect of negative $\Delta_v b_{eq}$ is taken into account, the proposed scaling relation adequately predicts the isentropic slope in all our simulations (Figure 5-7). Notice that consideration of the statically unstable restoring profile affects the scaling only quantitatively but not qualitatively. For moderately unstable restoring profiles, the simplified relation in Eq. (5.22) thus provides a good qualitative model for the steepening of the isentropic slope with γ.

5.5 Conclusions

We showed that the equilibration of an idealized primitive equation model can be understood in terms of a scaling relation derived from a balance between the radiative forcing and the adiabatic eddy fluxes. The scaling relation predicts the weak dependence of ξ to changes in the radiative restoring that has been observed in previous studies, but also shows that the criticality parameter can change strongly in response to changes in other external parameters, such as the planetary size or rotation rate. This result is confirmed by a series of numerical simulations in a primitive equation, beta-plane, channel model, with varying Coriolis parameters, f, and planetary vorticity gradients, β.

To the extent that the idealized dry system considered here can be used to make inferences about Earth's atmosphere, our results suggest that changes in the criticality parameter in response to changes in the radiative forcing, as expected in past and future climate change, are likely to be small. However, if other parameters are varied,

or if the forcing is varied strongly enough, the criticality parameter can become much larger than one. The assumption that large scale turbulence generally equilibrates planetary atmospheres to states of marginally criticality, does not hold.

Finally, the criticality parameter (which implies a constraint on the isentropic slope) was used to predict both the bulk stability and the horizontal buoyancy gradient. We derived a scaling relation for both the equator-to-pole temperature gradient and bulk stability as a function of the isentropic slope and the radiative temperature gradient (and stratification). We found that both are to first order proportional to the radiative equilibrium horizontal temperature gradient. In addition, the horizontal temperature gradient increases towards its radiative equilibrium value with increasing isentropic slopes. The bulk stability instead is only weakly sensitive to the isentropic slope, for slopes typically found in Earth's atmosphere. It is thus almost directly proportional to the radiative equilibrium equator-to-pole temperature gradient.

Our results have interesting implications for our understanding of planetary climates, as well as past climate changes. They push our understanding of climate sensitivity beyond the 0-dimensional picture of the global mean temperature response to global mean changes in the forcing. For instance, we find that a change in the radiative equilibrium equator-to-pole temperature gradient is associated with a proportional change in the bulk stability. The bulk stability in turn has a strong effect on the surface temperature, as it relates the latter to the temperature at the effective emission level. Yet, energy balance models discussed in the existing literature typically assume a constant static stability (e.g. Huybers and Tziperman, 2008; Rose and Marshall, 2009). Our results will hopefully motivate a more thorough consideration of the possible role of changes in the static stability for the dynamics and thermodynamics of the atmosphere.

APPENDIX A

The Meridional Buoyancy Gradient and Bulk Stability in the Presence of Finite $\Delta_v b_{eq}$

We here want to generalize the results for the horizontal buoyancy contrast and bulk stabilty in Eqs. (5.19) and (5.20), to account for a radiative restoring, which acts towards a stratification that is not statically neutral, i.e. $\Delta_v b_{eq} \sim H\langle\partial_z b_{eq}\rangle \neq 0$. The arguably most realistic representation of the real atmosphere is given by a radiative restoring to a statically unstable state, i.e. $\Delta_v b_{eq} < 0$. The case where $\Delta_v b_{eq} > 0$, is primarily of theoretical interest, since it allows us to recover the QG limit, in which the stratification converges to that prescribed by the restoring condition (see also Zurita-Gotor and Vallis, 2010).

Re-arrangement of Eq. (5.18), generally yields that

$$\Delta_h \overline{b} \approx \Delta_h b_{eq} \frac{1 + \hat{s}_{eq}^{-1}\hat{s}^{-1}}{1 + \hat{s}^{-2}} . \tag{5.A1}$$

where we defined $\hat{s}_{eq} \equiv \Delta_h b_{eq}/\Delta_v b_{eq}$. Using that $\Delta_v \overline{b} = \hat{s}^{-1}\Delta_h \overline{b}$, we directly find that

$$\Delta_v \overline{b} \approx \Delta_h b_{eq} \frac{1 + \hat{s}_{eq}^{-1}\hat{s}^{-1}}{\hat{s} + \hat{s}^{-1}} . \tag{5.A2}$$

As in Eqs. (5.19) and (5.20), we find that both, the horizontal buoyancy contrast and the bulk stability, can be expressed as a function of the radiative equilibrium buoyancy profile and the normalized isentropic slope. However, both, the horizontal buoyancy contrast and the stratification of the radiative equilibrium profile, now influence the resulting mean state.

As in the simplified Eqs. (5.19) and (5.20), the normalized horizontal buoyancy contrast approaches its radiative equilibrium value, i.e. $\Delta_h \overline{b} \approx \Delta_h b_{eq}$, in the limit that $\hat{s} \gg 1$. Any further increase in the isentropic slope in this limit is accomplished

primarily by a further reduction of the normalized stratification, $\Delta_v\bar{b}/\Delta_h b_{eq}$. Also as for Eqs. (5.19) and (5.20), the normalized stratification, $\Delta_v\bar{b}/\Delta_h b_{eq}$, has a maximum at an O(1) normalized isentropic slope, as long as $|\hat{s}_{eq}^{-1}| \lesssim 1$ (i.e. $|\Delta_v b_{eq}| \lesssim |\Delta_h b_{eq}|$). The exact location of this maximum depends on the exact value of $\hat{s}_{eq}$. For a radiative restoring acting to a statically unstable profile, i.e. $\hat{s}_{eq} < 0$, the maximum in the normalized stratification, $\Delta_v\bar{b}/\Delta_h b_{eq}$, is shifted to larger values of $\hat{s}$. The effect of adding a moderate radiative destabilization, $\Delta_v b_{eq} = -0.3\Delta_h b_{eq}$, is shown in figure $5-6$.

Notice, that Eq. (5.A2) would predict a negative stratification if $\hat{s} < -\hat{s}_{eq}^{-1}$. In the case of restoring to a statically unstable mean state, Eq. (5.A2), thus does not have a physical solution for normalized isentropic slopes weaker than $-\hat{s}_{eq}^{-1}$. In the limit of very effective eddy mixing, the isentropic slope may thus not be expected to go to zero. Instead the mean state is expected to equilibrate such that $\hat{s} = -\hat{s}_{eq}^{-1}$, with both $\Delta_v\bar{b}, \Delta_h b \to 0$. This result can also be obtained directly from Eq. (5.18), taking the limit where $|\partial_y\bar{b}| \ll |\partial_y b_{eq}|$ and $|\partial_z\bar{b}| \ll |\partial_z b_{eq}|$. In how far the scaling argument in Eq. (5.A2) holds in such a limit, is however yet to be tested. It is also possible that a system in this limit equilibrates to a state which is strongly inhomogeneous over the domain, such that "characteristic" isentropic slopes, buoyancy gradients, and stratifications, as defined here, become meaningless, and the presented scaling arguments break down. Further, it may be questioned in how far the assumption of "adiabatic" eddy fluxes is appropriate in such a limit[5].

The QG limit is retained if the isentropic slope is weak, i.e. $\hat{s} \ll 1$, and the restoring acts to a statically stable state, in which $0 < \hat{s}_{eq} \lesssim 1$. In this limit, Eq (5.A2) reduces to $\Delta_v b = \Delta_v b_{eq}$, and changes in the isentropic slope are solely due to changes in the meridional buoyancy gradient. Notice, however, that this limit is likely to be of little relevance for the real atmosphere.[6]

[5]Notice that, even if eddies are adiabatic in the sense that $\overline{b'Q'} = 0$, the assumption implied here that $\overline{w'b'}/\overline{v'b'} = s$ requires that the advection of buoyancy variance (primarily associated with the triple correlation term in the variance budget) is negligible (e.g. Cerovečki et al., 2009, and references therein).

[6]One possible way to argue that this limit could become relevant for the atmosphere, is to consider latent heat release as an external forcing in a warm, moist, climate. One might argue that the latent heat release due to moist convection here acts as a restoring to a dry statically stable state. In

Notice that the radiative restoring profile used in the simulations of chapter 2 cannot trivially be characterized by a single equilibrium stratification $\partial_z b_{eq}$, as the latter varies strongly (and even changes sign) over the depth of the troposphere. For figure 5-6, we chose $\Delta_v b_{eq} = 0.3\Delta_h b_{eq}$, which produces a good fit to the data, and subjectively represents an adequate linear fit to the horizontal mean restoring profile. The horizontal radiative equilibrium potential temperature contrast $\Delta_h \theta_{eq} = \alpha^{-1}\Delta_h b_{eq}$ was chosen similar to the simulations with varying f and β, which is an obvious choice, as they share the same radiative convective equilibrium solution.

how far dry dynamics are at all relevant in such a case, and in how far latent heat release can be reasonably thought of as an external diabatic forcing, however, remains questionable.

APPENDIX B

Predicting the Normalized Isentropic Slope in the Presence of Finite $\Delta_v b_{eq}$

We here want to generalize the scaling relation for the normalized isentropic slope in Eq. (5.13), to account for a radiative restoring, which acts towards a stratification that is not statically neutral. Following the same arguments as presented in section 5.3, but keeping $\partial_z b_{eq} \neq 0$, we obtain a generalized version of Eq. (5.13) as

$$\xi \sim \left(\frac{1 - \frac{\partial_z b_{eq}}{\partial_z \bar{b}}}{f \tau_r} \right)^{1/5} \left(\frac{L_d}{a} \right)^{-3/5} . \tag{5.B1}$$

Using that $\xi \sim a/L\hat{s}$, $L_d \sim (\Delta_v \bar{b} H)^{1/2}/f$, and substituting Eq. 5.A2 for the static stability, we obtain after some re-arrangements that

$$\hat{s} \left(\frac{\hat{s} + \hat{s}^{-1}}{1 + \hat{s}_{eq}^{-1} \hat{s}^{-1}} \right)^{-3/10} \left(\frac{\hat{s}_{eq} + \hat{s}^{-1}}{\hat{s}_{eq} - \hat{s}} \right)^{1/5} = \gamma , \tag{5.B2}$$

where γ is defined as in Eq. (5.23) above, and $\hat{s}_{eq} \equiv \Delta_h b_{eq}/\Delta_v b_{eq}$, as in Appendix 5.5.

While the full equation in (5.B2) appears daunting, it should be noted that for a fixed restoring profile (and thus fixed $\hat{s}_{eq}$) Eq. (5.B2), just like its simplified counterpart in Eq. (5.13), implies that $\hat{s} = g(\gamma)$, where the function g is given by inverting Eq. (5.B2). Since g depends on $\hat{s}_{eq}$ as a parameter, it might generally be understood as denoting a family of functions $g(\gamma; \hat{s}_{eq})$. For $\Delta_v b_{eq} = 0$, i.e. $\hat{s}_{eq} = \infty$, we find that $g(\gamma; \infty) = f(\gamma)$, where $f(\gamma)$ is defined as in section 5.4.3.

Chapter 6

Applications to the Southern Ocean

6.1 Introduction

This thesis was motivated in parts by a comparison between the macroturbulent equilibration of the extra-tropical atmosphere and the Southern Ocean. While arguments brought forward for the extra-tropical atmosphere suggest that a baroclinic flow is expected to equilibrate to states near marginal criticality for a wide range of parameters, the Southern Ocean is generally understood to be considerably supercritical. One goal of this thesis was to resolve this apparent contradiction. In chapter 2 we showed that a thermally forced (and thus more atmosphere-like) baroclinic flow can equilibrate to states near marginal criticality as well as to supercritical states if only parameters describing properties of the fluid are varied. This called into question the validity of arguments for equilibration to marginal criticality, even in an atmosphere-like, thermally forced setting. The following chapters 3 through 5 therefore focussed on revising the arguments that have been brought forward for the extra-tropical atmosphere.

By showing that the arguments for equilibration to marginal criticality, brought forward in the atmospheric literature, are not generally valid (even in an atmosphere-like thermally forced setting), we were able to resolve the above mentioned contradic-

tion without further exploration of the equilibration process in an oceanic channel. Nevertheless it seems appropriate to briefly return to the oceanic problem here and analyze whether the arguments discussed in chapters 2 through 5 may be used to make inferences about the Southern Ocean.

Apart from parametric differences, which have been addressed in chapter 2, the most obvious difference between the more atmospheric models considered here and the Antarctic Circumpolar Current (ACC) in the Southern Ocean are given by the different forcing and boundary conditions. While the baroclinic flows discussed here are driven by differential radiative heating throughout the troposphere, diabatic forcing in the Ocean acts only at the surface boundary, and the flow is driven primarily by surface wind stress (e.g. Wunsch and Ferrari, 2004). Once we take account of this difference, the scaling arguments discussed in chapters 2 through 5 can be generalized for the problem of the equilibration of an oceanic channel. The largest remaining uncertainty in our understanding of the equilibration of the Southern Ocean will be argued to be the role of bottom topography in modifying the characteristics of the geostrophic turbulence.

In section 6.2 we will discuss how the scaling arguments for the equilibration of the criticality parameter and isentropic slope, discussed in chapters 2 and 5, can be modified to apply for a wind-driven oceanic channel. It will be shown that the corresponding diffusive scaling relation for the oceanic channel is known and has been discussed in the oceanographic literature. In section 6.2 we will discuss how the constraint for the vertical structure of the eddy diffusivity, discussed in chapters 3 and 4, can be applied to an oceanic channel.

6.2 Scaling Arguments for the Southern Ocean Mean State

The scaling relations for the turbulent equilibration of an atmosphere, discussed in chapters 2 and 5, are based on a balance between the diabatic forcing and the eddy

driven residual overturning circulation. Appropriate for the large-scale atmospheric circulation, we assumed that the mechanical forcing is weak. This is not the case for the Southern Ocean, whose circulation can be understood as being driven by the surface wind stress (e.g. Johnson and Bryden, 1989). Including a surface zonal wind stress ,τ^x, the zonal momentum budget integrated over the surface layer can be written as

$$Ds \approx \psi^\dagger + \frac{\overline{\tau^x}}{f}, \tag{6.1}$$

The isentropic slope s is here evaluated at the bottom of the surface layer, and D can be interpreted as a bulk eddy diffusivity in the surface layer. For vanishing wind stress, Eq. (6.1) reduces to Eq. (5.3), which provides a relation between the eddy driven mass transport, Ds, and the residual circulation, $\psi^\dagger$, which in turn can be related to the radiative forcing (see chapter 2 and 5). Eq. (6.1) is derived in Marshall and Radko (2003), using residual mean theory in z-coordinates, and assuming a diffusive closure for the horizontal component of the buoyancy flux. Using the formalism discussed in chapter 2, it can similarly be derived from the isentropic momentum budget with a diffusive closure for the isentropic eddy PV flux and the surface eddy buoyancy flux.

In the Southern Ocean the diabatic forcing approximately vanishes below the surface, implying that the residual overturning circulation must be weak. The first order balance in Eq. (6.1) must be between the mass transport associated with the eddy flux, Ds, and the transport induced by the wind stress, $\overline{\tau^x}/f$. This allows us to derive a relation between the isentropic slope, the eddy diffusivity, and the forcing (which is here given by the wind stress):

$$s \approx \frac{\tau}{fD}. \tag{6.2}$$

The relation in Eq. (6.2) has been discussed in the oceanographic literature (e.g. Marshall and Radko, 2003; Kuo et al., 2005). It tells us that the isentropic slope is set by a balance between the wind stress, which acts to steepen the isentropic slope, and diffusive eddy fluxes, which act to flatten the isentropes. As for the atmospheric

problem, we can obtain a closed expression for the oceanic mean state if the eddy diffusivity can be related to external parameters and the mean state itself.

For the simulations discussed in this thesis, the eddy diffusivity was well approximated by the scaling relation proposed by Held and Larichev (1996). The derivation of this relation assumes an inverse kinetic energy cascade in the barotropic mode, with an inertial range extending from the deformation scale to the Rhines scale. In the Southern Ocean, it is commonly assumed that the inverse energy cascade is strongly modified by topographic scattering and bottom friction (Rhines, 1979; Thompson and Young, 2007). Both can modify the up-scale energy flux in the inverse cascade, and bottom friction can cause energy to be dissipated before reaching the Rhines scale. Additionally, Smith and Vallis (2002) argue that barotropization is significantly suppressed for strongly surface-intensified stratifications, as typically found in the ocean. The scaling relation for the eddy diffusivity proposed by Held and Larichev (1996) may thus not provide a good predictor for the eddy diffusivity in the Southern Ocean. The discussion about how to best parameterize eddy fluxes in the ocean is still ongoing. Observational data and numerical studies point to the result that the eddy diffusivity increases with the wind stress such that the isentropic slope is rather insensitive to changes in the latter (e.g. Böning et al., 2008; Farneti et al., 2010). This bears some qualitative resemblance to the result found for the atmosphere that the isentropic slope is weakly sensitive to changes in the forcing due to strong eddy compensation.

Eq. (6.2) could be transformed into a condition for the criticality parameter, as done for the atmosphere in chapters 2 and 5. However, the criticality parameter is of only limited interest in the Southern Ocean. In particular, flow characteristics and the range of the inverse energy cascade are related to the criticality parameter only as long as we may assume an inertial range extending to the Rhines scale. As mentioned above, the inverse cascade in the Southern Ocean is instead strongly modified by topographic scattering and bottom friction, which can prevent the inertial range from reaching the Rhines scale. The oceanographic literature has thus commonly paid more attention to the isentropic slope itself, rather than the criticality parameter.

Eq. (6.2) is sometimes used to obtain a scaling relation for the depth of the thermocline (e.g. Marshall and Radko, 2003). The thermodynamic constraint requires that all isentropes intersect with the surface, since there is no diabatic forcing below the surface. Significant stratification is therefore only found on isentropes that intersect with the surface somewhere in the domain. These isentropes make up the stratified thermocline, which vanishes (or is poorly defined) on the cold side of the Antarctic Circumpolar Current (ACC) and increases in depth over the width of the ACC, following the slope of the isentropes. On the equatorward side of the ACC the thermocline depth, h_{TC}, scales with the width of the ACC, L, times the slope of the isentropes: $h_{TC} \sim sL$.

6.3 The Vertical Structure of the Eddy Diffusivity

In chapters 3 and 4 we discussed a constraint for the vertical structure of the eddy diffusivity, and its relation to the criticality parameter. These arguments can be generalized for the oceanic case. The major differences from the atmospheric problem are (1) the existence of isentropic outcrops on both the bottom and top boundaries, (2) the importance of wind- and frictional-stress at the top and bottom boundaries, and (3) the importance of bottom topography, which exerts a zonal form drag. In the following, we will argue that (1) and (2) can be included easily in the framework developed in this thesis, while (3) deserves further attention.

In keeping with the approximations made throughout this thesis, we want to start by considering a flat-bottomed channel (that is we are deferring the discussion of topographic effects). While this is not realistic for the Southern Ocean, it is an illuminating simplification for theoretical purposes, and it is also a common configuration in idealized numerical studies of the ACC. As discussed in the Appendix, we can then derive a constraint for the vertical structure of the eddy diffusivity in an oceanic channel as

$$\int_{b_{min}}^{b_{max}} D\left(\overline{h_b}\beta - f\partial_y\overline{h_b}\right) db \approx \overline{\tau^x}^s - \overline{\tau^x}^f \,. \tag{6.3}$$

Here b_{min} and b_{max} are the minimum and maximum buoyancy over the domain,

$h_b = \mathcal{H}(b - b_f)\mathcal{H}(b_s - b)\partial_b z$ is the generalized isentropic thickness, which vanishes on isentropes below the seafloor ($b < b_f$) or above the surface ($b > b_s$), τ_x is the zonal stress, $\overline{(\cdot)}^s$ denotes an average along the surface, and $\overline{(\cdot)}^f$ denotes an average along the seafloor. Notice, that the argument of the integral in Eq. (6.3) represents a generalized planetary PV gradient. Due to the Heaviside functions in the definition of the generalized thickness, h_b, the generalized PV gradient has additional δ-function contributions from the isentropic outcrops, which are analogous to the PV sheets in the QG approximation (Bretherton, 1966).

From the Eulerian zonal momentum budget it follows that the surface wind stress needs to be approximately balanced by the frictional bottom stress, i.e. $\overline{\tau^x}^f \approx \overline{\tau^x}^s$. Any mismatch between the two would have to be balanced by horizontal momentum flux convergence which is typically much smaller (e.g. Johnson and Bryden, 1989; Stevens and Ivchenko, 1997, and references therein). The R.H.S. of Eq. (6.3) then vanishes and we are left with the same result as discussed for the atmosphere in chapter 3. The contribution of the planetary vorticity gradient, β, to the generalized PV gradient has been shown to be small over much of the ACC, particularly in the upper ocean (Abernathey et al., 2010), which suggests that the flow is strongly supercritical[1]. To the extend that this holds true for the vertically integrated budget, Eq (6.3) implies that the momentum budget can be satisfied with an eddy diffusivity that is approximately constant in the vertical, as has been commonly used in ocean models. This is directly analogous to the strongly supercritical limit discussed in chapters 3 and 4. Recent analysis of ocean models, however, suggests that the eddy diffusivity does vary in the vertical and peaks near a critical level where the PV gradient changes sign (Abernathey, 2012, personal communication). The constraint in Eq. (6.3), however, still has to be fulfilled. Notice, that Eq. (6.3) does not imply that the eddy diffusivity cannot have any vertical structure. It only states that the

[1]This can be seen by noting that $\xi \sim (fs/H)/\beta \sim f\partial_z s/\beta$, where we assume that the slope of the isentropes varies over the depth scale H. There is some arbitrariness on what depth scale should be used when estimating the criticality parameter in the Southern Ocean. When the interest is on the supercriticality to baroclinic instability, $\xi \sim f\partial_z s/\beta$ is an appropriate choice, since the requirement for stability is a cancellation of the thickness gradient contribution $f\partial_z s$ by the planetary vorticity gradient β.

eddy diffusivity and the generalized PV gradient cannot be correlated in the vertical.

To the extent that the contribution of the planetary vorticity gradient, β, is not negligible in the vertically integrated budget, Eq. (6.3) suggests that the eddy diffusivity needs to be larger at levels where the generalized PV gradient is negative. If the generalized PV gradient changes monotonically from negative values at the bottom to positive values near the surface, this implies that the eddy diffusivity has to be larger in the deep ocean than near the surface. This result is directly analog to the atmospheric case, discussed in chapters 2 and 3. The same scaling relation between the vertical structure of the eddy diffusivity and the criticality parameter can be derived if the ocean is divided into two vertical layers, separated by the level where the PV gradient changes sign. The criticality parameter, which determines the vertical decay of the eddy diffusivity, would here have to be defined as $\xi \sim fs/(\beta H)$, with H the full depth of the domain and s the isentropic slope at the level where the PV gradient changes sign (which is typically near the level of steepest isentropic slope). Notice, that the criticality parameter so defined is only ~2-3 for the Southern Ocean, indicating that the contribution of β to the PV gradient is indeed not completely negligible when considering the momentum budget integrated over the full depth of the channel.

We now want to address the more realistic case where the momentum budget is influenced by the presence of bottom topography. The isentropic zonal momentum budget used to derive Eq. (6.3) holds similarly in the presence of topography. However, the contribution associated with isentropic outcrops is proportional to the geostrophic eddy buoyancy flux averaged zonally along the now undulated seafloor. That is the average in $\overline{v_g' b'}^f$ is to be taken following the bottom topography (and primed quantities denote deviations from this average). In the derivation of Eq. (6.3) we used a diffusive closure for the geostrophic eddy buoyancy flux at the seafloor (with a diffusivity assumed to be similar to the PV diffusivity in the deep ocean). Whether such a closure can be justified in the presence of topography is questionable, for reasons that will be discussed in the following.

The contribution from the geostrophic eddy buoyancy flux at the seafloor can

be understood as a generalized bottom form drag in isentropic coordinates. For small topography, it can be approximated as the sum of a contribution associated with undulations of the isentropes, corresponding to the buoyancy flux at a fixed z-level, and a contribution associated with undulations of the seafloor, representing the bottom form drag in z-coordinates: $\overline{v_g' b'}^f \approx \overline{v_g' b'}^z + \partial_z \bar{b}^f \overline{v_g' \eta'}^f$, where $\overline{(\cdot)}^z$ denotes an average at constant height (just above the topography), and η denotes the topographic elevation. Since the bottom form drag contribution is not obviously connected to the rate of eddy mixing, or the meridional buoyancy gradient, it is unclear in how far a diffusive closure for the full geostrophic eddy buoyancy flux at the seafloor can be justified in the presence of significant topography. A diffusive closure for the eddy buoyancy flux at fixed z-level, however, is similarly unjustified, since the flow above the topography is not expected to be purely horizontal. Instead, any closure for the momentum budget near the seafloor requires careful consideration of the flow near the undulating bottom boundary, which is beyond the scope of this thesis.

The eddy buoyancy flux at the seafloor is a major component of the vertically integrated isentropic momentum budget, with the bottom form drag contribution, $f\overline{v_g' \eta'}^f$, typically canceling the surface wind stress in the presence of significant topography (Johnson and Bryden, 1989; Stevens and Ivchenko, 1997). Much progress has been made recently to extend theories of the ACC beyond the highly idealized picture of an isolated flat-bottomed zonal channel. For example, Ito and Marshall (2008) and Nikurashin and Vallis (2011) developed theories of the deep ocean thermal structure and overturning circulation which account for the interaction between the circumpolar channel and the rest of the ocean; and LaCasce and Isachsen (2010) revisited the role of continents and topography impinging on the channel in the framework of linear equivalent barotropic theories. Yet, our theoretical understanding of how eddy fluxes, and thus the zonal momentum budget, can be closed near the bottom topography is still underdeveloped.

6.4 Conclusions

We showed that the arguments discussed in chapters 2 through 5 can be generalized for the problem of the equilibration of a wind-driven oceanic channel, if we take account of the different boundary conditions and in particular the strong momentum flux at the ocean's surface imposed by the wind stress. The scaling arguments for the equilibration of the criticality parameter and isentropic slope, discussed in chapters 2 and 5, were modified to apply for a wind-driven oceanic channel by adding the surface wind stress forcing while making use of the fact that the oceanic interior is essentially adiabatic. The resulting relation between the isentropic slope and the surface wind stress and eddy diffusivity is known and confirmed in the oceanographic literature (e.g. Marshall and Radko, 2003; Kuo et al., 2005). To obtain a closed expression for the oceanic mean state, one would need to relate the eddy diffusivity to external parameters and the mean state itself. How this is best done in an oceanographic setting, where bottom friction and topography are likely to be important in shaping the characteristics of the turbulence, is a question that is widely debated in the oceanographic community and shall not be addressed here.

We further discussed how the constraint for the vertical structure of the eddy diffusivity, discussed in chapters 3 and 4, can be applied to an oceanic channel. For a flat-bottomed wind-driven channel we were able to derive the same integral constraint for the vertical structure of the eddy diffusivity as discussed for the atmosphere in chapter 3. While this has relevance for many idealized modeling studies, the zonal momentum budget in the real Southern Ocean is understood to be strongly influenced by the presence of bottom form drag, associated with the large bottom topography. The vertically integrated momentum budget in the presence of bottom topography involves a contribution associated with intersections of isentropes with the topography. It remains unclear whether the latter can be related to the mean state and/or the surface wind stress.

Notice, that the purpose of this chapter is to provide only a general overview about how the arguments presented in this thesis may be applied to make inferences

about the turbulent equilibration of the Southern Ocean. A detailed discussion of the Southern Ocean equilibration problem, as well as a test of the presented arguments against numerical simulations and/or observations, is beyond the scope of this thesis but provides possible directions for future work.

APPENDIX

Isentropic Mass Flux Balance in the Presence of Stresses at the Boundaries

We here want to derive a constraint for the vertical structure of the eddy diffusivity in the presence of momentum fluxes at the upper and lower boundary. As in chapter 2, we start from the isentropic zonal momentum balance in a zonally re-entrant channel, which can be transformed into an equation for the mass transport upon division by the mean isentropic PV. Vertically integrated from the bottom to the top boundary, the equation can be written as

$$\int_{b_{min}}^{b_{max}} \overline{h}_b \, \overline{v}^* db \approx - \int_{b_{min}}^{b_{max}} \frac{\overline{h}_b \overline{\hat{v}\hat{P}}^* + \overline{h}_b \overline{J_F^y}^*}{\overline{P}^*} db + \frac{f}{\overline{P}^*(\overline{b}^s)} \overline{v_g' b'}^s - \frac{f}{\overline{P}^*(\overline{b}^f)} \overline{v_g' b'}^f . \quad \text{(6.A1)}$$

Here b_{min} and b_{max} are the minimum and maximum buoyancy over the domain, $h_b = \mathcal{H}(b - b_f)\mathcal{H}(b_s - b)\partial_b z$ is the generalized isentropic thickness, which vanishes on isentropes below the seafloor ($b < b_f$) or above the surface ($b > b_s$), the overbar denotes an isentropic average, $\overline{(\cdot)}^* = \overline{h_b(\cdot)}/\overline{h_b}$ is the thickness weighted average, $\overline{(\cdot)}^s$ denotes an average along the surface, and $\overline{(\cdot)}^f$ denotes an average along the seafloor. Other quantities are defined as in chapter 2. Eq. (6.A1) is analog to Eq. (2.4), except that it has contributions due to isentropic outcrops on both the bottom and top boundaries. As before these contributions are written in terms of an eddy buoyancy flux.

We now want to rewrite the contributions from the mechanical forcing, which we assume to be confined to two shallow Ekman layers at the top and bottom boundaries. We need to consider two contributions of the mechanical forcing in (6.A1). The first obvious contribution comes from the forcing term $\overline{h}_b \overline{J_F^y}^*$ in the integral on the R.H.S.. Additionally, the eddy PV flux $\overline{h}_b \overline{\hat{v}\hat{P}}^*$ contains a contribution due to the Ekman

transport $\overline{\overline{h_b}\hat{v}\hat{P}}^* = \overline{\overline{h_b}\hat{v}_{Ek}\hat{P}}^* + \overline{\overline{h_b}\hat{\tilde{v}}\hat{P}}^*$, where we defined $\tilde{v} = v - v_{Ek}$, as the part of the velocity not associated with the Ekman transport, but with the macroturbulence (for small Rossby numbers this is simply the geostrophic part of the velocity). If we want to use a diffusive closure for the Eddy PV flux, it is only the contribution from the macroturbulence, $\overline{\overline{h_b}\hat{\tilde{v}}\hat{P}}^*$, that we can hope to close this way.

Using that $h_b J_F^y = F^x \mathcal{H}(b_s - b)\mathcal{H}(b - b_f) \equiv -f v_{Ek}$, with the zonal force per unit mass F^x, we can write

$$\begin{aligned}
\int_{b_{min}}^{b_{max}} \frac{\overline{\overline{h_b}\hat{v}_{Ek}\hat{P}}^* + \overline{\overline{h_b}J_F^y}^*}{\overline{P}^*} db &= \int_{b_{min}}^{b_{max}} \frac{\overline{\overline{h_b}v_{Ek}\hat{P}}^* - f\overline{v_{Ek}}}{\overline{P}^*} db && \text{(6.A2)} \\
&= \int_{b_{min}}^{b_{max}} \frac{\overline{h_b v_{Ek}(P - \overline{P}^*)} - f\overline{v_{Ek}}}{\overline{P}^*} db && \text{(6.A3)} \\
&\approx \int_{b_i}^{b_{max}} \frac{\overline{v_{Ek}f} - \overline{h_b v_{Ek}}\,\overline{P}^* - f\overline{v_{Ek}}}{\overline{P}^*} db && \text{(6.A4)} \\
&= -\int_{b_{min}}^{b_{max}} \overline{h_b v_{Ek}} db && \text{(6.A5)} \\
&= \frac{1}{f}\overline{\int_{-H}^{0} F^x dz} && \text{(6.A6)} \\
&= \frac{\overline{\tau^x}^s}{f} - \frac{\overline{\tau^x}^f}{f} && \text{(6.A7)}
\end{aligned}$$

where τ^x is the zonal momentum flux trough the top and bottom boundaries (positive downwards on both boundaries). Plugging this back into (6.A1) and using that the total meridional mass transport has to vanish, we find that

$$-\int_{b_{min}}^{b_{max}} \frac{\overline{\overline{h_b}\hat{\tilde{v}}\hat{P}}^*}{\overline{P}^*} db + \frac{f}{\overline{P}^*(\overline{b}^s)}\overline{v_g' b'}^s - \frac{f}{\overline{P}^*(\overline{b}^f)}\overline{v_g' b'}^f \approx \frac{\overline{\tau^x}^s}{f} - \frac{\overline{\tau^x}^f}{f}. \qquad \text{(6.A8)}$$

Using a diffusive closure for the eddy flux of PV and the eddy buoyancy fluxes at the top and bottom boundaries, the L.H.S can be re-written as discussed in chapter 2, to yield

$$\int_{b_{min}}^{b_{max}} D\left(\overline{h_b}\beta - f\partial_y \overline{h_b}\right) db \approx \overline{\tau^x}^s - \overline{\tau^x}^f. \qquad \text{(6.A9)}$$

Notice, that the argument in the integral in Eq. 6.A9 denotes a generalized planetary

PV gradient, which contains a contribution associated with the planetary vorticity gradient β, as well the generalized thickness gradient $\partial_y \overline{h}_b$. The latter includes contributions from the buoyancy gradients at the boundaries, corresponding to the buoyancy flux terms Eq. (6.A8) . This can be seen by noting that the gradient of the generalized thickness, $h_b = \mathcal{H}(b - b_f)\mathcal{H}(b_s - b)\partial_b z$, includes gradients of the Heaviside functions, which in turn yield the buoyancy gradients at the top and bottom boundaries. As in chapter 2, we have ignored contributions of the relative vorticity to the PV gradient in deriving Eq. (6.A9).

Chapter 7

Summary and Conclusion

7.1 Summary

This thesis has analyzed the turbulent equilibration of an atmosphere, using theoretical arguments and idealized numerical simulations. Contrary to the suggestion of some previous studies (Stone, 1978; Schneider, 2004), we have shown that eddies do not generally equilibrate atmospheres to states of marginal criticality. Instead, any theory for the turbulent equilibration requires an understanding of how turbulent fluxes depend on the external parameters, as well as the equilibrated mean state itself.

Chapter 2 was motivated by the observed difference in the criticality of the extra-tropical atmosphere and Southern Ocean. The mean state of the extra-tropical atmosphere is believed to be near marginal criticality to baroclinic instability, with eddy-eddy interactions playing a minor role. The Southern Ocean instead is understood to be considerably supercritical, and eddy-eddy interactions may play a significant role in shaping the turbulent flow statistics and ultimately setting the mean state. We performed a series of numerical simulations, in a thermally forced zonally re-entrant channel model, varying the thermal expansion coefficient of the fluid from atmosphere-like values to ocean-like values. It was shown that this suffices to obtain atmosphere-like, marginally critical mean states, as well as significantly supercritical states, which resemble some of the properties observed in the Southern Ocean.

We further derived a scaling argument for the criticality parameter of the equilibrated mean state, which explains most of the variations found in the numerical simulations. The scaling relation suggests that the transition to supercritical mean states can be explained in terms of a reduction of the deformation radius in the limit of small, ocean-like, expansion coefficients. This ultimately renders eddies ineffective in maintaining a marginally critical state in the limit of small thermal expansion coefficients.

The results in chapter 2 are at odds with the theory of Schneider (2004), which advocates adjustment to marginal criticality as a general feature of turbulently equilibrated atmospheres. Schneider (2004) argued that marginally critical states arise as a consequence of the eddy diffusivity of PV being vertically constant. Strongly supercritical states would require an eddy diffusivity that increases strongly with height, which in turn is inconsistent with the expectation that eddies become essentially barotropic in the strongly supercritical limit (e.g. Held and Larichev, 1996).

In chapter 3 we showed that the result of Schneider (2004) appears to arise as a consequence his definition of an extended mean and eddy PV flux on isentropes that intersect the surface. Yet, the physical meaning of this extended eddy PV flux is unclear, and the assumed closure is not supported by numerical simulations. We thus revised Schneider's (2004) derivation, using the isentropic mean and eddy PV flux definitions proposed by Koh and Plumb (2004), which arise from averaging the conventional PV flux over only the above-surface part of each isentrope. A diffusive closure for the eddy PV flux under this definition is supported by an analysis of the PV variance budget, as well as idealized numerical simulations. Following this approach, it was shown that order one criticalities are obtained if the eddy diffusivity decays from its surface value to about zero over the depth of the troposphere, which is likely to be the case in Earth's atmosphere. Large criticality parameters, however, are possible if the eddy diffusivity decays only weakly in the vertical, consistent with the notion that eddies become essentially barotropic in this limit. The revised relation between the criticality parameter and the vertical structure of the eddy diffusivity is also in agreement with previous results based on the QG approximation (e.g. Green,

1970), which Schneider (2004, 2005) deemed inappropriate to describe the effects of large-scale turbulence in the atmosphere.

In chapter 4, the derived scaling relation between the criticality parameter and the vertical structure of the eddy diffusivity was confirmed in atmospheric re-analysis, as well as in a series of numerical simulations. The performed numerical simulations used a widely varying Coriolis parameter, f, and planetary vorticity gradient, β, which proved to be an efficient way to obtain mean states with a wide range of criticality parameters. In agreement with the scaling relation proposed in chapter 3, simulations with marginally critical mean states were found to be associated with an eddy diffusivity which decreases strongly over the depth of the troposphere, while strongly supercritical mean states were found to be associated with an eddy diffusivity which is approximately constant over the entire troposphere.

While putting to rest the often stated belief that the criticality parameter cannot be much larger than one, the revised relation between the criticality parameter and the vertical structure of the eddy diffusivity does not provide a predictive theory for the equilibrated thermal mean state. Instead our results imply that any prediction of the equilibrated state requires a theory for what sets the eddy diffusivity.

In chapter 5 we thus returned to the challenge of predicting changes in the equilibrated mean state in response to changes in the forcing or other external parameters. We argued that changes in the criticality parameter are best understood in terms of a balance between the diabatic forcing and the eddy driven overturning circulation, as first discussed in chapter 2. Unlike the relation derived in chapter 3 we are here not concerned with the vertical structure of the eddy diffusivity, but require a scaling argument only for the magnitude of the bulk diffusivity in the lower troposphere. For the simulations discussed in this thesis the lower tropospheric eddy diffusivity follows the scaling relation of Held and Larichev (1996), which is based on the strength of the atmospheric energy cycle. Using this closure for the eddy diffusivity, one can derive a scaling relation for the criticality parameter, which reproduces the numerical results of chapter 2 (where we varied the thermal expansion coefficient), as well as the large variations in the criticality parameter found in the simulations of chapter 4 (where

we varied f and β).

The scaling arguments discussed in chapters 2 and 5, are also in qualitative agreement with previous numerical results, which showed weak dependence of the criticality parameter to changes in the external forcing (e.g. Schneider, 2004). It supports the notion that changes in the criticality parameter in response to moderate changes in the thermal forcing, as might be expected in past and future climate change, are likely to be small. The criticality parameter can, however, change strongly if the forcing is changed enough, or other parameters (such as the planets size and/or rotation rate) are varied. The assumption that atmospheres on other planets, or other fluid systems (such as the ocean), always equilibrate to states of marginal criticality is thus not generally justified.

Finally, we showed in chapter 5 that both the equator to pole temperature gradient and the bulk static stability are constrained by the thermodynamic budget, once the criticality parameter is known. For the idealized dry simulations discussed in this thesis, we were thus able to explain, and predict, the response of both the meridional temperature gradient, and bulk stability, to changes in the forcing and other external parameters.

In chapter 6 we offered a brief comparison between our results for the turbulent equilibration of an atmosphere, and the corresponding equilibration problem of the Southern Ocean, which was part of the motivation for this thesis. It was shown that the arguments discussed in chapters 2 through 5 can be generalized for the problem of the equilibration of a wind-driven oceanic channel, if we take account of the different boundary conditions and in particular the strong momentum flux at the ocean's surface imposed by the wind stress. The resulting relation between the isentropic slope, surface wind stress and eddy diffusivity has been known and confirmed in the oceanographic literature (e.g. Marshall and Radko, 2003; Kuo et al., 2005). The largest uncertainty in our understanding of the equilibration of the Southern Ocean was argued to be the role of bottom topography in modifying the characteristics of the geostrophic turbulence.

7.2 Concluding Remarks

This thesis resolved an apparent contradiction in our understanding of atmospheric and oceanic equilibration by large scale turbulence. In contrast with previous atmospheric literature, but in agreement with our understanding of the Southern Ocean, it was shown that atmospheres do not generally equilibrate to states of marginal criticality. Instead, any argument for the turbulent equilibration requires an understanding of the dependence of eddy fluxes on the mean state.

The results discussed in this thesis extend much of our understanding from quasi-geostrophic models to primitive equation systems. Using the isentropic zonal momentum budget, we derived constraints for the equilibrated mean state, and its relation to the magnitude and vertical structure of the eddy diffusivity. The results represent direct generalizations of quasi-geostrophic theory. Our simulations further confirmed the relations between the criticality parameter and the characteristics of the turbulent flow, originally proposed for the two-layer quasi-geostrophic model by Held and Larichev (1996). In particular we showed that increasing criticality parameters allow for an increasing inverse energy cascade, between the deformation scale (where most of the eddy kinetic energy is produced from conversion of available potential energy) to the Rhines scale (where the inverse kinetic energy cascade is halted).

We thus provide an important step in a hierarchy of models required to generate a fundamental understanding of how atmospheres equilibrate. To fully appreciate the key processes in Earth's extra-tropical atmosphere, or other planetary atmospheres, new models will need to be added to the hierarchy. These will need to address the role of processes that have been left out here for the sake of simplicity. For example, the influence of the planets spherical geometry, where the eddy-mediated extra-tropics are connected to the tropical Hadley-cell regime. The effect of applying a realistic radiative forcing, as opposed to the idealized thermal restoring considered here. The impact of the myriad of processes encountered in the atmospheric boundary layer. And, maybe most importantly for Earth's atmosphere, the role of moisture and convection. While some progress has already been made on all of these issues in the

existing literature, they still provide ample opportunities for future work.

Bibliography

Abernathey, R., J. Marshall, M. Mazloff, and E. Shuckburgh, 2010: Enhancement of mesoscale eddy stirring at steering levels in the Southern Ocean. *J. Phys. Oceanogr.*, **40**, 170–184.

Andrews, D. G., 1983: A finite-amplitude eliassen-palm theorem in isentropic coordinates. *J. Atmos. Sci.*, **40**, 1877–1883.

Andrews, D. G., J. R. Holton, and C. B. Leovy, 1987: *Middle Atmosphere Dynamics.*, International Geophysics Series, Vol. 40. Academic Press, 489 pp.

Barry, L., G. C. Craig, and J. Thuburn, 2000: A GCM investigation into the nature of baroclinic adjustment. *J. Atmos. Sci.*, **57**, 1141–1155.

Bartels, J., D. Peters, and G. Schmitz, 1998: Climatological Ertel's potential-vorticity flux and mean meridional circulation in the extratropical troposphere – lower stratosphere. *Ann. Geophysicae*, **16**, 250–265.

Boer, G. J. and T. G. Shepherd, 1983: Large-scale two-dimensional turbulence in the atmosphere. *J. Atmos. Sci.*, **40**, 164–184.

Böning, C. W., A. Dispert, M. Visbeck, S. R. Rintoul, and F. U. Schwarzkopf, 2008: The response of the Antarctic Circumpolar Current to recent climate change. *Nature Geoscience*, **1 (12)**, 864–869.

Bretherton, F. P., 1966: Critical layer instability in baroclinic flows. *Quart. J. Roy. Meteor. Soc.*, **92 (393)**, 325–334.

Cerovečki, I., R. A. Plumb, and W. Heres, 2009: Eddy transport and mixing in a wind and buoyancy-driven jet on the sphere. *J. Phys. Oceanogr.*, **39**, 1133–1149.

Farneti, R., T. L. Delworth, A. J. Rosati, S. M. Griffies, and F. Zeng, 2010: The role of mesoscale eddies in the rectification of the southern ocean response to climate change. *J. Phys. Oceanogr.*, **40**, 1539–1557.

Farrell, B. F. and P. J. Ioannou, 2009: A theory of baroclinic turbulence. *J. Atmos. Sci.*, **66**, 2444–2454.

Ferrari, R. and M. Nikurashin, 2010: Suppression of eddy mixing across jets in the southern ocean. *J. Phys. Oceanogr.*, **40**, 1501–1519.

Gent, P. R. and J. C. McWilliams, 1990: Isopycnal mixing in ocean circulation models. *J. Phys. Oceanogr.*, **20**, 150–155.

Green, J. S. A., 1970: Transfer properties of the large-scale eddies and the general circulation of the atmosphere. *Quart. J. Roy. Meteor. Soc.*, **96**, 157–185.

Haynes, P. and E. Shuckburgh, 2000: Effective diffusivity as a diagnostic of atmospheric transport 2. troposphere and lower stratosphere. *J. Geophys. Res.*, **105 (D18)**, 22,795–22,810.

Held, I. M., 1978: The vertical scale of an unstable baroclinic wave and its importance for eddy heat flux parameterizations. *J. Atmos. Sci.*, **35**, 572–576.

Held, I. M., 1982: On the height of the tropopause and the static stability of the troposphere. *J. Atmos. Sci.*, **39**, 412–417.

Held, I. M., 2007: Progress and problems in large-scale atmospheric dynamics. *The Global Circulation of the Atmosphere*, T. Schneider and A. H. Sobel, Eds., Princeton University Press, 1–21.

Held, I. M. and V. D. Larichev, 1996: A scaling theory for horizontally homogeneous baroclinically unstable flow on a beta plane. *J. Atmos. Sci.*, **53 (7)**, 946–952.

Held, I. M. and T. Schneider, 1999: The surface branch of the mass transport circulation in the troposphere. *J. Atmos. Sci.*, **56**, 1688–1697.

Held, I. M. and M. J. Suarez, 1994: A proposal for the intercomparison of the dynamical cores of atmospheric general circulation models. *Bull. Am. Meteorol. Soc.*, **75 (10)**, 1825–1830.

Huybers, P. and E. Tziperman, 2008: Integrated summer insolation controls 40,000 year glacial cycles in an ice-sheet energy-balance model. *Paleoceanography*, **23**, PA1208.

Ito, T. and J. Marshall, 2008: Control of lower-limb overturning circulation in the Southern Ocean by diapycnal mixing and mesoscale eddy transfer. *J. Phys. Oceanogr.*, **38**, 2832–2845.

James, I. N. and L. J. Gray, 1986: Concerning the effect of surface drag on the circulation of a baroclinic planetary atmosphere. *Quart. J. Roy. Meteor. Soc.*, **1112**, 1231–1250.

Jansen, M. and R. Ferrari, 2012: Macroturbulent equilibration in a thermally forced primitive equation system. *J. Atmos. Sci.*, **69**, 695–713.

Johnson, G. C. and H. L. Bryden, 1989: On the size of the antarctic circumpolar current. *Deep Sea Research Part A. Oceanographic Research Papers*, **36 (1)**, 39 – 53.

Juckes, M. N., I. N. James, and M. Blackburn, 1994: The influence of antarctica on the momentum budget of the southern extratropics. *Quart. J. Roy. Meteor. Soc.*, **120 (518)**, 1017–1044.

Karsten, R. and J. Marshall, 2002: Constructing the residual circulation of the ACC from observations. *J. Phys. Oceanogr.*, **32**, 3315–3327.

Koh, T.-Y. and R. A. Plumb, 2004: Isentropic zonal average formalism and the near-surface circulation. *Quart. J. Roy. Meteor. Soc.*, **130**, 1631–1653.

Koshyk, J. N. and K. Hamilton, 2001: The horizontal kinetic energy spectrum and spectral budget simulated by a high-resolution troposphere-stratosphere mesosphere GCM. *J. Atmos. Sci.*, **58 (4)**, 329–348.

Kuo, A., R. A. Plumb, and J. Marshall, 2005: Transformed eulerian-mean theory. part II: potential vorticity homogenization and the equilibrium of a wind and buoyancy-driven zonal flow. *J. Phys. Oceanogr.*, **35**, 175–187.

LaCasce, J. and P. Isachsen, 2010: The linear models of the ACC. *Progress In Oceanography*, **84**, 139 – 157.

Lapeyre, G. and I. M. Held, 2003: Diffusivity, kinetic energy dissipation, and closure theories for the poleward eddy heat flux. *J. Atmos. Sci.*, **60**, 2907–2916.

Marshall, J., C. Hill, L. Perelman, and A. Adcroft, 1997: Hydrostatic, quasie-hydrostatic, and nonhydrostatic ocean modeling. *J. Geophys. Res.*, **102**, 5753–5766.

Marshall, J. and T. Radko, 2003: Residual mean solutions for the antarctic circumpolar current and its associated overturning circulation. *J. Phys. Oceanogr.*, **33 (11)**, 2341–2354.

Marshall, J. C., 1981: On the parameterization of geostrophic eddies in the ocean. *J. Phys. Oceanogr.*, **11**, 257–271.

Merlis, T. M. and T. Schneider, 2009: Scales of linear baroclinic instability and macroturbulence in dry atmospheres. *J. Atmos. Sci.*, **66**, 1821–1833.

Nakamura, N., 1996: Two-dimensional mixing, edge formation, and permeability diagnosed in area coordinates. *J. Atmos. Sci.*, **53**, 1524–1537.

Nikurashin, M. and G. A. Vallis, 2011: A theory of deep stratification and overturning circulation in the ocean. *J. Phys. Oceanogr.*, **41**, 485–502.

O'Gorman, P. A. and T. Schneider, 2007: Recovery of atmospheric flow statistics in a general circulation model without nonlinear eddy-eddy interactions. *Geophys. Res. Lett.*, **34**, L22 801.

Panetta, R. L. and I. M. Held, 1988: Baroclinic eddy fluxes in a one–dimensional model of quasi–geostrophic turbulence. *J. Atmos. Sci.*, **45**, 3354–3365.

Pavan, V. and I. Held, 1996: The diffusive approximation for eddy fluxes in baroclinically unstable jets. *J. Atmos. Sci.*, **53 (9)**, 1262–1272.

Plumb, R., 1979: Eddy fluxes of conserved quantities by small-amplitude waves. *J. Atmos. Sci.*, **36 (9)**, 1699–1704.

Plumb, R. and R. Ferrari, 2005: Transformed Eulerian-mean theory. Part I: Nonquasigeostrophic theory for eddies on a zonal-mean flow. *J. Phys. Oceanogr.*, **35**, 165–174.

Plumb, R. and J. Mahlman, 1987: The zonally averaged transport characteristics of the gfdl general circulation/transport model. *J. Atmos. Sci.*, **44**, 298–327.

Rhines, P. and W. Young., 1982: Homogenization of potential vorticity in planetary gyres. *J. Fluid Mech.*, **122**, 347–367.

Rhines, P. B., 1979: Geostrophic turbulence. *Annu. Rev. Fluid Mech.*, **11**, 401–441.

Rose, B. and J. Marshall, 2009: Ocean heat transport, sea ice, and multiple climate states: insights from energy balance models. *J. Atmos. Sci.*, **66**, 2828–2843.

Schneider, T., 2004: The tropopause and the thermal stratification in the extratropics of a dry atmosphere. *J. Atmos. Sci.*, **61 (12)**, 1317–1340.

Schneider, T., 2005: Zonal momentum balance potential vorticity dynamics, and mass fluxes on near-surface isentropes. *J. Atmos. Sci.*, **62**, 1884–1900.

Schneider, T., I. M. Held, and S. T. Garner, 2003: Boundary effects in potential vorticity dynamics. *J. Atmos. Sci.*, **60**, 1024–1040.

Schneider, T. and J. Liu, 2009: Formation of jets and equatorial super rotation on jupiter. *J. Atmos. Sci.*, **66**, 579–601.

Schneider, T. and C. C. Walker, 2006: Self-organization of atmospheric macroturbulence into critical states of weak nonlinear eddy-eddy interactions. *J. Atmos. Sci.*, **63**, 1569–1586.

Scott, R. and F. Wang, 2005: Direct evidence of an oceanic inverse kinetic energy cascade from satellite altimetry. *J. Phys. Oceanogr.*, **35**, 1650–1666.

Shapiro, R., 1970: Smoothing, filtering, and boundary effects. *Reviews of Geophysics and Space Physics*, **8 (2)**, 359–387.

Smith, K. S., 2007: The geography of linear baroclinic instability in earth's oceans. *J. Mar. Res.*, **65**, 655–683.

Smith, K. S. and G. K. Vallis, 2002: The scales and equilibration of midocean eddies: Forced-dissipative flow. *J. Phys. Oceanogr.*, **32**, 1699–1721.

Stevens, D. and V. Ivchenko, 1997: The zonal momentum balance in an eddy resolving general circulation model of the Southern Ocean. *Quart. J. Roy. Meteor. Soc.*, **123**, 929–951.

Stone, P. H., 1972: A simplified radiative-dynamical model for the static stability of rotating atmospheres. *J. Atmos. Sci.*, **29 (3)**, 405–418.

Stone, P. H., 1978: Baroclinic adjustment. *J. Atmos. Sci.*, **35**, 561–571.

Thompson, A. and W. Young, 2007: Two-layer baroclinic eddy heat fluxes: Zonal flows and energy balance. *J. Atmos. Sci.*, **64**, 3214–3231.

Thuburn, J. and G. C. Craig, 1997: GCM tests of theories for the height of the tropopause. *J. Atmos. Sci.*, **54**, 869–882.

Tulloch, R., J. Marshall, C. Hill, and K. S. Smith, 2011: Scales, growth rates and spectral fluxes of baroclinic instability in the ocean. *J. Phys. Oceanogr.*, **41**, 1057–1076.

Tung, K. K., 1986: Nongeostrophic theory of zonally averaged circulation.Part 1: Formulation. *J. Atmos. Sci.*, **43 (22)**, 2600–2618.

Vallis, G. K., 2006: *Atmospheric and Oceanic Fluid Dynamics.* Cambridge University Press, Cambridge, U.K., 745 pp.

Wunsch, C. and R. Ferrari, 2004: Vertical mixing, energy, and the general circulation of the oceans. *Annu. Rev. Fluid Mech.*, **36**, 281–314.

Zurita-Gotor, P., 2008: The sensitivity of the isentropic slope in a primitive equation dry model. *J. Atmos. Sci.*, **65**, 43–65.

Zurita-Gotor, P. and R. S. Lindzen, 2007: Theories of baroclinic adjustment and eddy equilibration. *The Global Circulation of the Atmosphere*, T. Schneider and A. H. Sobel, Eds., Princeton University Press, 22–46.

Zurita-Gotor, P. and G. K. Vallis, 2009: Equilibration of baroclinic turbulence in primitive-equation and quasi-geostrophic models. *J. Atmos. Sci.*, **66**, 837–863.

Zurita-Gotor, P. and G. K. Vallis, 2010: Circulation sensitivity to heating in a simple model of baroclinic turbulence. *J. Atmos. Sci.*, **67**, 1543–1558.

Zurita-Gotor, P. and G. K. Vallis, 2011: Dynamics of midlatitude tropopause height in an idealized model. *J. Atmos. Sci.*, **68**, 823–838.